LUND UNIVERSITY

# SURVEY OF EXPERIMENTAL DATA ON THE STRENGTH OF ANNEALED FLOAT GLASS PANES IN THE AS-RECEIVED CONDITION TESTED IN AN AMBIENT ENVIRONMENT

DAVID KINSELLA

Structural Mechanics

DEPARTMENT OF CONSTRUCTION SCIENCES
DIVISION OF STRUCTURAL MECHANICS

ISRN LUTVDG/TVSM--18/7166--SE (1-73) | ISSN 0281-6679

# SURVEY OF EXPERIMENTAL DATA ON THE STRENGTH OF ANNEALED FLOAT GLASS PANES IN THE AS-RECEIVED CONDITION TESTED IN AN AMBIENT ENVIRONMENT

DAVID KINSELLA



For information, address:
Div. of Structural Mechanics,
Faculty of Engineering LTH, Lund University, Box 118, SE-221 00 Lund, Sweden.
Homepage: www.byggmek.lth.se

*Division of Structural Mechanics*
*Faculty of Engineering, LTH*
*Lund University, Sweden*

# SURVEY OF EXPERIMENTAL DATA ON THE STRENGTH OF ANNEALED FLOAT GLASS PANES IN THE AS-RECEIVED CONDITION TESTED IN AN AMBIENT ENVIRONMENT

David Kinsella
*david.kinsella@construction.lth.se*

A detailed overview is provided for the strength of monolithic annealed float glass panes according to experiments carried out over the past four decades. The experiments were conducted with the coaxial double ring bending device, the three-point bending device, the four-point bending device, and the arrangement that allows for laterally supported plates to be subjected to uniform pressure. When the stress history was linear, the 2 MPa $s^{-1}$ stress rate-equivalent strength was calculated and compared with the nominal value of the strength. The data was obtained from the open literature. Only new glass in the as-received condition was considered. Only glass that was tested in an ambient environment was included in the survey. The strength is visualized in the form of boxplots and probability plots. The three following types of probability plots were considered, viz. the Weibull, the normal, and the lognormal. The goodness-of-fit was tested numerically with the Anderson-Darling statistic.

**Keywords:** Glass, fracture data

# Contents

## 1. Introduction

Glass in structures is commonly formed by monolithic, laminated, or insulated units of annealed, heat-strengthened or toughened float glass panes. According to the codes, e.g. DIN 18008-1:2010 and prEN 16612:2017, the strength design is based on the characteristic value of the fracture stress of a monolithic pane of annealed float glass. Hence, the distribution of strength in monolithic panes of annealed float glass is of paramount importance. In the open literature and up to date, there has been no comprehensive survey providing a detailed overview of the experimental results on the strength of monolithic panes of annealed float glass. This report was put together to provide such a detailed overview. The purpose is furthermore to enable an in-depth analysis of the most important statistics such as the characteristic value of the strength, the difference in strength between edge and surface failures, the goodness-of-fit for standard distributions, etc. The aim is moreover to enable a general assessment of phenomena such as static fatigue and the size effect. The investigation is restricted to new glass in the as-received condition that was tested in an ambient environment. The examined experiments were conducted with the following testing devices, viz. the coaxial double ring bending device, the three-point bending device, the four-point bending device, and the device that enables the application of uniform lateral pressure to plates that are continuously supported along all four edges. The empirical data was obtained from original articles, conference proceedings, reports, and dissertations from the following sources, viz. scientific publishers, societies, organizations, and universities. According to all accounts, great care was taken in the handling of the glass prior to testing and during mounting of the specimens into the respective testing rigs. The glass was always stored for some time before testing.

## 2. Environmental conditions

The ambient environment is somewhat represented by an indoor climate. The ambient temperature is about 20 ºC and the relative humidity ranges between 40-70%. However, due to regional as well as seasonal differences and variations, the ambient temperature and relative humidity in the examined experiments was sometimes found to deviate significantly from these values. For instance, during the tests carried out in Australia (Calderone 1999), the relative humidity once reached 99%. And while tests were conducted in Canada (Johar 1982), the measured temperature dropped to 16 ºC.

## 3. Bending test arrangements and strength calculations

The surveyed experiments were conducted using one of the following bending arrangements, viz. the three-point bending device, the four-point bending device, the coaxial double ring bending device, and the device that allows for four-sided laterally supported panes to be subjected to uniform lateral pressure. The bending strength was determined either using an analytical formula, with the use of the finite element method, or based on strain gauge measurements combined with some extrapolation method. Here follows a description of the analytical formulae used for calculating the ultimate stress at failure. The bending strength $\sigma_f$ is generally determined according to

$$\sigma_f = \frac{M}{W} \tag{1}$$

where $M$ is the maximum bending moment and $W$ is the section modulus of the specimen. For a rectangular cross-section

$$W = \frac{hb^2}{6} \tag{2}$$

where $b$ denotes the thickness and $h$ the width of the specimen. In the case of the three and four-point bending setup, the terms in-plane and out-of-plane bending, respectively, refer to the orientation of the specimen in the cross-sectional plane, i.e. whether the specimen is lying down or standing up on its edge. The difference is illustrated in Fig. 1.

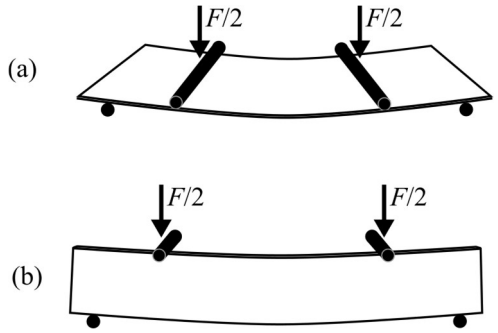


Fig. 1 (a) Out-of-plane (specimen lying down) and (b) in-plane (specimen standing on its edge) bending in a four-point setup.

*Three-point bending*

A schematic view of the three-point bending arrangement is given in Fig. 2. The largest bending moment is $Fl/4$ where $F$ is the fracture load and $l$ is the distance between the supports. With reference to Eqs. (1) and (2), the bending strength is found to be

$$\sigma_f = \frac{3}{2}\frac{Fl}{hb^2} \tag{3}$$

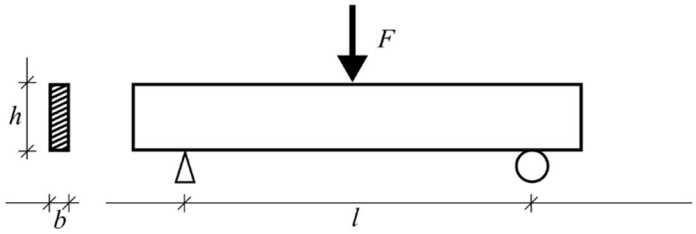


Fig. 2 The three-point bending arrangement.

*Four-point bending*

A schematic of the four-point bending arrangement is shown in Fig. 3. The bending strength is calculated with

$$\sigma_f = 3\frac{Fl_1}{hb^2} \tag{4}$$

where $l_1$ is the distance between the outer and inner supports. In the case of four-point bending tests, only the data was included that corresponds to fracture within the load span limits. In some experiments, the analytical formula, Eq. (4), was combined with finite element calculations in the calculation of the bending strength in the following way. When taking into account the stress concentration that occurs at the points where the load is introduced and supposing that fracture occurs under the loading points, the fracture stress increases by about 5%, see e.g. Vandebroek et al. (2014). As a matter of fact, it was not unusual for the fracture origin to be located at the load introduction points in four-point bending tests (Vandebroek et al. 2014).

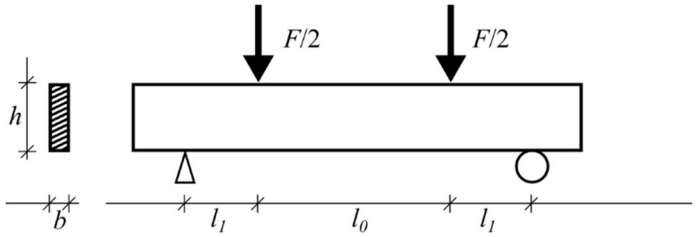

Fig. 3 The four-point bending arrangement.

*Coaxial double ring bending*

Fig. 4 shows a schematic of the double ring bending arrangement which uses two opposing coaxial rings of unequal diameters, one loading ring and one reaction ring. The test specimen is positioned between the rings and a load is transmitted through the smaller concentric loading ring. A uniform biaxial tensile stress is produced in the surface of the sample plate within the loading ring area. The stresses on the tensile surface of a specimen in coaxial double ring bending have radial and circumferential components and are given by a set of approximate analytical solutions (Kirstein and Woolley 1967). Geometrical nonlinearity is not accounted for by Eq. (*5*), (*7*), and (*8*). In the case of bending of thin plates, membrane stresses are activated and become significant when the deflection exceeds about half the plate thickness. The uniform biaxial stress within the loading ring area is

$$\sigma_r = \sigma_\theta = \frac{3F}{2\pi t^2}\left((1+\nu)\,ln\left(\frac{r_1}{r_0}\right) + (1-\nu)\frac{r_1^2-r_0^2}{2r_2^2}\right), r \le r_0 \tag{5}$$

where $\nu$ is Poisson's ratio, $r_0$ and $r_1$ are the radii of the inner and outer supports, respectively. $r_2$ is the equivalent outer radius used for a square shaped specimen with side length $2L$ and is given by

$$r_2 = L(1+\sqrt{2}) \tag{6}$$

The radial stress outside the loading ring area at the distance $r$ from the plate centre point is

$$\sigma_r = \frac{3F}{2\pi t^2}\left((1+\nu)\,ln\left(\frac{r_1}{r}\right) + (1-\nu)\frac{r_0^2(r_1^2-r^2)}{2r^2r_2^2}\right), r > r_0 \tag{7}$$

while the circumferential stress is

$$\sigma_\theta = \frac{3F}{2\pi t^2}\left((1+\nu)\,ln\left(\frac{r_1}{r}\right) - (1-\nu)\frac{r_0^2(r_1^2+r^2)}{2r^2r_2^2} + 2(1-\nu)\frac{r_1^2}{r_2^2}\right), r > r_0 \tag{8}$$

When the fracture occurred outside the loading ring area in coaxial double ring bending tests and provided that the fracture location was recorded, the test results were recalculated by this author with Eq. (7) to reflect the maximum principal tensile stress at the fracture location rather than the stress within the loading ring. This applies only in one case, viz. Simiu et al. (1984), and as a matter of fact, Simiu et al. (1984) used the analytical formula, Eq. (5), to calculate the fracture stress. Hence, our calculation method for the adjustment of the fracture stress harmonizes well with the original method.

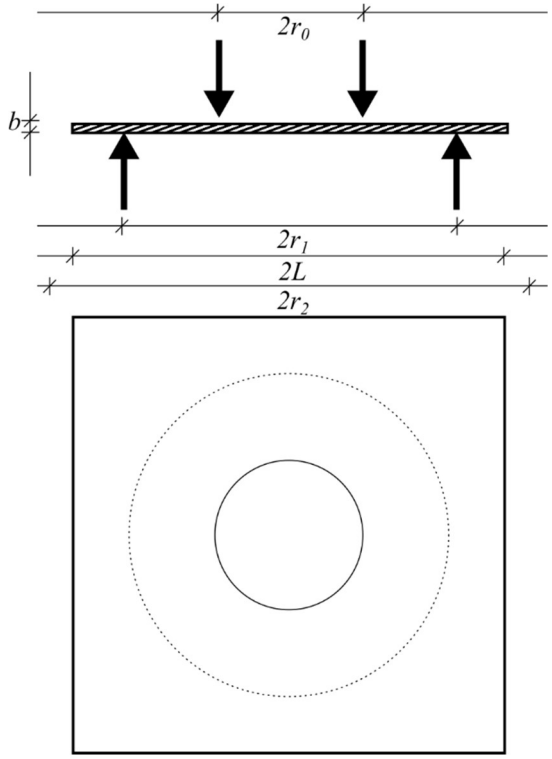


Fig. 4 The coaxial double ring bending arrangement.

*Uniform pressure applied to laterally supported plates*

In the case of laterally supported plates subjected to uniform pressure, analytical formulae based on plate equations were not used in any of the examined experiments. Instead, the fracture stress was determined with the finite element method or based on strain gauge measurements. Fig. 5 illustrates the general test arrangement. The boundary conditions in the experiments varied substantially. The rigidness in the supports varied depending on the gasket material in use and the clamping force applied along the edges as well as the stiffness of the surrounding frame.

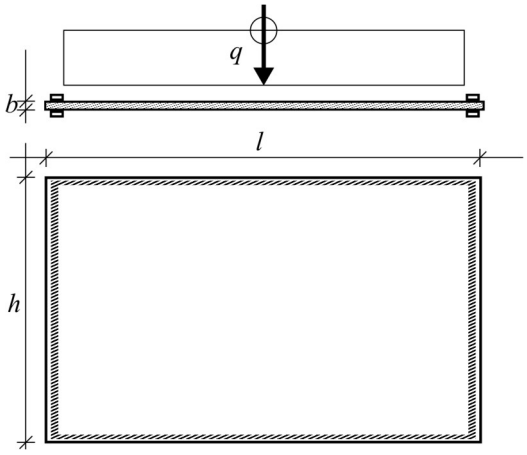


Fig. 5 The arrangement with a laterally supported plate subjected to uniform pressure.

## 4. Stochastic models

The following three probability distributions are considered as models for the fracture stress in glass, viz. the Weibull distribution, the normal distribution and the lognormal distribution. The

distribution parameters are estimated using the maximum likelihood method. It is supposed that the fracture stress, $x$, is an observation of some random variable $X$.

*Weibull distribution*
The Weibull distribution (Weibull 1939) has the cumulative distribution function

$$F(x) = 1 - exp\left(-\left(\frac{x}{k}\right)^m\right) \tag{9}$$

where $k$ and $m > 0$ denote the scale and shape parameters, respectively.

*Normal distribution*
The normal distribution has the probability density function (Forbes et al 2011)

$$f(x) = \frac{1}{\sqrt{2\pi\sigma^2}} exp\left(-\frac{(x-\mu)^2}{2\sigma^2}\right) \tag{10}$$

where $\mu$ and $\sigma^2$ are the mean and variance, respectively.

*Lognormal distribution*
The lognormal distribution is related to the normal distribution in the following way. If $Y$ denotes a normally distributed random variable, then $X = \exp(Y)$ is lognormally distributed with the probability density function (Forbes et al 2011)

$$f(x) = \frac{1}{x\sqrt{2\pi\sigma^2}} exp\left(-\frac{(log(x)-\mu)^2}{2\sigma^2}\right) \tag{11}$$

In Eq. (11), $\mu$ and $\sigma^2$ denote the mean and variance of the associated normal distribution, Eq. (10).

## 5. Adjusting for static fatigue

Following the theory of stress corrosion (Charles 1958a, 1958b) and the Load Duration Theory (Brown 1972), the nominal value of the strength can be associated with a 2 MPa $s^{-1}$ stress rate-equivalent strength providing that the stress history is known. In other words, the recorded value of the fracture stress is associated with an equivalent strength value that would have been, were the specimen subjected in an identical environment to a ramp stress until failure at a rate of 2 MPa $s^{-1}$. Supposing that the actual stress history was linear, i.e. $\dot{\sigma} = $ constant, the transformation is carried out using the following equation

$$\sigma_{f,eq} = \sigma_f \cdot \sqrt[n+1]{\frac{\dot{\sigma}_{eq}}{\dot{\sigma}}} \tag{12}$$

where $\sigma_{f,eq}$ is the 2 MPa $s^{-1}$ stress rate-equivalent strength, $\sigma_f$ is the nominal or received strength, $\dot{\sigma}_{eq}$ is 2 MPa $s^{-1}$, and $n$ is the static fatigue parameter. It is assumed that $n = 16$ (Mencik 1992). In the experiments considered in this report, the stress history at the fracture location was linear in nearly all cases. Typically, the experimenter recorded the calculated rate of stress or else recorded the rate of deflection. In the latter case when the four-point bending test rig was used, the stress rate was determined by this author using the following equation

$$\dot{\sigma} = \dot{u}\frac{3E}{l_1(3l_0+2l_1)} \tag{13}$$

where $\dot{u}$ is the rate of deformation, see also Fig. 3. The stress rate together with the fracture stress are used to adjust the value of strength for the effect of static fatigue. When Eq. (13) is

used, it is assumed that Young's modulus $E = 72$ GPa. With the 2 MPa $s^{-1}$ stress rate-equivalent strength, Eq. (12), it is possible in theory to benchmark various measurements of the strength when the glass material was exposed to different levels of static fatigue due to different rates of stress. The word nominal is used to denote the as-received strength value which has not been adjusted with respect to static fatigue.

## 6. Graphical description

The histogram, the empirical cumulative distribution function (ECDF), the boxplot, and the probability plot are frequently employed in descriptive statistics to depict a data set graphically. Graphical techniques are useful because of their ease and informality while providing for powerful analyses in conjunction with formal numerical techniques (D'Agostino and Stephens 1986).

*Histogram*

The histogram is a bar graph that reflects the probability distribution of a continuous random variable. The range of sample values is grouped into $m$ contiguous intervals, each interval having the length $m^{-1}$. The intervals are usually called bins. The number of observations falling into each bin is counted. A bar is constructed over each bin the height of which is proportional to the frequency (Sheshkin 2004). The bin width is selected to cover the data range and reveal the shape of the underlying distribution.

*Empirical distribution function*

The empirical cumulative distribution function (ECDF) is a step function that estimates the cumulative distribution function (CDF) that generated the observed data points. Suppose we have a random sample $X_1, \dots, X_n$ drawn from a distribution with CDF $F(x)$. The ECDF is constructed by plotting $i/n$ on the $y$-axis against the $i$th ordered value of the sample, i.e. $X_{(i)}$, on the x-axis (Forbes et al 2011). The ECDF $\hat{F}_n(x)$ is defined as (Wasserman 2006)

$$\hat{F}_n(x) = \frac{1}{n}\sum_{i=1}^{n} I(X_i \leq x) \tag{14}$$

where $I$ is the indicator function defined by

$$I(X_i \leq x) = \begin{cases} 1 \; if \; X_i \leq x \\ 0 \; if \; X_i > x \end{cases} \tag{15}$$

*Boxplot*

The boxplot provides a visual summary of batches of data through their quartiles (McGill et al. 1978). The central mark on each box represents the second quartile, i.e. the median, while the bottom and top edges of the box represent the first and third quartiles, i.e. the 25$^{th}$ and 75$^{th}$ percentiles. The whiskers extend to 1.5 times the Interquartile Range (IQR) which is the distance between the first and third quartiles. Hence, the whiskers indicate variability outside the upper and lower quartiles. Data points that are located beyond the ends of the whiskers are indicated by a plus sign. Variability of the median value between samples is indicated by triangular markers. If the interval between the triangles in a boxplot does not overlap with the interval from another boxplot, then the samples have different medians at the 5% significance level, assuming normally distributed data. In fact, comparisons of medians are reasonably robust even for other distributions than the normal (Mathworks 2018). The interval endpoint lies at the centre of the triangle marker. The endpoints are calculated from

$$q_2 \pm \frac{1.57(q_3 - q_1)}{\sqrt{n}} \tag{16}$$

where $q_2$ is the second quartile, i.e. the median, and $q_1$ and $q_3$ are the first and third quartiles, respectively. $n$ is the number of observations in the sample. The boxplot is useful for depicting a range of statistics, including the IQR, the range, the mid-range, the skewness, etc.

*Probability plot*

The classic form of the probability plot assumes a parameter model that can be written as

$$F(x) = F_0\left(\frac{x-a}{b}\right) \tag{17}$$

where $b > 0$ is a scale parameter, and $-\infty < a < \infty$ is a location parameter. Suppose $x_{(1)} < x_{(2)} < \cdots < x_{(n)}$ are the order statistics in a random sample of size $n$ from the distribution of $X$. In the probability plot, the $x_{(i)}$ are plotted against $F_0^{-1}(u_i)$ where $u_i$ are termed the plotting positions. The most common choice of plotting position is (Lawless 2003, Mathworks 2018)

$$u_i = \frac{\left(i-\frac{1}{2}\right)}{n} \tag{18}$$

The plot of the points $\left(x_{(i)}, F_0^{-1}(u_i)\right)$ should be approximately linear if the choice of model is reasonable. In the probability plot, the scale of the $y$-axis is based on the values of $F_0^{-1}(u)$. A reference line that goes through the first and third quartiles is superimposed (Mathworks 2018). In the case of the Weibull distribution, Eq. (9), the distribution function can be rewritten to conform with the location-scale parameter model, Eq. (17). From Eq. (9) we deduce that

$$ln\big(1 - F(x)\big) = -\left(\frac{x}{k}\right)^m \tag{19}$$

from which it follows that

$$ln\big(-ln\big(1 - F(x)\big)\big) = m\,ln(x) - m\,ln(k) \tag{20}$$

Hence, in a Weibull probability plot, the $x$-axis scaling is logarithmic and the $y$-axis scaling is such that it maps the function $y = \ln(-ln(1-u))$. In the lognormal probability plot, the $x$-axis scaling is also logarithmic. With the normal distribution, the $x$-axis scaling is linear.

## 7. Goodness-of-fit

The experimental data was compared with standard distributions and the goodness-of-fit was evaluated in a formal numerical test using the Anderson-Darling statistic. Suppose the sample $x_1, x_2, \ldots, x_n$ contains $n$ observations of a set of independent and identically distributed random variables $X$. The general test of fit is a test of the null hypothesis

$$H_0\text{: a random sample of } n \text{ observations of } X \text{ comes from } F\left(x; \vec{\theta}\right) \tag{21}$$

where $\vec{\theta}$ is a vector of parameters associated with the continuous distribution F. An empirical distribution function statistic measures the vertical difference between $\hat{F}_n(x)$ and $F(x)$. The quadratic class of EDF statistics is based on the class of measures with the following functional form (D'Agostino and Stephens 1986)

$$Q = n\int_{-\infty}^{\infty}\left(\hat{F}_n(x) - F(x)\right)^2 \psi(x)dF(x) \tag{22}$$

where $\psi(x)$ is a weighting function. The Anderson-Darling (1952) statistic is obtained by choosing

$$\psi(x) = \frac{1}{F(x)(1-F(x))} \tag{23}$$

## 8. Supplementary data

In a few cases, viz. Veer et al. (2006), Muniz-Calvente et al. (2016), Navarrete et al. (2016) and Osnes and Börvik (2018), supplementary information about the experiment was obtained through private correspondence with the respective author. The displacement rate that was used in the in-plane four-point bending tests as reported by Veer et al. (2006) was 1 mm $s^{-1}$. The fracture origin mode, i.e. edge or surface, in the out-of-plane four-point bending tests were recorded but not published by Muniz-Calvente et al. (2016). The loading ring and support ring diameters in the double ring bending tests conducted by Navarrete et al. (2016) was 51 mm and 127 mm, respectively. The data on the edge failures in the out-of-plane four-point bending tests in the experiment conducted by Osnes et al. (2018) was recorded but not published.

## 9. General overview

Tab. 1 contains a list of the experiments included in the survey. Also indicated in Tab. 1 are the total number of test specimens per experiment, the type of test device, the type of stress history at the fracture origin, and the edge condition of the glass as reported by the respective author.

Table 1: Summary of surveyed experiments. 4PB=Four-point bending, 3PB=Three-point bending, CDR=Coaxial double ring, ULP=Uniform lateral pressure, C=As-cut, A=Arrised, G=Ground, P=Polished, W=Water-jet cut.

| Reference | No. of spec's | Testing device | Stress history | Edge proc. |
|---|---|---|---|---|
| Johar (1981) | 78 | ULP | Nonlinear | Not recorded |
| Johar (1982) | 106 | ULP | Nonlinear | Not recorded |
| Simiu et al. (1984) | 85 | CDR | Linear | Not recorded |
| Kanabolo and Norville (1985) | 206 | ULP | Nonlinear | Not recorded |
| Carre (1996) | 81 | 4PB | Linear | P |
| Calderone (1999) | 195 | ULP | Nonlinear | Not recorded |
| Hess (2000) | 15 | 4PB | Nonlinear | G |
| Fink (2000) | 127 | CDR | Linear | Not recorded |
| Overend (2002) | 30 | CDR | Linear | Not recorded |
| Haldimann (2006) | 20 | CDR | Linear | Not recorded |
| Veer et al. (2006) | 32 | 4PB | Linear | G |
| Sglavo (2007) | 115 | 3PB | Linear | CAGP |
| Veer et al. (2009) | 54 | 4PB | Linear | P |
| Veer and Rodichev (2011) | 177 | 4PB | Linear | C |
| Consuelo-Huerta et al. (2011) | 66 | CDR, 4PB | Linear | Not recorded |
| Veer and Rodichev (2012) | 60 | 4PB | Linear | W |
| Vandebroek et al. (2012) | 77 | 4PB | Linear | CP |
| Lindqvist (2013) | 478 | 4PB | Linear | CAGPW |
| Vandebroek et al. (2014) | 202 | 4PB | Linear | CG |
| Kozlowski (2014) | 6 | 4PB | Linear | P |
| Kleuderlein et al. (2014) | 830 | 4PB | Linear | CAG |
| Schula (2015) | 15 | CDR | Linear | Not recorded |
| Kinsella and Persson (2016) | 58 | 4PB | Linear | P |
| Muniz-Calvente et al. (2016) | 73 | CDR, 4PB | Linear | P |
| Navarrete et al. (2016) | 69 | CDR | Linear | C |
| Yankelevsky et al. (2017) | 56 | 4PB | Linear | C |
| Osnes et al. (2018) | 93 | 4PB | Linear | C |
| Sum: | 3404 | | | |

## 10. Experiments

Here follows a detailed summary of the experiments in the survey. The summary contains a description of the testing device employed with information about the specimen geometry and edge condition. The fracture stress data is represented graphically in the form of boxplots. Triangular markers indicate the inter-sample variation of the median only when the average sample sizes were large enough, i.e. usually greater than 7. The sample data is also visualized in the form of probability plots for the Weibull, normal, and lognormal distributions, but only when the sample size was deemed sufficiently large. Edge failures in the data are marked with a crossed circle in the probability plots. All other types of failure, i.e. surface failure or failures that were ambiguous with respect to the origin, are marked with an empty circle. When applicable, the stress rate-equivalent data is also depicted.

*Johar (1981)*

The experiment was conducted using a setup that enabled a monotonically increasing uniform lateral pressure to be applied to laterally supported plates. The glass panels were mounted vertically between continuous 12.7 mm wide neoprene gaskets in the front face of the testing rig. The front face was hinged and could be opened like a door to reveal the test chamber. Inside the chamber a negative pressure was produced. The specified loading rate was achieved by controlling the rate of movement of a hydraulically driven piston. Three different pressure rates were employed, viz. 0.15 kPa $s^{-1}$, 1.5 kPa $s^{-1}$, and 15 kPa $s^{-1}$. The panels were supported on two 150 mm long neoprene setting blocks at the quarter points of the bottom edge. The outside surface, i.e. the compression side, was taped with polypropylene tape. A distributed clamping force of 1 kN $m^{-1}$ was applied along the four edges. The lateral support was continuous along the entire perimeter. The glass plates were cut out from panes with the nominal thickness 6 mm. The mean thickness was found to be 5.8 mm. The glass was obtained from three different manufacturers denoted by M1, M2, and M3. It was not specified if the glass edges were processed in any way. Presumably, the edge condition was as-cut. The tin side was always placed in the tension side. During the experiments, the temperature was maintained at 20-25 ºC and the relative humidity was 28-55%. The length of load-duration ranged from 0.2 to 53 seconds. Nondestructive tests were carried out on a strain-gauged and tempered glass panel having 41 strain gauges bound to its surface. The fracture stress, i.e. the maximum principal tensile stress at the fracture origin, was determined based on the nondestructive tests. However, the calculation method used was not detailed in the report. Dalgliesh and Taylor (1990) discuss the Ontario Research Foundation test results and indicate that a power law relation was fitted in order to interpolate the stresses, $\sigma$, for pressures, $P$, up to failure using the following equation

$$\sigma = KP^{\beta} \tag{24}$$

where $K$ is a constant and $\beta$ varies with the failure location. In most cases, $\beta$ was in the range 0.85-0.95. In fact, $\beta$ is also a function of aspect ratio and thickness. A summary of details on the experiment is given in Tab. 2. In Fig. 6, a set of boxplots depict the fracture stress characteristics for the nominal strength data. Fig. 7 shows the recorded fracture origins. NB., in some cases, there was an ambiguity as to the specific fracture origin due to the existence of multiple potential fracture sites, including, in a few cases, a mixture of potential surface and edge failures. Fig. 7 shows the primary choice of origins according to the reference in the case when the fracture origin could be uniquely determined as being either an edge failure or a surface failure.

Table 2: Details on the experiment as reported by Johar (1981). L=Low, M=Medium, H=High loading rate, ULP=Uniform lateral pressure.

| Sample ID | No. of spec's | No. of unamb. edge fail's | No. of unamb. surf. fail's | Bending mode | Dimensions ($mm^3$) | Pressure rate (kPa $s^{-1}$) |
|---|---|---|---|---|---|---|
| L-M1 | 9 | 3 | 5 | ULP | 6x1525x2440 | 0.15 |
| L-M2 | 9 | 4 | 5 | ULP | 6x1525x2440 | 0.15 |
| L-M3 | 10 | 1 | 9 | ULP | 6x1525x2440 | 0.15 |
| M-M1 | 8 | 0 | 8 | ULP | 6x1525x2440 | 1.5 |
| M-M2 | 7 | 4 | 2 | ULP | 6x1525x2440 | 1.5 |
| M-M3 | 9 | 1 | 8 | ULP | 6x1525x2440 | 1.5 |
| H-M1 | 9 | 1 | 6 | ULP | 6x1525x2440 | 15 |
| H-M2 | 9 | 2 | 6 | ULP | 6x1525x2440 | 15 |
| H-M3 | 8 | 0 | 7 | ULP | 6x1525x2440 | 15 |

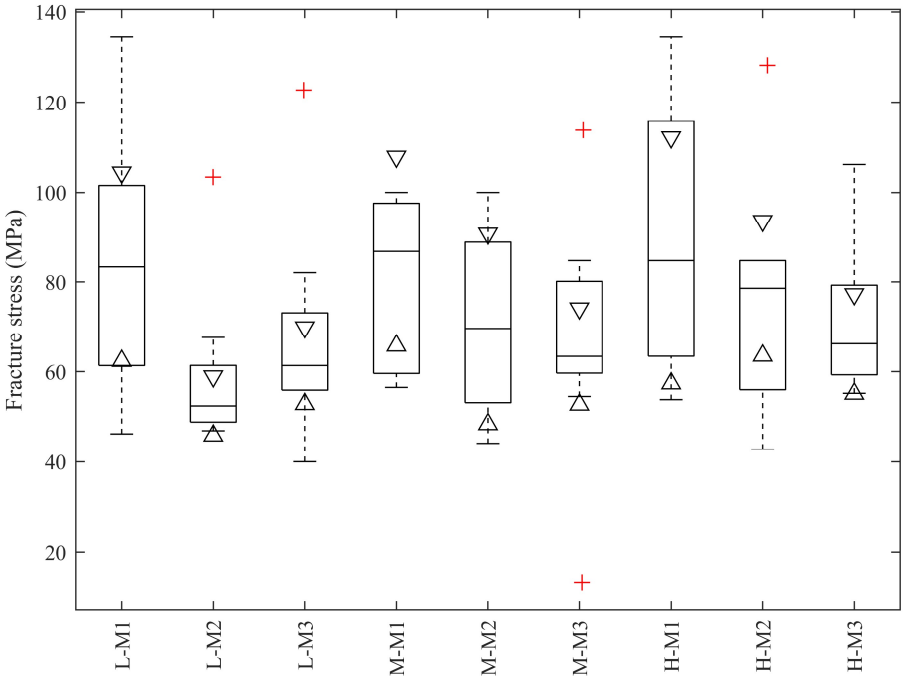


Fig. 6 Boxplots of the strength according to Johar (1981).

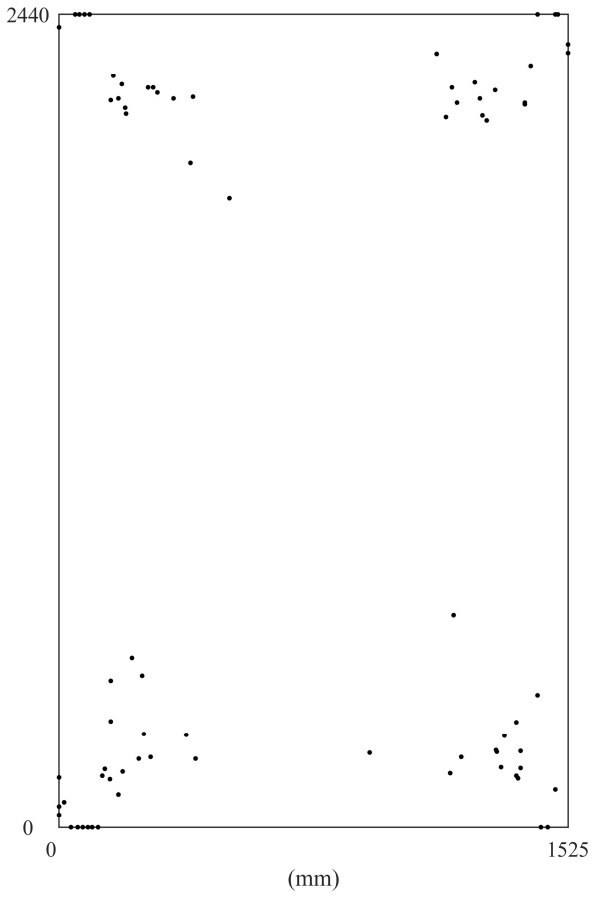


Fig. 7 Fracture locations according to Johar (1981).

*Johar (1982)*

The experiment was conducted with the same test rig and specimen geometry as in Johar (1981). In the following, the main differences are mentioned. The glass was obtained from one manufacturer only. During the experiments, the temperature was maintained at 16-24 ºC and the relative humidity was 26-57%. A summary of details on the experiment is given in Tab. 3. In Fig. 8, a set of boxplots depict the fracture stress characteristics for the nominal strength data divided into the following categories, viz. 1) all failures irrespective of failure mode, i.e. surface or edge origin, 2) only edge failures that were unambiguously identified as such, and 3) only surface failures that were unambiguously identified as such. A set of three probability plots for each sample is shown in Fig. 10 including the respective maximum-likelihood parameter estimates and the Anderson-Darling goodness-of-fit statistic. Fig. 9 shows the recorded fracture origins.

Table 3: Details on the experiment as reported by Johar (1982).

| Sample ID | No. of spec's | No. of unamb. edge fail's | No. of unamb. surf. fail's | Bending mode | Dimensions ($mm^3$) | Pressure rate ($kPa\ s^{-1}$) |
|---|---|---|---|---|---|---|
| 1 | 21 | 4 | 15 | ULP | 6x1525x2440 | 0.0025 |
| 2 | 21 | 7 | 13 | ULP | 6x1525x2440 | 0.025 |
| 3 | 22 | 5 | 16 | ULP | 6x1525x2440 | 0.25 |
| 4 | 23 | 5 | 18 | ULP | 6x1525x2440 | 2.5 |
| 5 | 19 | 2 | 13 | ULP | 6x1525x2440 | 25 |

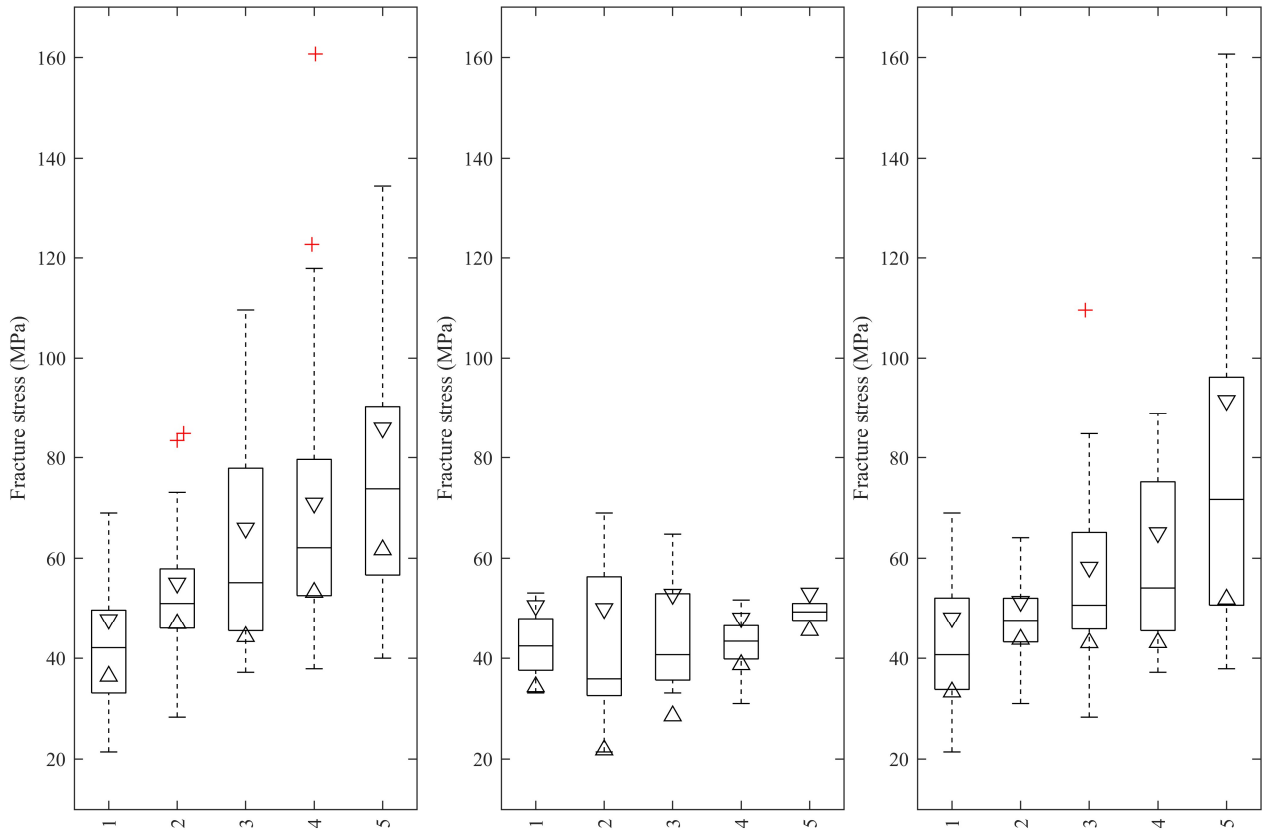


Fig. 8 Boxplots of the strength according to Johar (1982). Left: both edge and surface failures. Middle: only edge failures that were unambiguously identified as such. Right: only surface failures that were unambiguously identified as such.

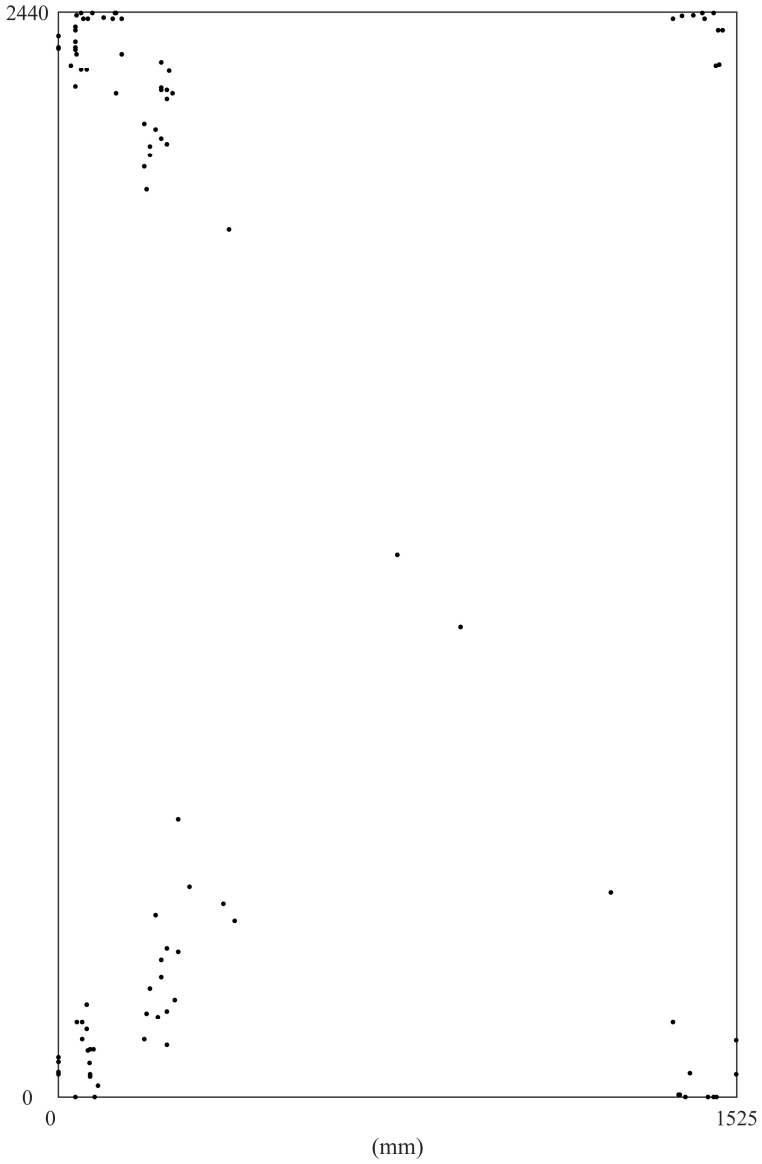


Fig. 9 Fracture locations according to Johar (1982).

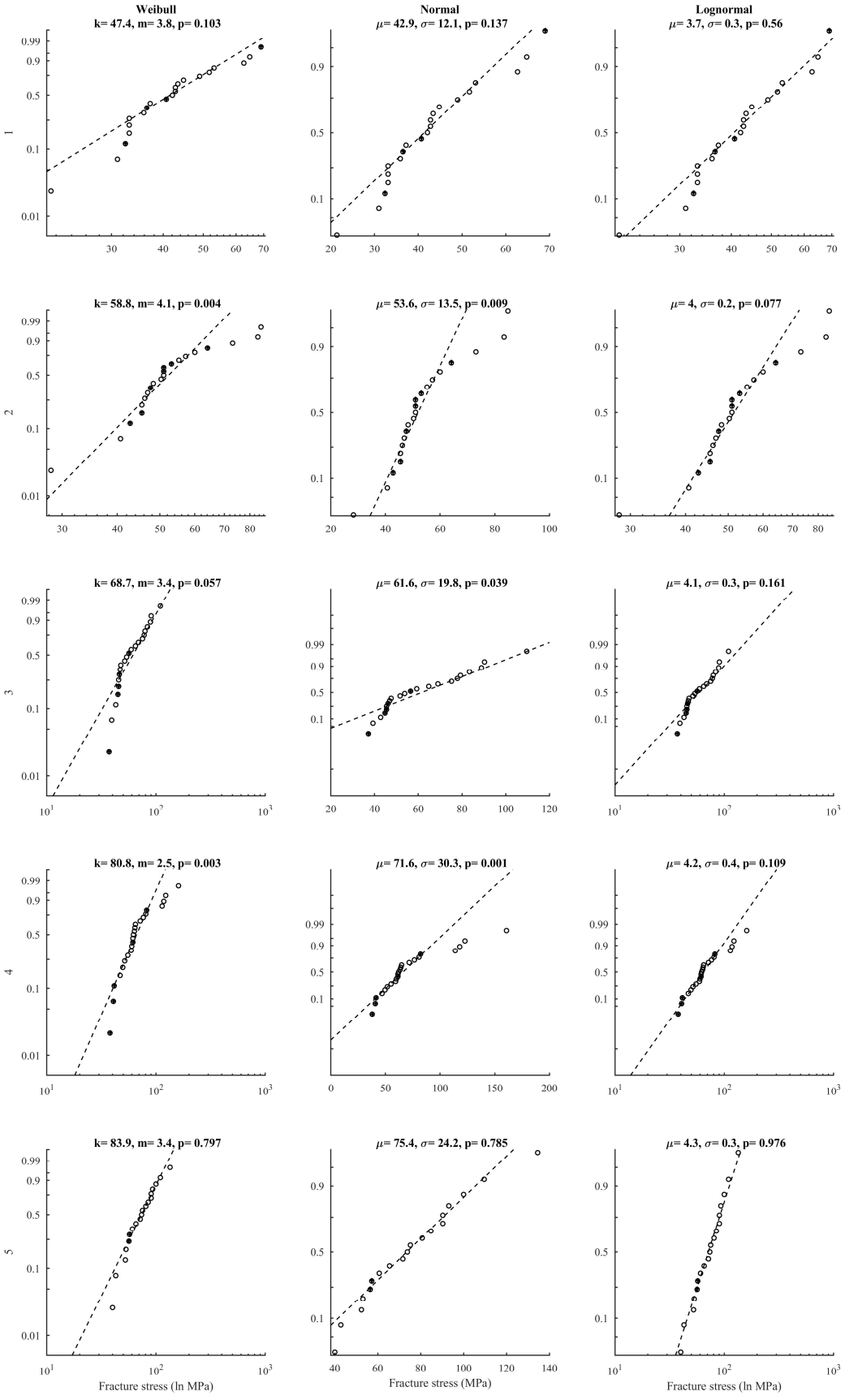


Fig. 10 Probality plots for the data samples in Johar (1982). Edge failures are marked with a crossed circle.

*Simiu et al. (1984)*

The experiment was conducted with a coaxial double ring bending device in combination with a Universal Testing Machine. The loading ring diameter was 51 mm and the support ring diameter was 121 mm. The support ring consisted of a segmented circular ring. The loading ring consisted of a closely wound coil. The load was transmitted to the coil by a rubber diaphragm covering a circular groove filled with water, the purpose of which was to equalize the loading along the coils. Two types of plate geometries were employed corresponding to two samples. In data sample 1, the plates were square specimens. In sample 2, the plates were circular discs. All specimens were cut out from panes with the nominal thickness 6 mm and the glass was obtained from the same manufacturer and batch. The overall mean thickness of the plates was found to be 5.44 mm. The square plate dimensions were 179x179 $mm^2$. The round plates measured 178 mm in diameter. The applied loading produced a linear stress rate with the average values 0.8 MPa $s^{-1}$ and 1.1 MPa $s^{-1}$, respectively. The load-duration until failure ranged from 31 sec to 1 min and 57 sec. It was not recorded which of the tin versus air side of the glass that was placed in the tension zone. The fracture stress was calculated using Eqs. (*5*) and (*6*). During the experiments, the temperature was maintained at room temperature and the relative humidity was 60-74%. A summary of details on the experiment is given in Tab. 4. In Fig. 11, a set of boxplots depict the fracture stress characteristics for the nominal and stress rate-equivalent strength data. A set of three probability plots for each sample is shown in Fig. 12 including the respective maximum-likelihood parameter estimates and the Anderson-Darling goodness-of-fit statistic. Fig. 13 illustrates the recorded failure origins in the radial direction from the centre point of the plate.

Table 4: Details from the experiment of Simiu et al. (1984).

| Sample ID | No. of spec's | Bending mode | Dimensions ($mm^3/mm^2$) | Load. ring diameter (mm) | Stress rate (MPa $s^{-1}$) |
|---|---|---|---|---|---|
| Square | 56 | CDR | 6x179x179 | 51 | 0.8 |
| Circular | 29 | CDR | 6x178 | 51 | 1.1 |

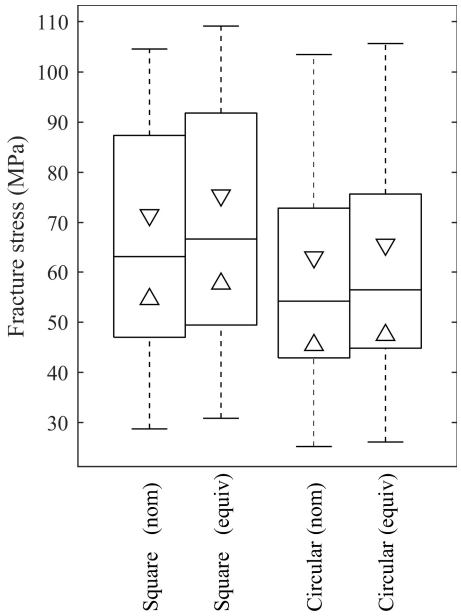


Fig. 11 Boxplots of the nominal fracture stress values and the stress rate-equivalent values for the data samples in Simiu et al. (1984).

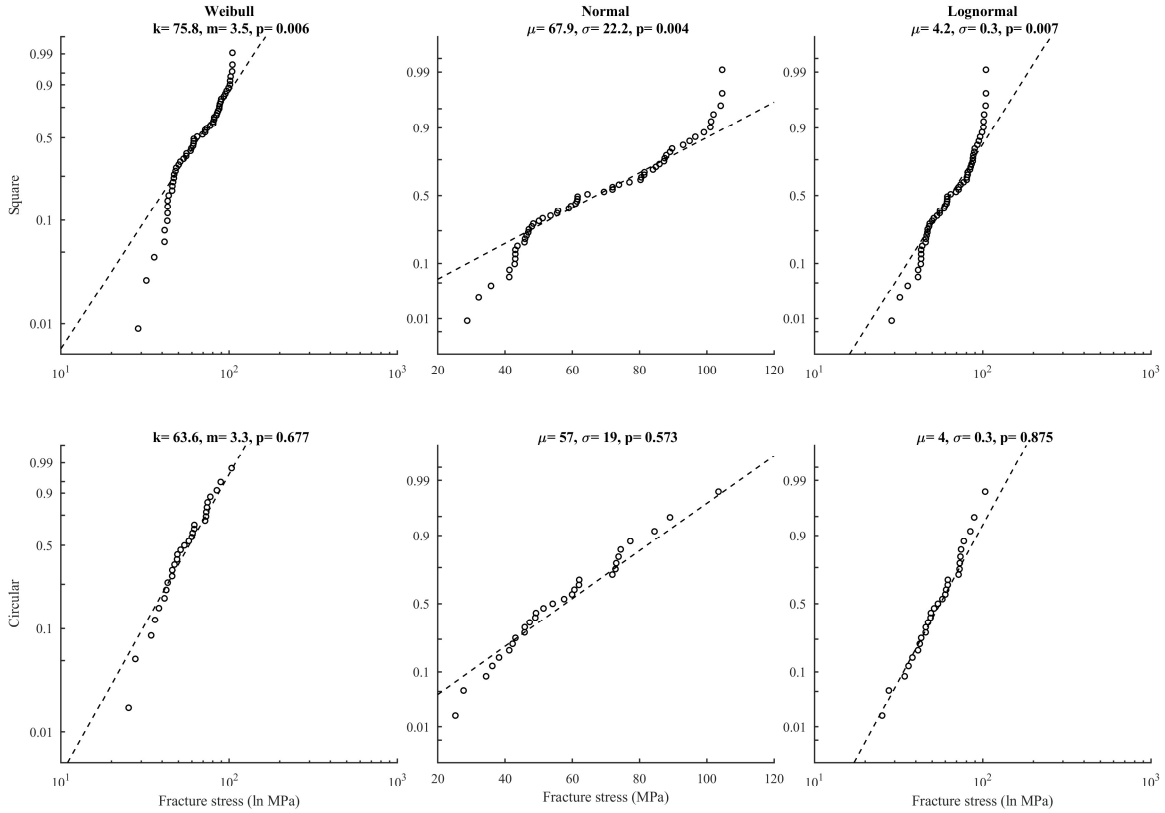


Fig. 12 Probability plots for each data sample in Simiu et al. (1984).

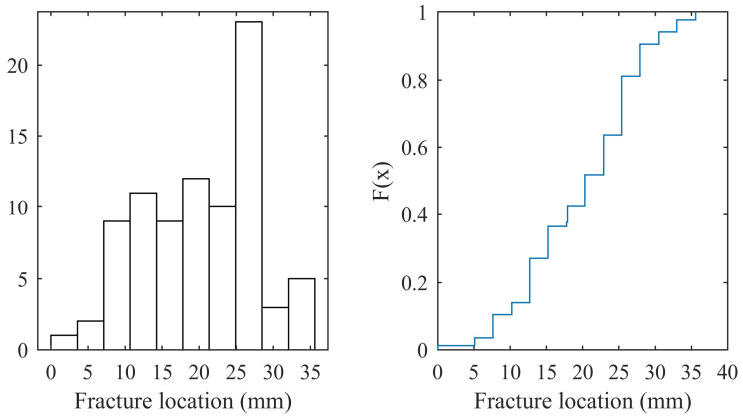


Fig. 13 Fracture locations in the radial direction from the centre point of the plate specimen, according to Simiu et al. (1984). Histogram (left) and empirical distribution function (right). NB., loading ring radius was 25.4 mm.

*Kanabolo and Norville (1985)*

The experiment was conducted using a setup that enabled a monotonically increasing uniform lateral pressure to be applied to laterally supported plates. The test rig consisted of a plywood deck to which a base structure of steel channels was mounted. Neoprene strips were set onto the base structure. The test specimens were mounted on the base structure and clamped between two neoprene gaskets to form an air-tight chamber. The testing procedure provided boundary conditions similar in concept to those in actual window installations. With a vacuum accumulator a negative pressure was applied to the glass surface in the test chamber. The compression surface, i.e. the surface outside the test chamber, of the specimens was taped to enable an identification of the fracture origin. The tin side of the glass was always placed in the tension side. It was not specified if the edges were processed in any way. Presumably, the edge condition was as-cut. The specimens were cut out from panes with the nominal thickness 6 mm. The overall mean thickness was 5.8 mm. The panes were obtained from two different manufacturers. A set of seven different plate dimensions were used. The various plate dimensions are detailed in Tab. 5 which also includes a summary of details on the experiment. The load-duration until failure ranged from about 0.5 sec to almost 25 min. The fracture stress was not calculated. However, Natividad (2014) calculated the MPTS at the fracture locations based on the 60 second-equivalent failure loads. Fig. 14 depicts the recorded fracture locations.

Table 5: Details on the experiment as reported by Kanabolo and Norville (1985).

| Sample ID | No. of spec's | No. of edge fail's | Bending mode | Dimensions (mm$^3$) | Pressure rate (kPa s$^{-1}$) |
|---|---|---|---|---|---|
| w-1 – w-24 | 20 | 3 | ULP | 6x965x1930 | 60.2 |
| w-25 – w-48 | 18 | 6 | ULP | 6x 965x1930 | 17.7 |
| w-49 – w-70 | 15 | 7 | ULP | 6x 965x1930 | 1.9 |
| SS | 19 | 2 | ULP | 6x 838x1676 | 87.7 |
| SL | 16 | 8 | ULP | 6x 1118x2362 | 33.6 |
| Z | 19 | 5 | ULP | 6x 1372x1372 | 50.1 |
| SQ | 18 | 6 | ULP | 6x 1181x1181 | 87.7 |
| V | 12 | 8 | ULP | 6x 1930x1930 | 37.6 |
| H | 15 | 9 | ULP | 6x 1524x2438 | 35.1 |

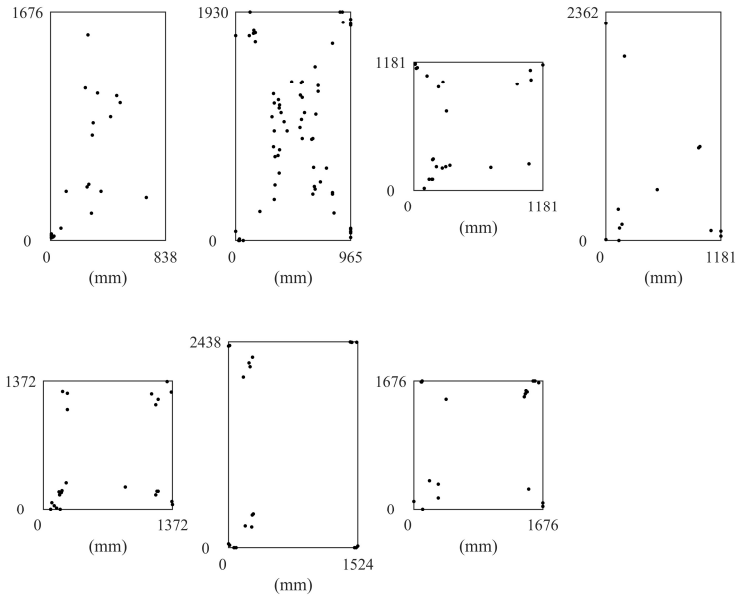


Fig. 14 Fracture locations according to Kanabolo and Norville (1985).

*SURVEY OF EXPERIMENTAL DATA ON THE STRENGTH OF ANNEALED FLOAT GLASS*

*Carre (1996)*

The experiment was conducted with the four-point bending arrangement. The load span dimension was 125 mm. The specimens were cut out from glass panes with the thickness 19 mm. Two different specimen dimensions were employed, viz. 37.5x250 $mm^2$ and 300x2000 $mm^2$. Moreover, two different edge polishing machines were utilized corresponding to the sample ID's A and B, respectively. The beams were subjected to in-plane loading generating an approximate stress rate of 0.05 MPa $s^{-1}$, 0.5 MPa $s^{-1}$, and 5.0 MPa $s^{-1}$, respectively. Failures that occurred outside the load span or outside the polished edge (i.e. on the surface) were excluded from the data. During the experiment, the temperature ranged between 15-20 ºC while the relative humidity was 40-70%. The length of load-duration ranged from about 9 sec to over 20 min according to calculations. A summary of details on the experiment is given in Tab. 6. In Fig. 15, a set of boxplots depict the fracture stress characteristics for the nominal and stress rate-equivalent strength data. A set of three probability plots for the samples is shown in Fig. 16 including the respective maximum-likelihood parameter estimates and the Anderson-Darling goodness-of-fit statistic. The last sample was not included in the probability plot due to its limited size. The data results were extracted from the digitized graphs by this author.

Table 6: Details on the experiment as reported by Carre (1996). L=Low, M=Medium, H=High stress rate, 4PB=Four-point bending, IP=In-plane.

| Sample ID | No. of spec's | Bending mode | Dimensions ($mm^3$) | Edge proc. | Load. span (mm) | Stress rate (MPa $s^{-1}$) |
|---|---|---|---|---|---|---|
| M-A | 28 | 4PB IP | 19x37.5x250 | Polished | 125 | 0.5 |
| L-A | 14 | 4PB IP | 19x37.5x250 | Polished | 125 | 0.05 |
| H-B | 9 | 4PB IP | 19x37.5x250 | Polished | 125 | 5.0 |
| M-B | 15 | 4PB IP | 19x37.5x250 | Polished | 125 | 0.5 |
| L-B | 12 | 4PB IP | 19x37.5x250 | Polished | 125 | 0.05 |
| L | 3 | 4PB IP | 19x300x2000 | Polished | 667 | 0.05 |

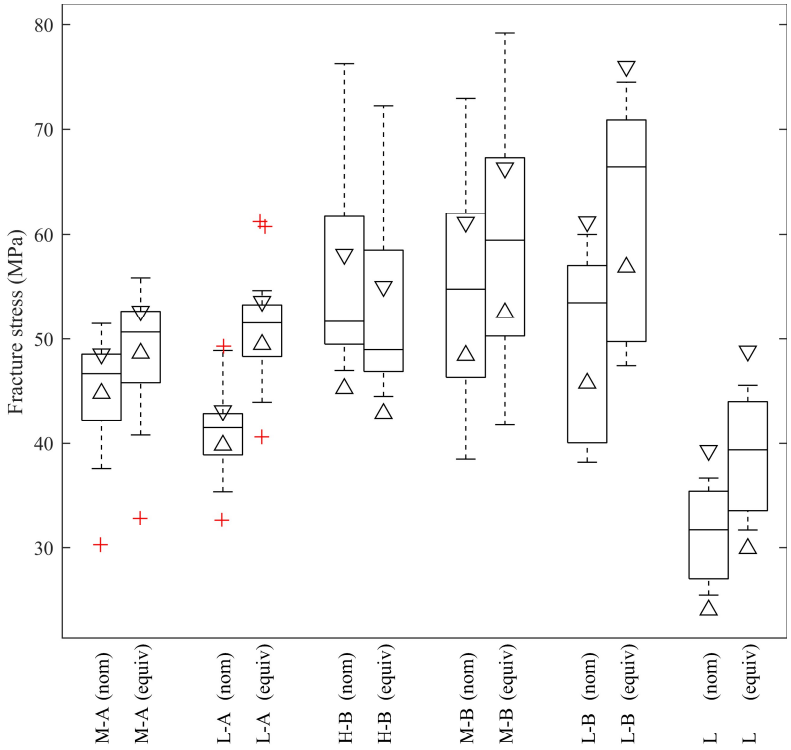


Fig. 15 Boxplots for the nominal fracture stress and the stress rate-equivalent strength according to Carre (1996).

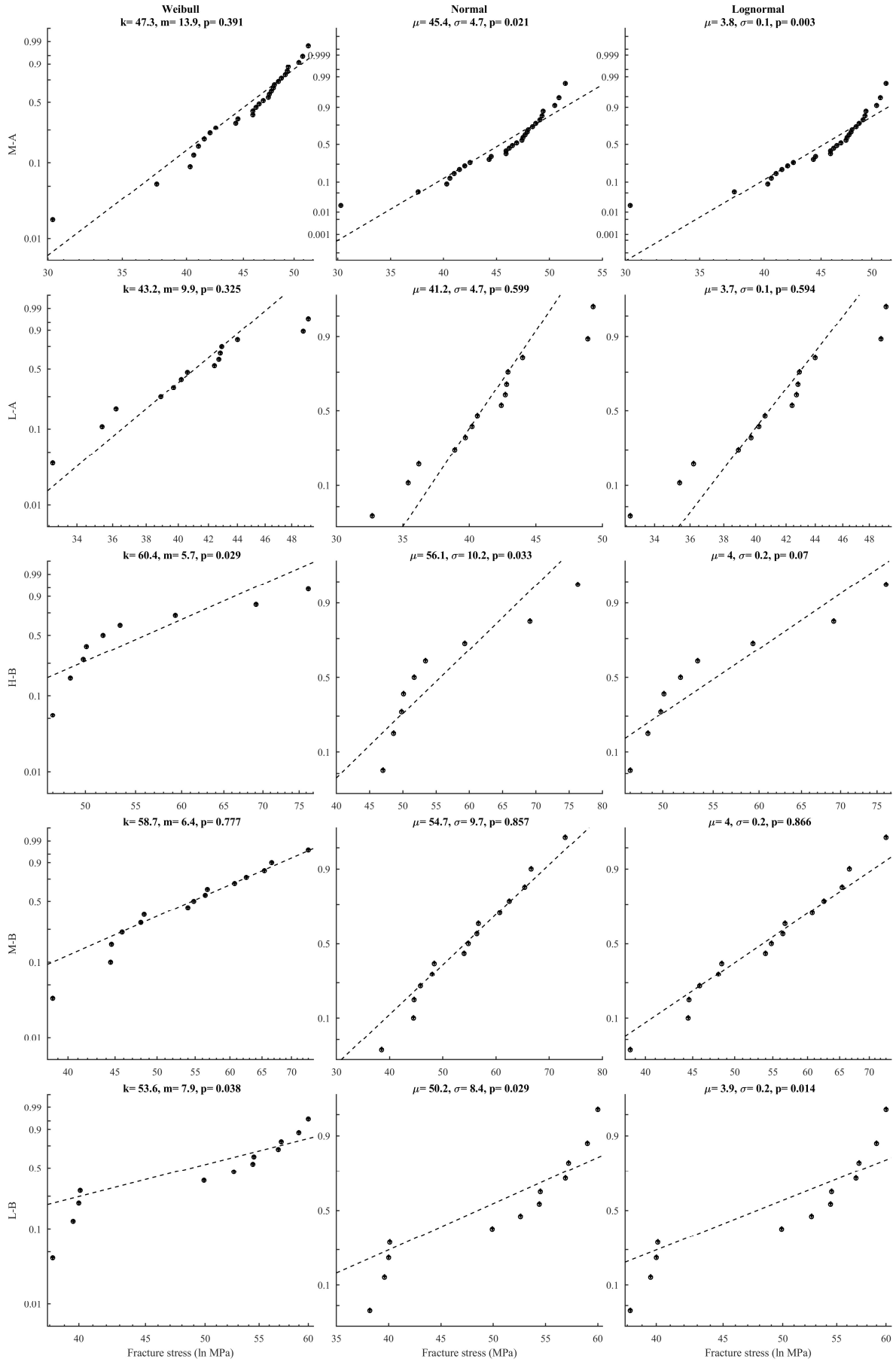


Fig. 16 Probability plots for the data sets according to Carre (1996).

*Calderone (1999)*

The experiment was conducted using a setup that enabled a uniform lateral pressure to be applied to laterally supported plates. The glass panes were mounted with their plane horizontally in the test rig. Water was used for applying the load to the glass. The test rig had the form of a horizontal table on legs. The tabletop was formed from a flat steel plate. A supporting structure was used below the table. A base frame was constructed above the tabletop and bolted to the structure below. The tabletop and the base frame formed the water reservoir. Hence, the loading was applied to the bottom surface of the glass. The specimens were mounted on continuous 20 mm thick nylon blocks which were set on the base frame. The blocks had a groove at the edge forming a support rebate. An upper frame was constructed above the base frame and bolted to it. The upper frame provided support for the glass edges from the top between a set of continuous 20 mm thick nylon in-fills. The flow of inlet and outlet water was controlled using butterfly valves. The water was supplied from a large tank which was six meters high. The water was retained within the test rig without leakage upon fracture using a soft plastic bag. The stresses at the observed fracture origins were calculated with FE software while assuming that the glass edges were restrained so that they remained in plane. However, no measurements were made on any plates using strain gauges. The specimens were cut out from panes with the nominal thickness 6 mm. The overall mean thickness was measured to be 5.9 mm. Eight different specimen dimensions were employed providing a range of different aspect ratios. The loading was applied in four different ways producing either a slow ramp pressure, a medium ramp pressure, a fast ramp pressure, or a cyclic loading. The tin surface of the glass was always placed in the tension zone, i.e. upwards. During the experiments, the temperature ranged between 12-31 ºC and the relative humidity was 39-99%. The length of load-duration ranged from 48 sec to over 23 min. A summary of details on the experiment is given in Tab. 7. In Fig. 17, a set of boxplots depict the fracture stress characteristics for the nominal strength data. Fig. 18 shows the recorded fracture origins. NB. in some cases there was an ambiguity as to the specific fracture origin due to the existence of multiple potential fracture sites. Fig. 18 shows the primary choice of origins according to Calderone (1999).

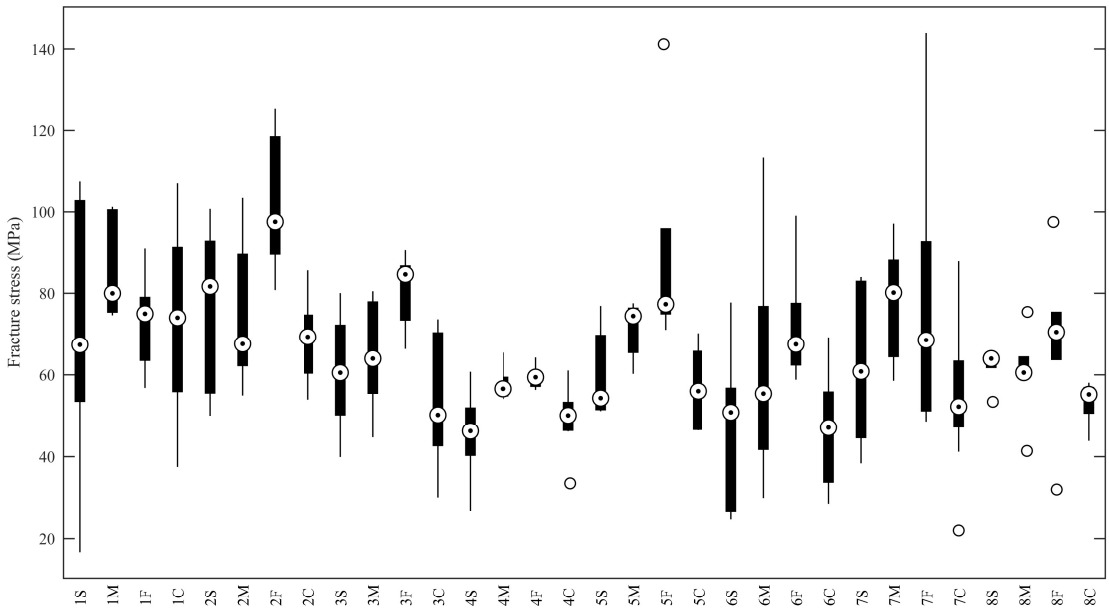


Fig. 17 Boxplots of the fracture stress according to Calderone (1999).

Table 7: Details on the experiment reported by Calderone (1999). S=Slow, M=Medium, F=Fast, C=Cyclic loading, ULP=Uniform Lateral Pressure.

| Sample ID | No. of spec's | No. of unamb. edge fail's | No. of unamb. surf. fail's | Bending mode | Dimensions ($mm^3$) | Edge proc. | Pressure rate ($kPa\ s^{-1}$) |
|---|---|---|---|---|---|---|---|
| 1S | 6 | 1 | 5 | ULP | 6x400x2000 | Unknown | Slow ramp |
| 1M | 5 | 0 | 5 | ULP | 6x400x2000 | Unknown | Med. ramp |
| 1F | 5 | 0 | 5 | ULP | 6x400x2000 | Unknown | Fast ramp |
| 1C | 9 | 0 | 9 | ULP | 6x400x2000 | Unknown | Cyclic loading |
| 2S | 6 | 0 | 6 | ULP | 6x500x2000 | Unknown | Slow ramp |
| 2M | 7 | 0 | 7 | ULP | 6x500x2000 | Unknown | Med. ramp |
| 2F | 5 | 0 | 5 | ULP | 6x500x2000 | Unknown | Fast ramp |
| 2C | 7 | 0 | 7 | ULP | 6x500x2000 | Unknown | Cyclic loading |
| 3S | 5 | 0 | 5 | ULP | 6x670x2000 | Unknown | Slow ramp |
| 3M | 5 | 0 | 5 | ULP | 6x670x2000 | Unknown | Med. ramp |
| 3F | 5 | 0 | 5 | ULP | 6x670x2000 | Unknown | Fast ramp |
| 3C | 9 | 0 | 9 | ULP | 6x670x2000 | Unknown | Cyclic loading |
| 4S | 5 | 1 | 4 | ULP | 6x1000x2000 | Unknown | Slow ramp |
| 4M | 6 | 2 | 4 | ULP | 6x1000x2000 | Unknown | Med. ramp |
| 4F | 5 | 0 | 5 | ULP | 6x1000x2000 | Unknown | Fast ramp |
| 4C | 9 | 1 | 8 | ULP | 6x1000x2000 | Unknown | Cyclic loading |
| 5S | 6 | 3 | 3 | ULP | 6x1335x2000 | Unknown | Slow ramp |
| 5M | 5 | 3 | 2 | ULP | 6x1335x2000 | Unknown | Med. ramp |
| 5F | 5 | 0 | 5 | ULP | 6x1335x2000 | Unknown | Fast ramp |
| 5C | 6 | 3 | 3 | ULP | 6x1335x2000 | Unknown | Cyclic loading |
| 6S | 6 | 2 | 4 | ULP | 6x1600x2000 | Unknown | Slow ramp |
| 6M | 6 | 1 | 5 | ULP | 6x1600x2000 | Unknown | Med. ramp |
| 6F | 5 | 2 | 3 | ULP | 6x1600x2000 | Unknown | Fast ramp |
| 6C | 7 | 3 | 4 | ULP | 6x1600x2000 | Unknown | Cyclic loading |
| 7S | 5 | 1 | 4 | ULP | 6x2000x2000 | Unknown | Slow ramp |
| 7M | 5 | 1 | 4 | ULP | 6x2000x2000 | Unknown | Med. ramp |
| 7F | 6 | 3 | 3 | ULP | 6x2000x2000 | Unknown | Fast ramp |
| 7C | 9 | 3 | 5 | ULP | 6x2000x2000 | Unknown | Cyclic loading |
| 8S | 6 | 1 | 4 | ULP | 6x2000x3000 | Unknown | Slow ramp |
| 8M | 6 | 3 | 3 | ULP | 6x2000x3000 | Unknown | Med. ramp |
| 8F | 6 | 3 | 3 | ULP | 6x2000x3000 | Unknown | Fast ramp |
| 8C | 7 | 3 | 4 | ULP | 6x2000x3000 | Unknown | Cyclic loading |

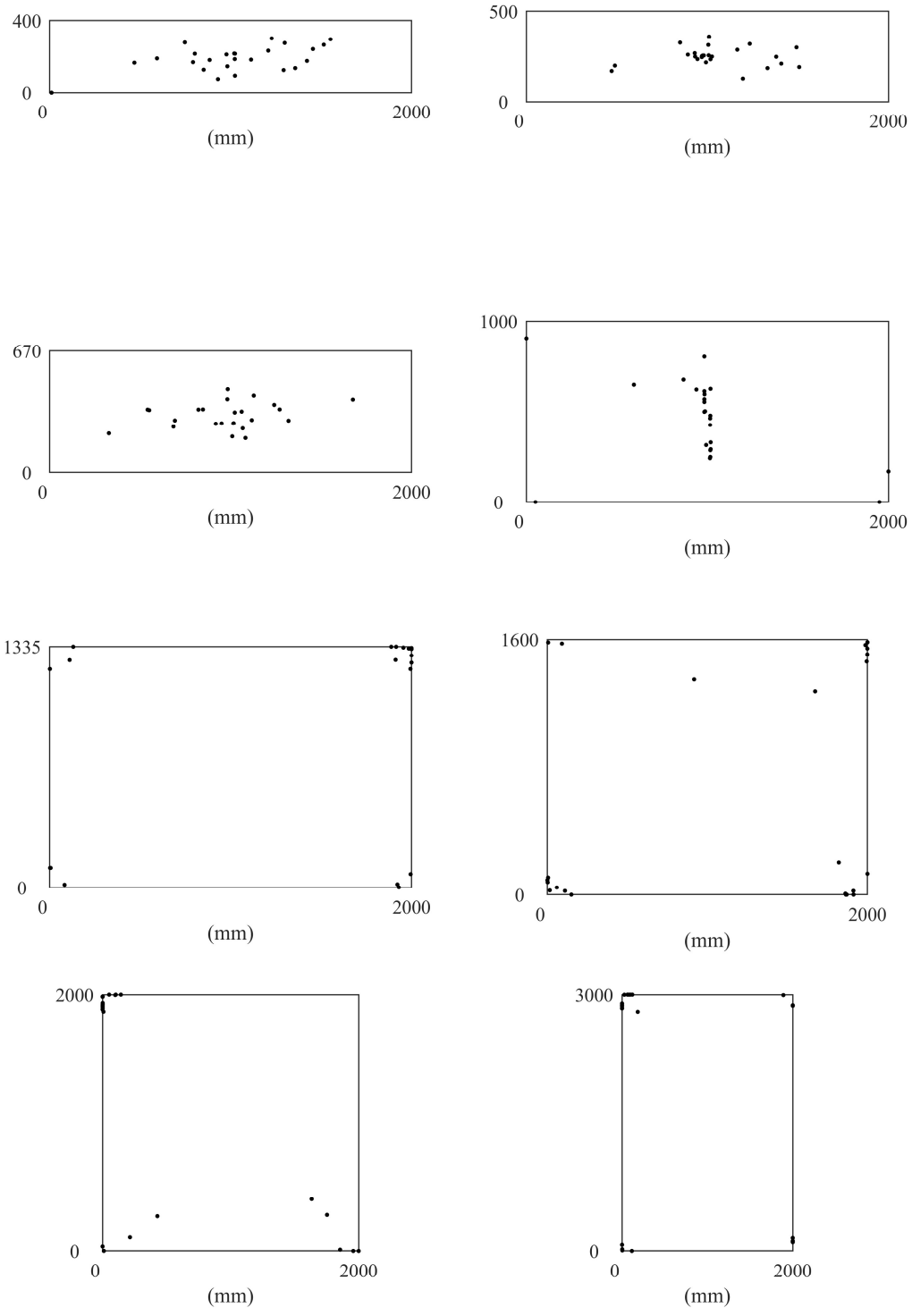


Fig. 18 Fracture locations according to Calderone (1999).

*Hess (2000)*

The experiment was conducted with a four-point bending device. The loading rate was controlled using a hand-driven hydraulic piston. Hence, a strictly linear stress rate could not be produced. The load span and support span were varied between 1400 mm and 4200 mm, respectively, and 200 mm and 1000 mm, respectively. All glass specimens were cut out from 10 mm thick panes except for the small set of large specimens which measured 12 mm in thickness. The glass edge was ground. Two different specimen dimensions were employed, viz. 400x4500 $mm^2$ and 360x1100 $mm^2$. Three samples of specimens were subjected to in-plane and out-of-plane loading. In one of the samples with in-plane loading, however, the stress history between the load span was nonlinear due to the high ratio of cross-sectional height to beam length. In the case of the beams which were subjected to out-of-plane loading, the type of failure, i.e. edge failure or surface failure, was not recorded. During the experiment, the temperature was maintained at 23 ºC. The relative humidity was not recorded but can be assumed to be the same as in room conditions. A summary of details on the experiment is given in Tab. 8. The length of load-duration ranged from about 17 sec to 6 min and 23 sec according to calculations. Fig. 19 shows a set of boxplots for the fracture stress. Fig. 20 shows a set of probability plots for some of the data samples.

Table 8: Details on the experiment as reported by Hess (2000). 4PB=Four-point bending, IP=In-plane.

| Sample ID | No. of spec's | Bending mode | Dimensions ($mm^3$) | Edge proc. | Load. span (mm) | Approx. stress rate ($MPa\ s^{-1}$) |
|---|---|---|---|---|---|---|
| 1 | 4 | 4PB IP | 12x400x4500 | Ground | 1400 | 0.13 |
| 2 | 10 | 4PB IP | 10x360x1100 | Ground | 200 | N/A |
| 3 | 11 | 4PB OP | 10x360x1100 | Ground | 200 | 3.0 |

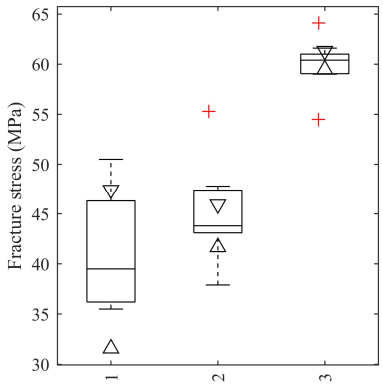


Fig. 19 Boxplots for the fracture stress according to Hess (2000).

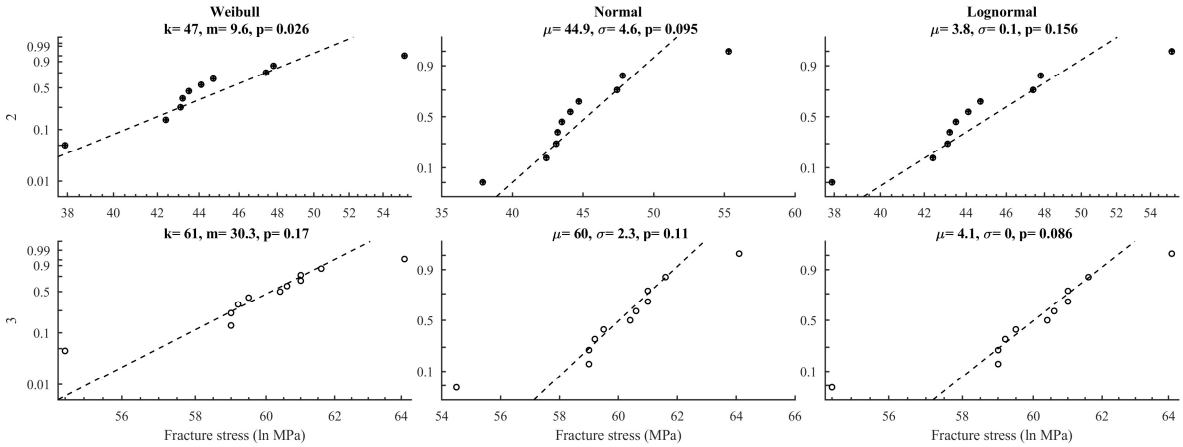


Fig. 20 Probability plots for the strength according to Hess (2000).

*Fink (2000)*

The experiment was conducted with the coaxial double ring bending device. The loading ring diameter was 55 mm and the support ring diameter was 145 mm. The specimens were cut out from panes with the nominal thickness 4 mm and obtained from two different suppliers in this report denoted by M1 and M2. The specimens had the dimensions 225x225 $mm^2$. The applied loading generated an approximate stress rate of 2 MPa $s^{-1}$. In the case of the M1 sample data, the tin side of the plates was placed in the tension zone. However, for the M2 sample, it was not recorded which of the tin versus air side that was placed in the tension zone. A piece of machine writing paper was applied to the contact surface between the glass and steel parts. The temperature during testing was 23 ºC and the relative humidity was 60%. The load-duration until failure ranged from about 28 sec to 1 min and 41 sec according to calculations. A summary of details on the experiment is given in Tab. 9. In Fig. 21, a set of boxplots depict the fracture stress characteristics for the nominal strength data. A set of three probability plots for each sample is shown in Fig. 22 including the respective maximum-likelihood parameter estimates and the Anderson-Darling goodness-of-fit statistic.

Table 9: Details on the experiment as reported by Fink (2000).

| Sample ID | No. of spec's | Bending mode | Dimensions ($mm^3$) | Load. ring diameter (mm) | Stress rate (MPa $s^{-1}$) |
|---|---|---|---|---|---|
| M1 | 20 | CDR | 4x225x225 | 55 | 2 |
| M2 | 107 | CDR | 4x225x225 | 55 | 2 |

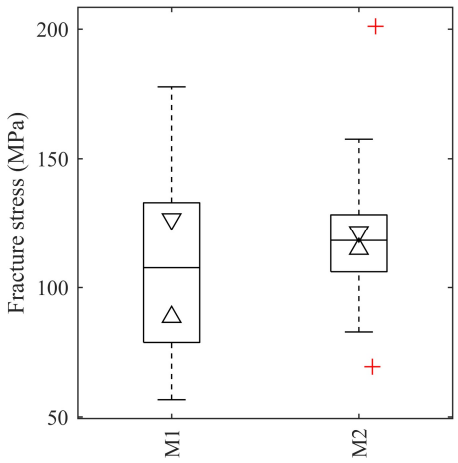


Fig. 21 Boxplots of the nominal fracture stress according to Fink (2000).

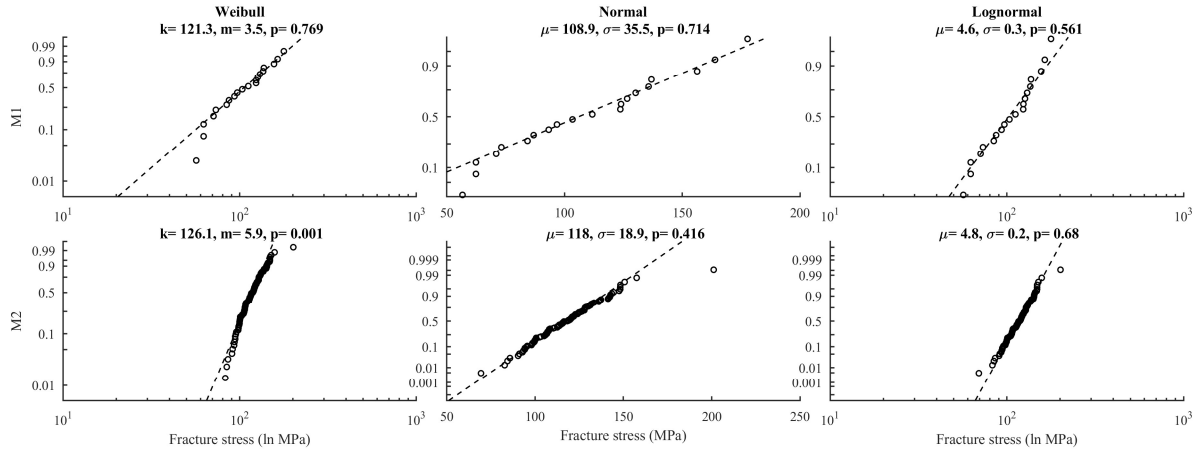


Fig. 22 Probability plots for each data sample in Fink (2000).

*SURVEY OF EXPERIMENTAL DATA ON THE STRENGTH OF ANNEALED FLOAT GLASS*

*Overend (2002)*

The experiment was conducted with the coaxial double ring bending setup using a Satec Universal testing machine under displacement control. The loading ring diameter was 51 mm and the support ring diameter was either 65 mm, 127 mm or 200 mm, corresponding to three samples of tests. The specimens were cut out from panes with a thickness of 6 mm. The specimen dimensions were 300x300 $mm^2$. The out-of-plane loading generated an approximate stress rate of 0.65 MPa $s^{-1}$, 0.90 MPa $s^{-1}$, and 0.64 MPa $s^{-1}$, respectively. Transparent adhesive tape was applied to the compression side. One specimen in each sample was strain gauged using two rosettes located at the center on the tension side of the glass and directly under the loading ring. It was not recorded which of the air versus tin side of the glass that were placed in the tension zone. The load-duration until failure ranged from about 1 min to 8 min and 43 sec. The temperature and relative humidity during testing was not specified but it can be assumed that an indoor environment represents the climatic conditions. A summary of details on the experiment is given in Tab. 10. In Fig. 23, a set of boxplots depict the fracture stress characteristics for the nominal and stress rate-equivalent strength data. The fracture stress values are the experimental values recorded by Overend (2002) which were based on strain gauge measurements and extrapolation methods. A set of three probability plots for each sample is shown in Fig. 24 including the respective maximum-likelihood parameter estimates and the Anderson-Darling goodness-of-fit statistic. The recorded fracture origins are depicted in Fig. 25.

Table 10: Details on the experiment as reported by Overend (2002). S=Small, M=Medium, L=Large reaction ring diameter, CDR=Coaxial double ring,

| Sample ID | No. of spec's | Bending mode | Dimensions ($mm^3$) | Load. ring diameter (mm) | Stress rate (MPa $s^{-1}$) |
|---|---|---|---|---|---|
| S | 10 | CDR | 6x300x300 | 51 | 0.65 |
| M | 10 | CDR | 6x300x300 | 51 | 0.90 |
| L | 10 | CDR | 6x300x300 | 51 | 0.64 |

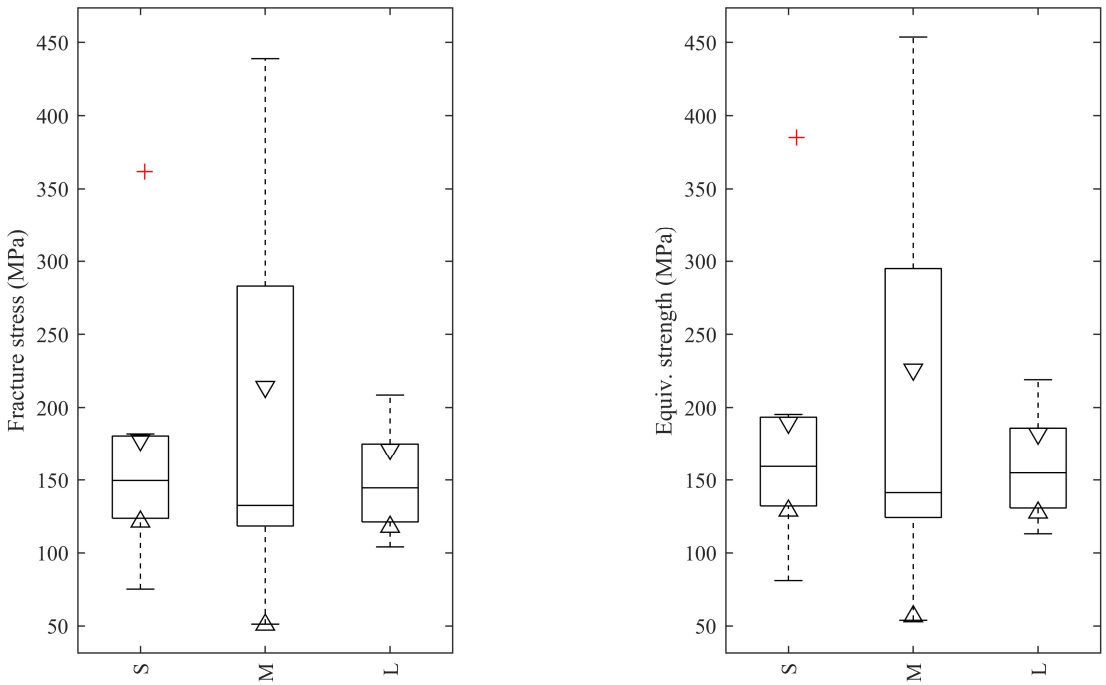


Fig. 23 Boxplots of the (left) nominal and (right) stress rate-equivalent fracture stress for the data in Overend (2002). Comb.=Combined data set.

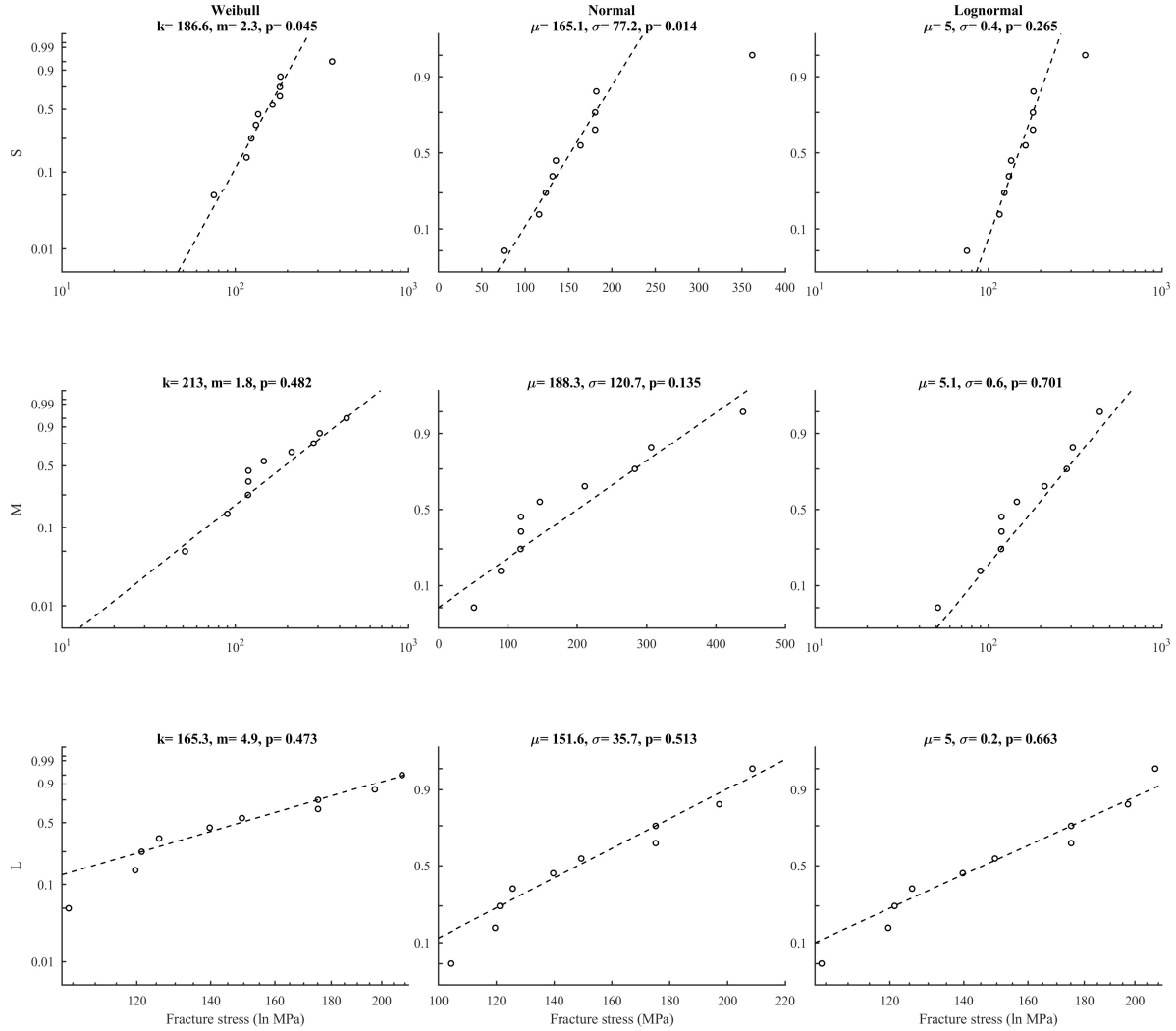


Fig. 24 Probability plots for the data samples in Overend (2002).

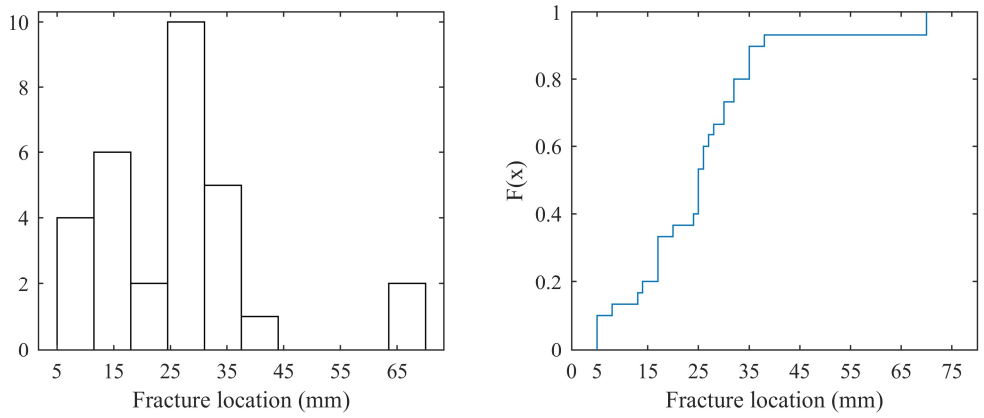


Fig. 25 Fracture locations in the radial direction from the centre point of the plate specimen, according to Overend (2002). Histogram (left) and empirical distribution function (right). NB., loading ring radius was 25.4 mm.

*SURVEY OF EXPERIMENTAL DATA ON THE STRENGTH OF ANNEALED FLOAT GLASS*

*Haldimann (2006)*

The experiment was conducted with a coaxial double ring bending setup using a universal testing machine. The loading ring diameter was 51 mm and the support ring diameter was 127 mm. The specimens were cut out from panes with the nominal thickness 6 mm. The specimen dimensions were 200x200 $mm^2$. Two different loading rates were employed which produced stress rates of approximately 0.21 MPa $s^{-1}$ and 21.2 MPa $s^{-1}$, respectively. The temperature during testing was 23-24 ºC and the relative humidity varied between 51-55%. The load-duration until failure ranged from approximately 6 sec to 6 min and 59 sec. A summary of details on the experiment is given in Tab. 11. In Fig. 26, a set of boxplots depict the fracture stress characteristics for the nominal and stress rate-equivalent strength data. A set of three probability plots for each sample is shown in Fig. 27 including the respective maximum-likelihood parameter estimates and the Anderson-Darling goodness-of-fit statistic.

Table 11: Details on the experiment as reported by Haldimann (2006). L=Low stress rate, H=High stress rate, CDR=Coaxial double ring.

| Sample ID | No. of spec's | Bending mode | Dimensions ($mm^3$) | Load. ring diameter (mm) | Stress rate (MPa $s^{-1}$) |
|---|---|---|---|---|---|
| L | 10 | CDR | 6x200x200 | 51 | 0.21 |
| H | 10 | CDR | 6x200x200 | 51 | 21.2 |

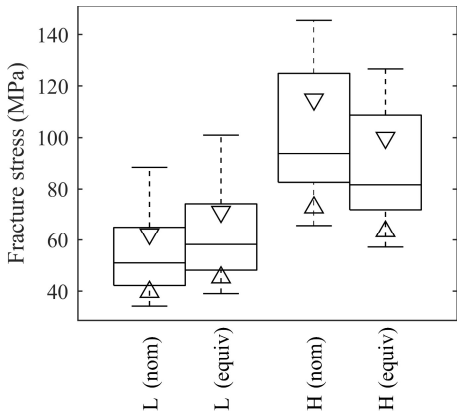


Fig. 26 Boxplots of the nominal and stress rate-equivalent fracture stress according to Haldimann (2006).

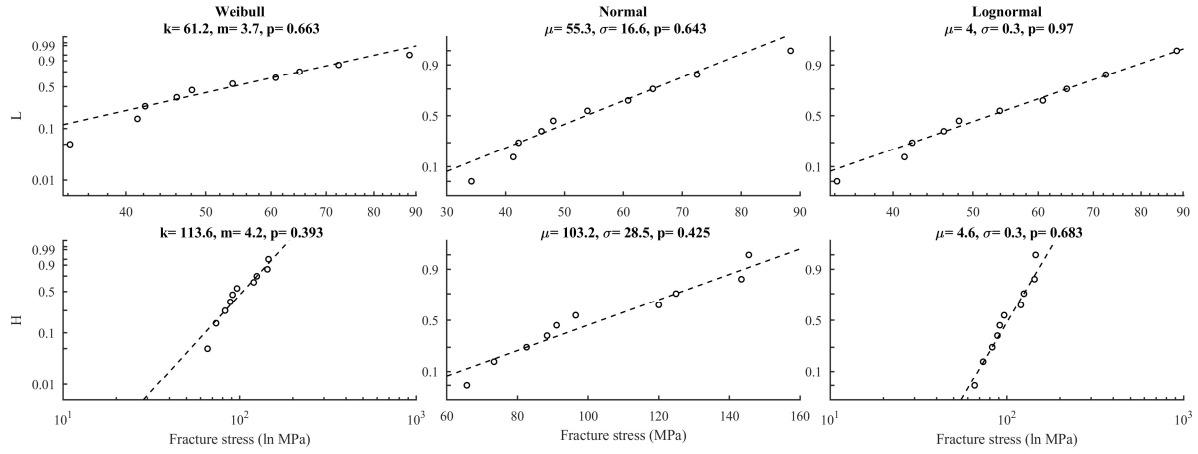


Fig. 27 Probability plots for the data samples in Haldimann (2006).

*Veer et al. (2006)*

The experiment was conducted with a four-point bending arrangement under displacement control using a Zwick Z100 universal testing machine. The load and support span were 230 mm and 850 mm, respectively. The specimens were cut from a single pane with the thickness 10 mm. The specimen dimensions were 125x1000 $mm^2$. The edges were machine ground on three different lines. On each line, the specimens were processed in one whole set, i.e. continuosly without interruption. In fact, prior to processing the grinding lines were inspected to ensure the proper cleaning and the due replacement of grinding heads. One set of plates, Sample 1, had edges ground on a twelve years old manually controlled line. A second set, Sample 2, had edges ground on an eight year old manually controlled lone. Finally, a third set, Sample 3, had edges ground on a new computer controlled line less than three months old. The specimens were subjected to in-plane loading generating an approximate stress rate of 1.0 MPa $s^{-1}$. The specimens were mounted in the test rig using an anti-buckling support at the centre of the support span. The temperature and relative humidity during testing was not specified but it can be assumed that an indoor environment represents the climatic conditions. The range of load-duration was approximately 26 sec to 1 min and 4 sec. No fractures occurred from outside the load span. A summary of details on the experiment is given in Tab. 12. In Fig. 28, a set of boxplots depict the fracture stress characteristics for the nominal strength data as well as the stress rate-equivalent data. A set of three probability plots for each sample is shown in Fig. 29 including the respective maximum-likelihood parameter estimates and the Anderson-Darling goodness-of-fit statistic.

Table 12: Details on the experiment as reported by Veer et al. (2006). 4PB=Four-point bending, IP=In-plane, L=Line no.

| Sample ID | No. of spec's | Bending mode | Dimensions ($mm^3$) | Edge proc. | Load. span (mm) | Stress rate (MPa $s^{-1}$) |
|---|---|---|---|---|---|---|
| gro-L1 | 10 | 4PB IP | 10x125x1000 | Ground | 230 | 1.1 |
| gro-L2 | 11 | 4PB IP | 10x125x1000 | Ground | 230 | 1.1 |
| gro-L3 | 11 | 4PB IP | 10x125x1000 | Ground | 230 | 1.1 |

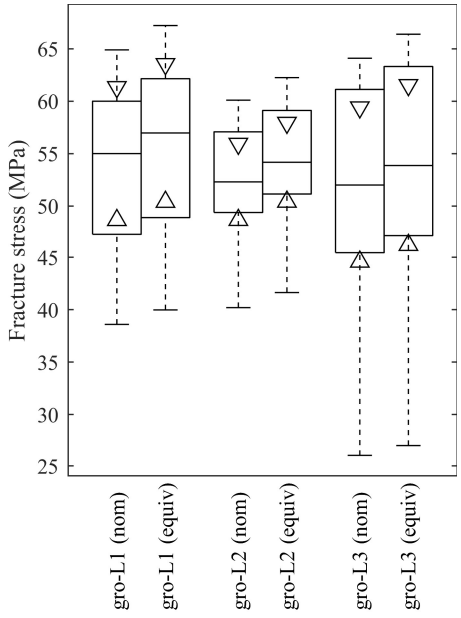


Fig. 28 Boxplots for the nominal fracture stress and the stress rate-equivalent strength according to Veer et al. (2006).

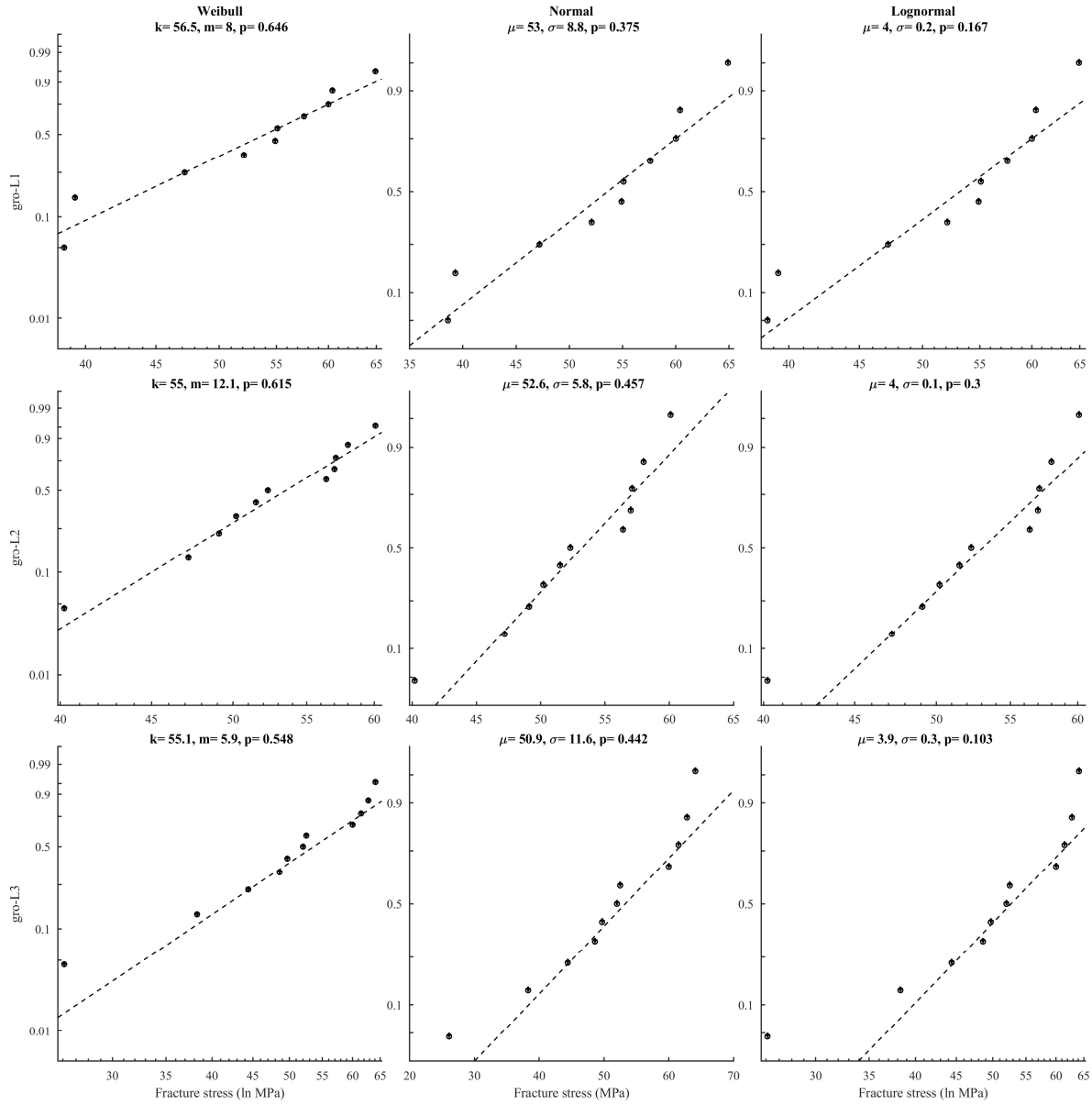


Fig. 29 Probability plots of the data sets according to Veer et al. (2006).

*SURVEY OF EXPERIMENTAL DATA ON THE STRENGTH OF ANNEALED FLOAT GLASS*

*Sglavo et al. (2007)*

The experiment was conducted with a three-point bending arrangement using displacement control. The support span was 280 mm. The specimens were cut from a set of panes with the thickness 4 mm on an industrial process line. The specimen dimensions were 200x300 $mm^2$. The edge processing types were the following, viz. as-cut, manually arrised through abrasion by traditional hand tools, machine ground, and machine polished. The specimens were subjected to out-of-plane loading producing a stress rate of approximately 3.5 MPa $s^{-1}$. Half of the out-of-plane loaded specimens were mounted with the mechanically scribed edge placed in the compression zone while half were positioned with the scribed edge in the tension zone. It was not recorded which of the tin side and air side that was placed in the tension zone. The compression side of the specimens were covered in adhesive transparent tape. The temperature and relative humidity during testing was estimated at about 25 ºC and 40%, respectively. The range of load-duration was approximately 17 sec to 55 sec. The fracture origin mode, i.e. edge or surface, was recorded. A summary of details on the experiment is given in Tab. 13. In Fig. 30, a set of boxplots depict the fracture stress characteristics for the nominal strength data. A set of three probability plots for each sample is shown in Fig. 31 including the respective maximum-likelihood parameter estimates and the Anderson-Darling goodness-of-fit statistic.

Table 13: Details on the experiment as reported by Sglavo et al. (2007). The mechanically scribed edge was alternatively positioned Up in the compression zone and Down in the tension zone. Legend: 3PB=Three-point bending, OP=Out-of-plane.

| Sample ID | No. of spec's | No. of edge fail's | Bending mode | Dimensions ($mm^3$) | Edge proc. | Stress rate (MPa $s^{-1}$) |
|---|---|---|---|---|---|---|
| cut-down | 12 | 5 | 3PB OP | 4x200x300 | Cut | 3.5 |
| cut-up | 15 | 13 | 3PB OP | 4x200x300 | Cut | 3.5 |
| arr-down | 13 | 4 | 3PB OP | 4x200x300 | Arrised | 3.5 |
| arr-up | 14 | 11 | 3PB OP | 4x200x300 | Arrised | 3.5 |
| gro-down | 16 | 7 | 3PB OP | 4x200x300 | Ground | 3.5 |
| gro-up | 15 | 14 | 3PB OP | 4x200x300 | Ground | 3.5 |
| pol-down | 15 | 5 | 3PB OP | 4x200x300 | Polished | 3.5 |
| pol-up | 15 | 15 | 3PB OP | 4x200x300 | Polished | 3.5 |

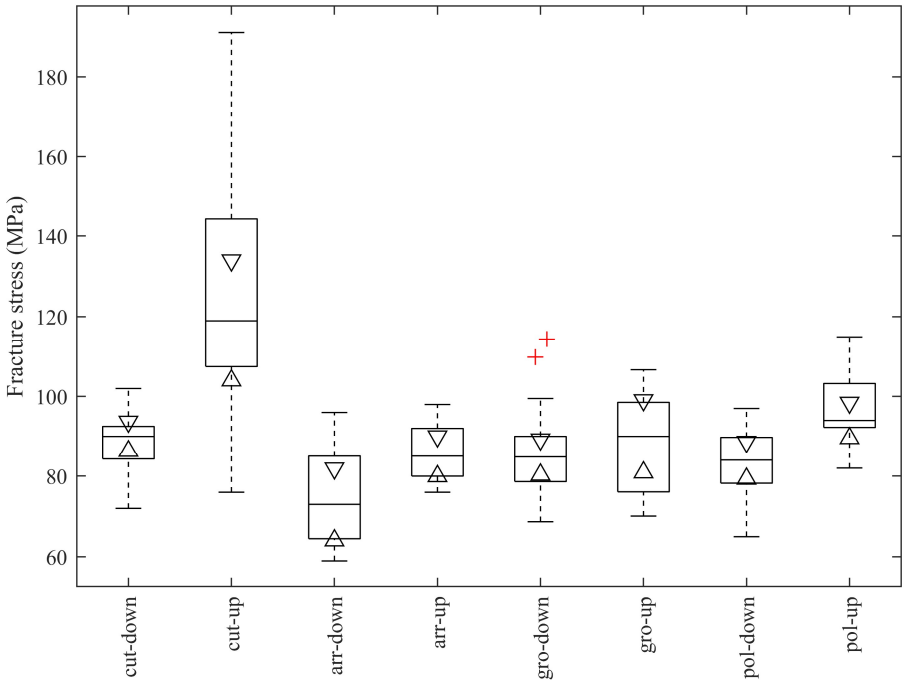


Fig. 30 Boxplots of the nominal fracture stress for each data sample in Sglavo et al. (2007). Legend: Comb=Combined data set.

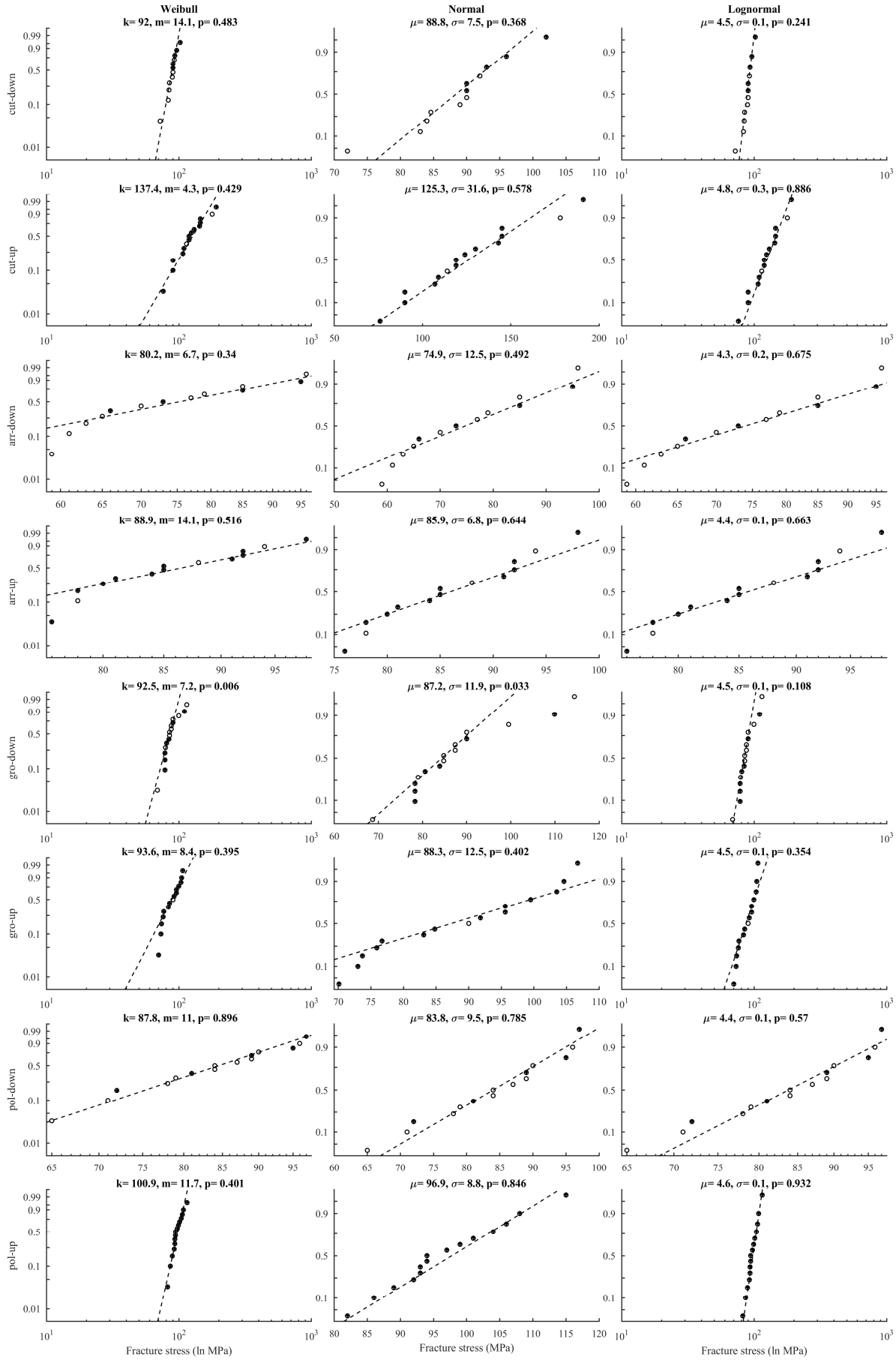


Fig. 31 Probability plots of the data samples in Sglavo et al. (2007). Edge failures are marked with a crossed circle.

*SURVEY OF EXPERIMENTAL DATA ON THE STRENGTH OF ANNEALED FLOAT GLASS*

*Veer et al. (2009)*

The experiment was conducted with a four-point bending arrangement under displacement control using a Zwick Z100 universal testing machine. The load and support span were 230 mm and 850 mm, respectively, according to private correspondence. The specimens were cut from a single pane with the thickness 10 mm using an automated cutting machine. The specimen dimensions were 100x1000 $mm^2$. The edges were processed on a single line by automated grinding and polishing. Some of the specimens were subjected to in-plane loading whereas others were subjected to out-of-plane loading generating an approximate stress rate of 0.8 MPa $s^{-1}$ and 0.1 MPa $s^{-1}$, respectively. The in-plane loaded specimens were mounted in the test rig using a 1 mm thick Teflon sheet as an intermediary at the support locations. Anti-buckling supports were employed at five locations along the length of the beam. It was not recorded which of the tin side and air side that was placed in the tension zone. The specimens were wrapped in PET foil. The temperature and relative humidity during testing was not specified but it can be assumed that an indoor environment represents the climatic conditions. The range of load-duration was approximately 26 sec to 8 min and 51 sec. The fracture origin mode, i.e. edge or surface, was not recorded in the case of the out-of-plane loaded specimens. Fractures that initiated from outside the load span were not reported so it was assumed that all fractures occurred within the load span. A summary of details on the experiment is given in Tab. 14. In Fig. 32, a set of boxplots depict the fracture stress characteristics for the nominal strength data as well as the stress rate-equivalent data. A set of three probability plots for each sample is shown in Fig. 33 including the respective maximum-likelihood parameter estimates and the Anderson-Darling goodness-of-fit statistic.

Table 14: Details on the experiment as reported by Veer et al. (2009). Legend: 4PB=Four-point bending, IP=In-plane, OP=Out-of-plane.

| Sample ID | No. of spec's | Bending mode | Dimensions ($mm^3$) | Edge proc. | Load. span (mm) | Stress rate (MPa $s^{-1}$) |
|---|---|---|---|---|---|---|
| pol-IP | 30 | 4PB IP | 10x100x1000 | Polished | 230 | 0.9 |
| pol-OP | 24 | 4PB OP | 10x100x1000 | Polished | 230 | 0.1 |

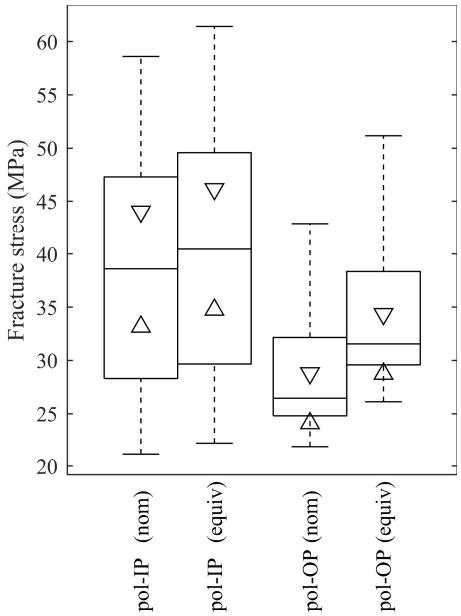


Fig. 32 Boxplots of the (left) nominal and (right) stress rate-equivalent fracture stress for each data sample in Veer et al. (2009). Legend: Comb=Combined data set.

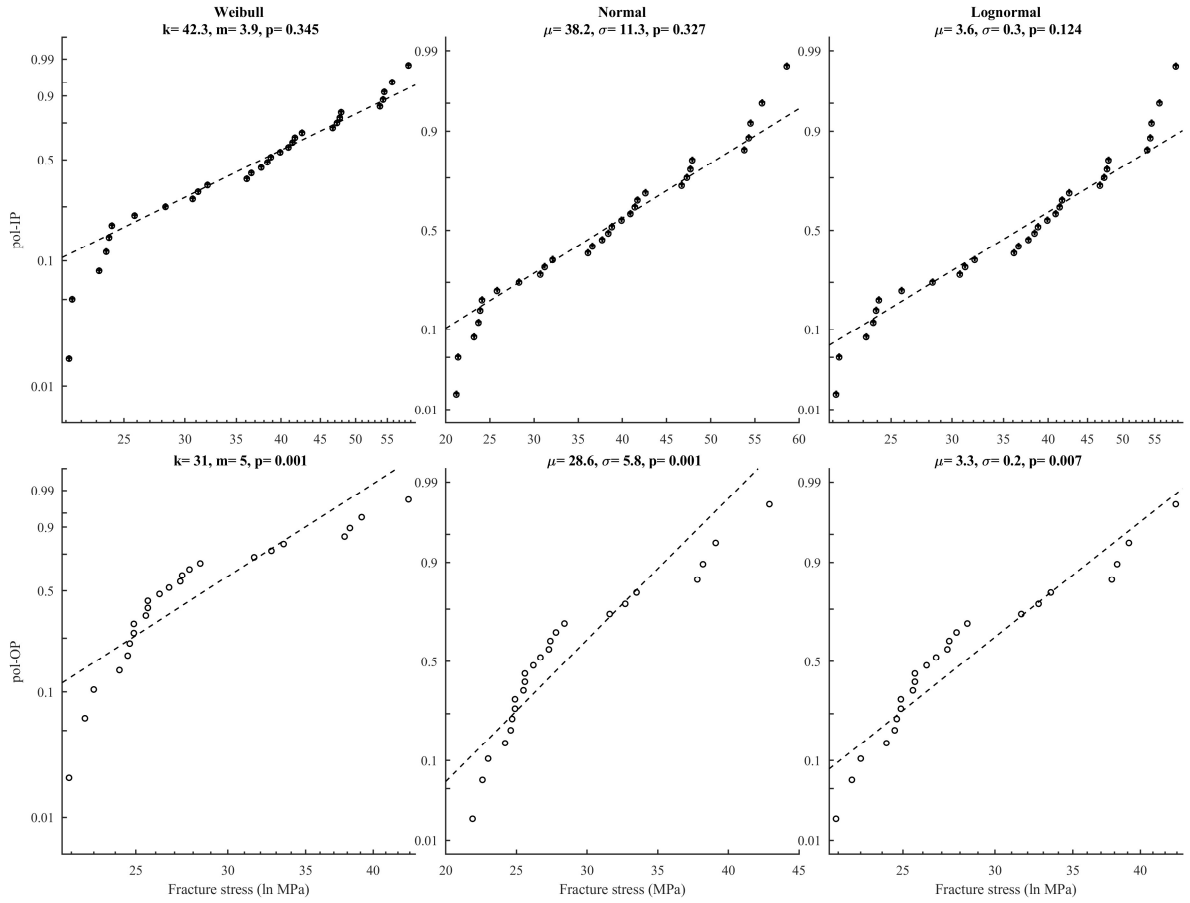


Fig. 33 Probability plots of the data sets in Veer et al. (2009).

*SURVEY OF EXPERIMENTAL DATA ON THE STRENGTH OF ANNEALED FLOAT GLASS*

*Consuelo-Huerta et al. (2011)*

In a conference article from 2011 following the proceedings of the Glass Processing Days, Maria Consuelo-Huerta and co-workers published the results from two series of tests, one of them was conducted with the four-point bending device and the other was conducted with the double ring bending device. The details regarding the specimen dimensions, loading rates, and so forth, are given in Tab. 15. Garcia-Prieto (2001) was cited as the source of the test results using the four-point bending device while Postigo (2010) was cited as the source of the results using the double ring bending device. However, upon acquiring a copy of Garcia-Prieto (2001), this author was unable to locate the original data in that reference (a PhD thesis). This author was unable to obtain a copy of Postigo (2010). Nevertheless, the experiments were detailed well enough by Consuelo-Huerta and co-workers. In the case of the specimens subjected to four-point bending, it was not recorded whether the fracture originated with the edge or the surface area of the glass. The load-durations for the two samples can be calculated to be approximately 47 secs to 1 min and 11 secs, and 15 secs to 1 min and 2 secs, respectively. Fig. 34 shows a set of boxplots for the data samples both in the case of the nominal fracture stress values and in the case of the stress rate-equivalent values. Figs. 35 and 36 show a set of probability plots for each data sample. The data results were extracted from the digitized graphs by this author.

Table 15: Details from the experiments reported of in Consuelo-Huerta et al. (2011). 4PB=Four-point bending, OP=Out-of-plane, CDR=Coaxial double ring.

| Sample ID | No. of spec's | Bending mode | Dimensions ($mm^3$) | Edge proc. | Load. span/Load. ring diam. (mm) | Stress rate (MPa $s^{-1}$) |
|---|---|---|---|---|---|---|
| 4PB | 25 | 4PB OP | 10x100x300 | Unknown | 150 | 1 |
| CDR | 41 | CDR | 5x300x300 | Unknown | 180 | 2.4 |

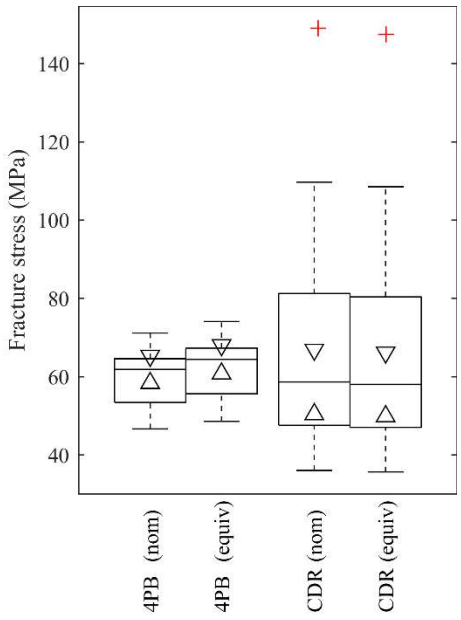


Fig. 34 Boxplot of the nominal and stress-rate equivalent fracture stress values according to the four-point bending experiment (Garcia-Prieto 2001) and the double ring bending experiment (Postigo 2010) as reported by Consuelo-Huerta et al. (2011).

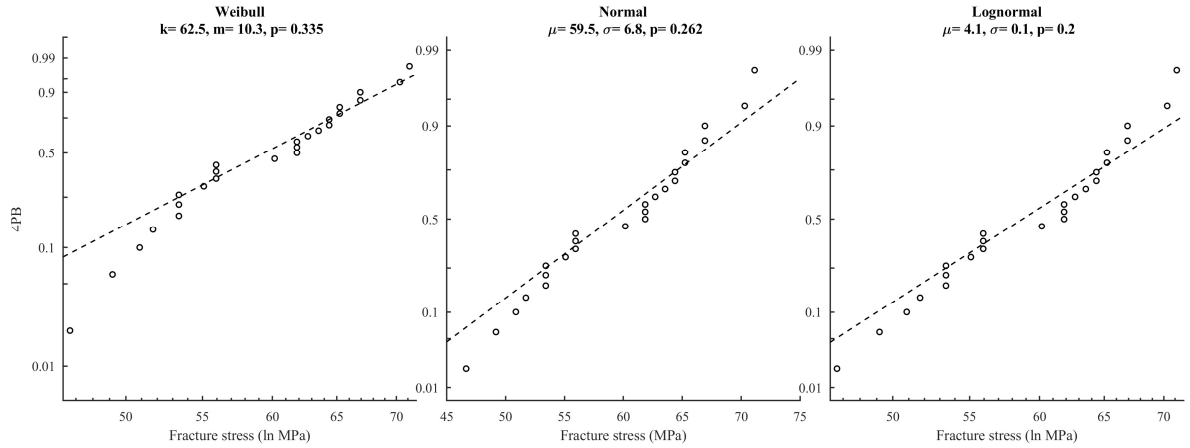


Fig. 35 Probability plots including estimated parameter values for the four-point bending experiment (Garcia-Prieto 2001) as reported by Consuelo-Huerta et al. (2011).

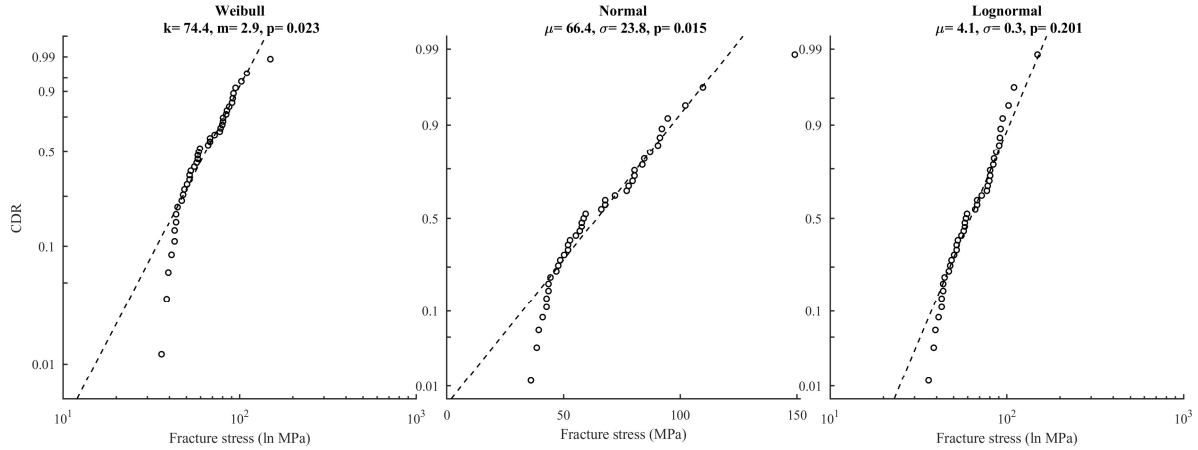


Fig. 36 Probability plots including estimated parameter values for the double ring bending experiment (Postigo 2010) as reported by Consuelo-Huerta et al. (2011).

*SURVEY OF EXPERIMENTAL DATA ON THE STRENGTH OF ANNEALED FLOAT GLASS*

*Veer and Rodichev (2011)*

The experiment was conducted with a four-point bending arrangement under displacement control using a Zwick Z100 universal testing machine. The load and support span were 175 mm and 350 mm, respectively. The specimens were cut from a single jumbo pane with the thickness 6 mm using an automated cutting table. The specimen dimensions were 50x400 $mm^2$. The edge condition was as-cut. Some of the specimens were subjected to in-plane loading whereas others were subjected to out-of-plane loading generating an approximate stress rate of 2.1 MPa $s^{-1}$ and 1.3 MPa $s^{-1}$, respectively. The in-plane loaded specimens were mounted in the test rig with frictionless anti-buckling supports. Half of the out-of-plane loaded specimens were mounted with the mechanically scribed edge placed in the compression zone and half were positioned with the scribed edge in the tension zone. It was not recorded which of the tin side and air side that was placed in the tension zone. The specimens were wrapped in self-adhesive foil. The temperature and relative humidity during testing was not specified but it can be assumed that an indoor environment represents the climatic conditions. The tests were carried out in a single week. The range of load-duration was approximately 15 sec to 1 min and 18 sec. The fracture origin mode, i.e. edge or surface, was recorded. Fractures that initiated from outside the load span were noted when occurring. A summary of details on the experiment is given in Tab. 16. In Fig. 37, a set of boxplots depict the fracture stress characteristics for the nominal strength data as well as the stress rate-equivalent data. A set of three probability plots for each sample is shown in Fig. 38 including the respective maximum-likelihood parameter estimates and the Anderson-Darling goodness-of-fit statistic.

Table 16: Details on the experiment as reported by Veer and Rodichev (2011). Legend: 4PB=Four-point bending, OP=Out-of-plane.

| Sample ID | No. of spec's | Bending mode | Dimensions ($mm^3$) | Edge condition | Load. span (mm) | Stress rate (MPa $s^{-1}$) |
|---|---|---|---|---|---|---|
| cut-IP.1 | 44 | 4PB IP | 6x50x400 | As-cut | 175 | 2.9 |
| cut-IP.2 | 44 | 4PB IP | 6x50x400 | As-cut | 175 | 2.9 |
| cut-OP.1 | 50 | 4PB OP | 6x50x400 | As-cut | 175 | 1.8 |
| cut-OP.2 | 39 | 4PB OP | 6x50x400 | As-cut | 175 | 1.8 |

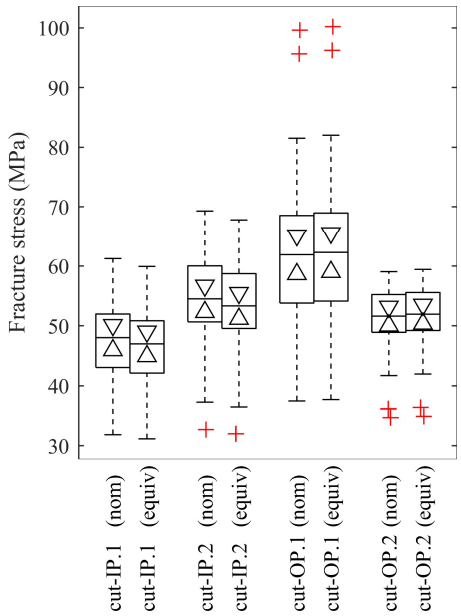


Fig. 37 Boxplots of the (left) nominal and (right) stress rate-equivalent fracture stress values for each data sample in Veer and Rodichev (2011).

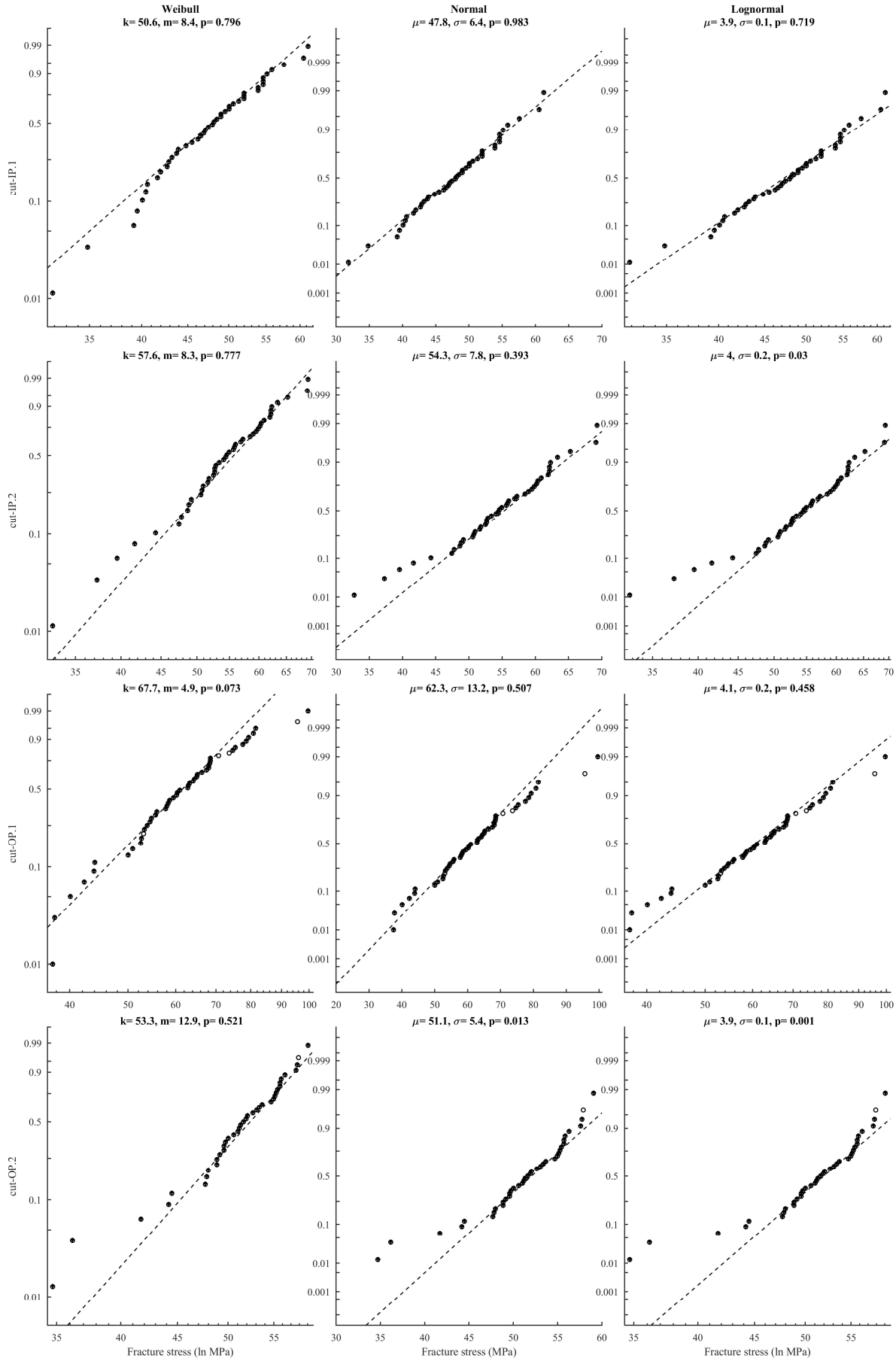


Fig. 38 Probability plots for the data samples in Veer and Rodichev (2011).

*Veer and Rodichev (2012)*

The experiment was conducted with a four-point bending arrangement under displacement control using a Zwick Z100 universal testing machine. The load and support span were 190 mm and 380 mm, respectively. The specimens were cut from panes with the thickness 6 mm using a water-jet cutting machine. The specimen dimensions were 40x400 $mm^2$. The water-jet cutting line was new and was optimized prior to the processing of the specimens. The specimens were subjected to out-of-plane loading generating an approximate stress rate of 1.1 MPa $s^{-1}$. Half of the specimens were mounted with the water-jet cut face placed in the compression zone (cut face up) and half were positioned with the cut edge in the tension zone (cut face down). It was not recorded which of the tin side and air side that was placed in the tension zone. The specimens were wrapped in self-adhesive foil. The temperature and relative humidity during testing was not specified but it can be assumed that an indoor environment represents the climatic conditions. The tests were carried out in a single day. The range of load-duration was approximately 20 sec to 33 sec according to calculations. The fracture origin mode, i.e. edge or surface, was recorded. The fractured specimens were inspected with respect to the breakage occurring between the load span. A summary of details on the experiment is given in Tab. 17. In Fig. 39, a set of boxplots depict the fracture stress characteristics for the nominal strength data as well as the stress rate-equivalent data. A set of three probability plots for each sample is shown in Fig. 40 including the respective maximum-likelihood parameter estimates and the Anderson-Darling goodness-of-fit statistic.

Table 17: Details on the experiment as reported by Veer and Rodichev (2012). Legend: 4PB=Four-point bending, OP=Out-of-plane.

| Sample ID | No. of spec's | Bending mode | Dimensions ($mm^3$) | Edge condition | Load. span (mm) | Stress rate (MPa $s^{-1}$) |
|---|---|---|---|---|---|---|
| cut-up | 30 | 4PB IP | 6x40x400 | As-cut | 190 | 1.5 |
| cut-down | 30 | 4PB IP | 6x40x400 | As-cut | 190 | 1.5 |

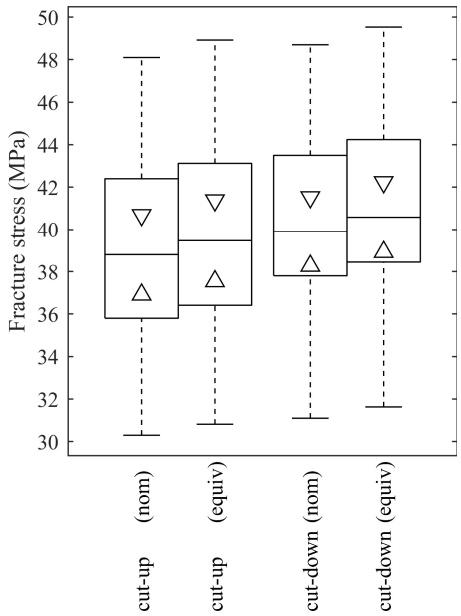


Fig. 39 Boxplots of the (left) nominal and (right) stress rate-equivalent fracture stress values for each data sample in Veer and Rodichev (2012).

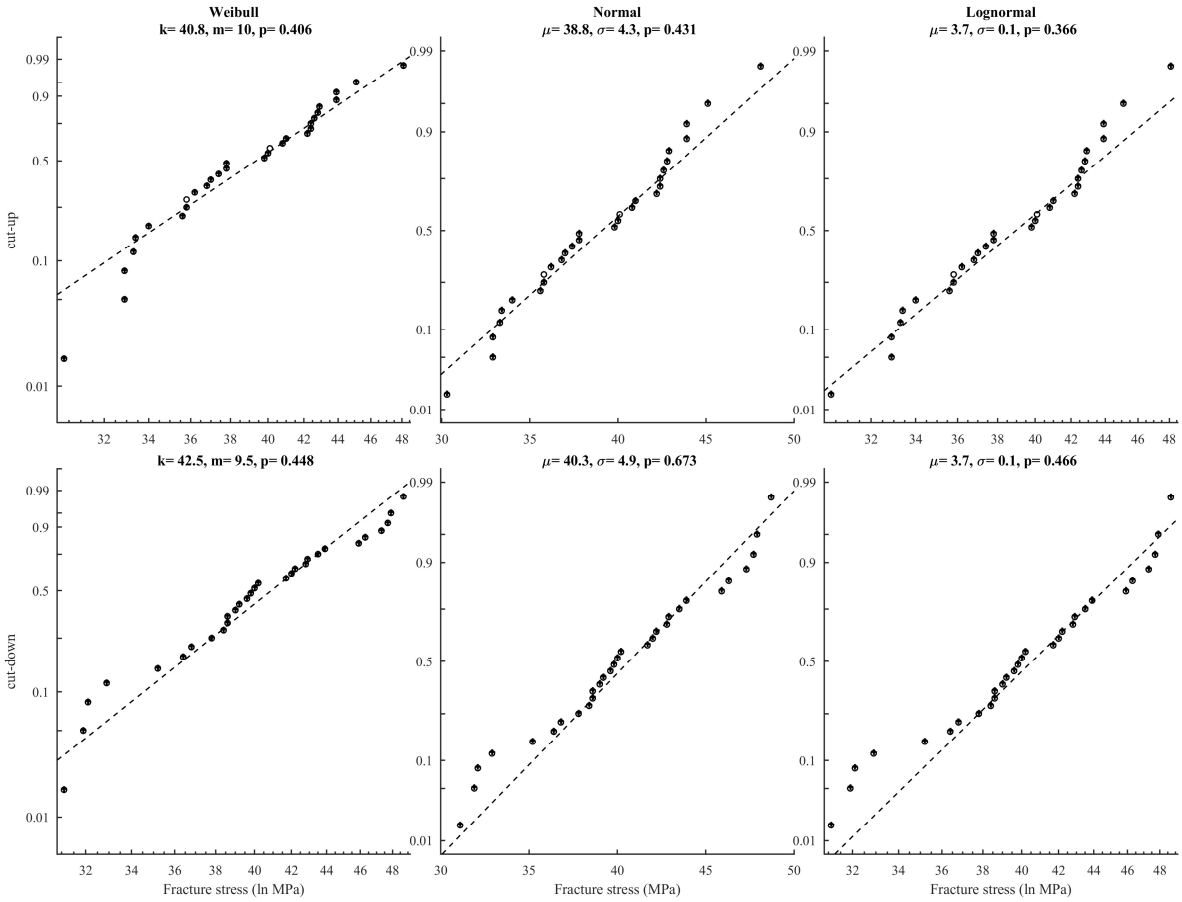


Fig. 40 Probability plots for the data samples in Veer and Rodichev (2012).

*SURVEY OF EXPERIMENTAL DATA ON THE STRENGTH OF ANNEALED FLOAT GLASS*

*Vandebroek et al. (2012)*

The experiment was conducted with a four-point bending arrangement using a universal UTS testing machine. The load and support span were 250 mm and 500 mm, respectively. The specimens were cut from panes with the thickness 4 mm. The specimen dimensions were 50x550 $mm^2$. Two types of edge condition were included, viz. the as-cut edge and the polished edge. The specimens were subjected to in-plane loading generating an approximate stress rate of 55 MPa $s^{-1}$ and 0.55 MPa $s^{-1}$, respectively. The temperature and relative humidity during testing was not specified but it can be assumed that an indoor environment represents the climatic conditions. The specimens that fractured outside the load span were identified and excluded from the analysis. The range of load-duration was approximately 1 sec to 2 min and 26 sec. A summary of details on the experiment is given in Tab. 18. In Fig. 41, a set of boxplots depict the fracture stress characteristics for the nominal strength data as well as the stress rate-equivalent data. A set of three probability plots for each sample is shown in Fig. 42 including the respective maximum-likelihood parameter estimates and the Anderson-Darling goodness-of-fit statistic.

Table 18: Details on the experiment as reported by Vandebroek et al. (2012). Legend: 4PB=Four-point bending, OP=Out-of-plane.

| Sample ID | No. of spec's | Bending mode | Dimensions ($mm^3$) | Edge condition | Load. span (mm) | Stress rate (MPa $s^{-1}$) |
|---|---|---|---|---|---|---|
| pol-High | 20 | 4PB IP | 4x50x550 | Polished | 250 | 55 |
| cut-High | 19 | 4PB IP | 4x50x550 | As-cut | 250 | 55 |
| pol-Low | 19 | 4PB IP | 4x50x550 | Polished | 250 | 0.55 |
| cut-Low | 19 | 4PB IP | 4x50x550 | As-cut | 250 | 0.55 |

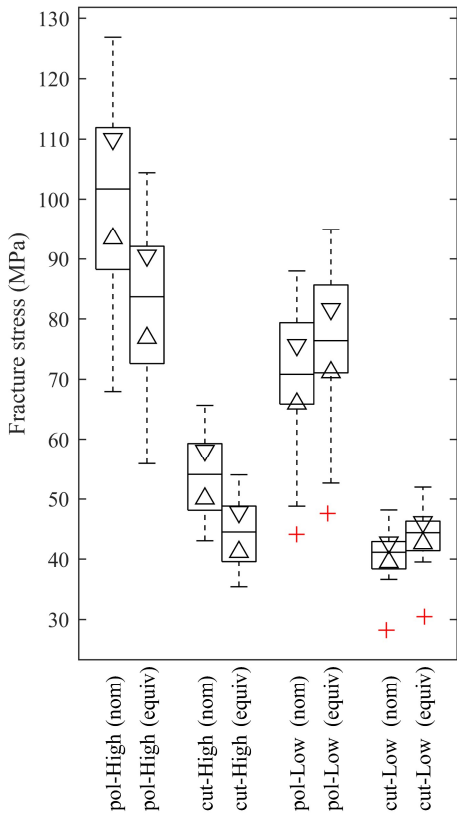


Fig. 41 Boxplots of the (left) nominal and (right) stress rate-equivalent fracture stress values for each data sample in Vandebroek et al. (2012).

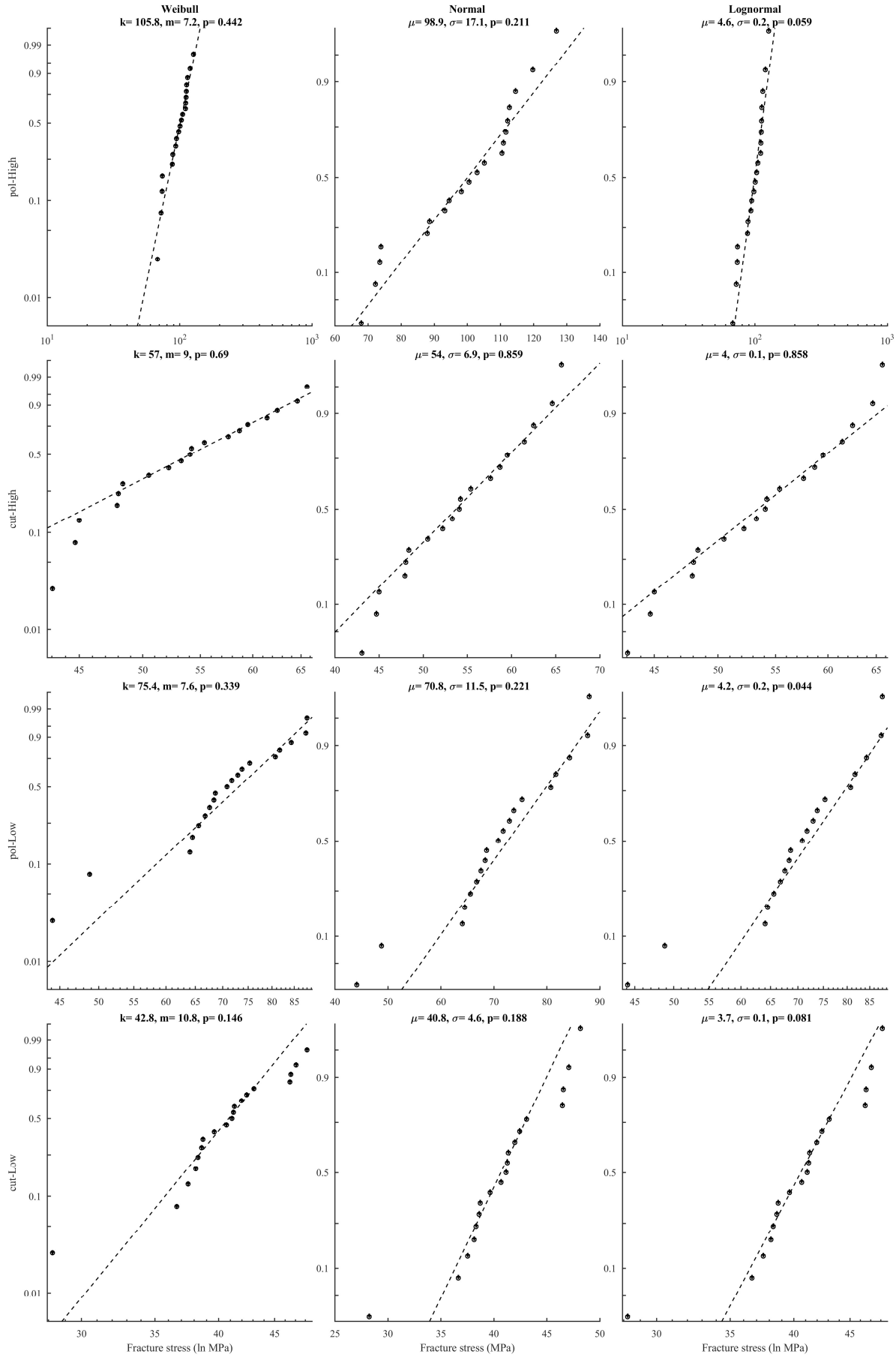


Fig. 42 Probability plots for the data samples in Vandebroek et al. (2012).

*Lindqvist (2013)*

The experiment was conducted with a four-point bending arrangement using a UTS test system and an Instron 5948 MicroTester. In most cases the testing was performed under displacement control or else under force control. The load span varied from 40 mm to 50 mm while the support span was maintained at 100 mm. The glass was obtained from seven different suppliers in total. The specimens were cut from panes with the nominal thickness 4 mm and 8 mm. The specimens were cut out manually or with a water-cutting machine to the approximate dimensions 10x110 $mm^2$. Five types of edge condition were included, viz. the as-cut edge, the arrised edge, the ground edge, the polished edge, and the water-jet cut edge. The specimens were subjected to in-plane loading, the generated stress rate ranging from low, i.e. 0.1 MPa $s^{-1}$ to 2 MPa $s^{-1}$, to high, i.e. 15 MPa $s^{-1}$ to 55 MPa $s^{-1}$. However, the stress rate could not be accurately determined in some cases. This is reflected in Fig. 43 below where a number of stress rate-equivalent data samples could not be computed and displayed. The surfaces of the glass (edges excluded) were covered in a transparent and highly plastic tape. The temperature ranged between 18-23 ºC while the relative humidity was between 23-69%. The range of load-duration was approximately 1 sec to 8 min and 57 sec according to calculations. A summary of details on the experiment is given in Tab. 19. The dimensional measurements and stress rates given in Tab. 19 represent the mean values. In Fig. 43, a set of boxplots depict the fracture stress characteristics for the nominal strength data as well as the stress rate-equivalent data. A set of three probability plots for each sample is shown in Figs. 44 to 47 including the respective maximum-likelihood parameter estimates and the Anderson-Darling goodness-of-fit statistic.

Table 19: Details on the experiment as reported by Lindqvist (2013). Legend: 4PB=Four-point bending, IP=In-plane, H=High stress rate, L=Low stress rate.

| Sample ID | No. of spec's | Bending mode | Supplier ID | Dimensions ($mm^3$) | Edge condition | Load. span (mm) | Stress rate ($MPa\ s^{-1}$) |
|---|---|---|---|---|---|---|---|
| cut-M1.H:4mm | 20 | 4PB IP | M1 | 3.83x10.20x110 | As-cut | 40 | 17.2 |
| cut-M1.L:4mm | 20 | 4PB IP | M1 | 3.83x10.11x110 | As-cut | 40 | 1.4 |
| cut-M2.H:4mm | 19 | 4PB IP | M2 | 3.78x10.00x110 | As-cut | 40 | 18.1 |
| cut-M2.L:4mm | 16 | 4PB IP | M2 | 3.78x9.97x110 | As-cut | 40 | N/A |
| cut-M3.H:4mm | 17 | 4PB IP | M3 | 3.86x12.75x110 | As-cut | 50 | 49.3 |
| cut-M3.L:4mm | 19 | 4PB IP | M3 | 3.85x12.65x110 | As-cut | 50 | 2.0 |
| cut-M4.H:4mm | 20 | 4PB IP | M4 | 3.83x12.41x110 | As-cut | 50 | 53.3 |
| cut-M4.L:4mm | 20 | 4PB IP | M4 | 3.84x12.33x110 | As-cut | 50 | 2.1 |
| arr-M4.H:4mm | 20 | 4PB IP | M4 | 3.82x12.40x110 | Arrised | 50 | 49.3 |
| arr-M4.L:4mm | 24 | 4PB IP | M4 | 3.83x12.29x110 | Arrised | 50 | 2.0 |
| arr-M5.H:4mm | 20 | 4PB IP | M5 | 3.74x12.13x110 | Arrised | 50 | 49.5 |
| arr-M5.L:4mm | 26 | 4PB IP | M5 | 3.74x12.15x110 | Arrised | 50 | 2.0 |
| gro-M3.H:4mm | 16 | 4PB IP | M3 | 3.80x12.13x110 | Ground | 50 | 50.3 |
| gro-M3.L:4mm | 21 | 4PB IP | M3 | 3.82x12.17x110 | Ground | 50 | 2.0 |
| gro-M5.H:4mm | 11 | 4PB IP | M5 | 3.80x12.24x110 | Ground | 50 | 50.0 |
| gro-M5.L:4mm | 23 | 4PB IP | M5 | 3.79x12.24x110 | Ground | 50 | 2.0 |
| gro-M6.H:4mm | 16 | 4PB IP | M6 | 3.82x12.19x110 | Ground | 50 | 48.6 |
| gro-M6.L:4mm | 23 | 4PB IP | M6 | 3.82x12.09x110 | Ground | 50 | 2.0 |
| wat-M7.H:4mm | 20 | 4PB IP | M7 | 3.82x10.44x110 | Water-cut | 40 | 20.9 |
| wat-M7.L:4mm | 19 | 4PB IP | M7 | 3.81x10.42x110 | Water-cut | 40 | 0.16 |
| pol-M1.H:4mm | 37 | 4PB IP | M1 | 3.82x9.93x110 | Polished | 40 | 20.6 |
| pol-M1.L:4mm | 33 | 4PB IP | M1 | 3.82x10.04x110 | Polished | 40 | 0.15 |
| pol-M2.H:4mm | 19 | 4PB IP | M2 | 3.78x10.80x110 | Polished | 40 | N/A |
| pol-M2.L:4mm | 20 | 4PB IP | M2 | 3.78x10.92x110 | Polished | 40 | N/A |
| cut-M3.H:8mm | 20 | 4PB IP | M3 | 7.84x12.00x110 | As-cut | 50 | N/A |
| cut-M4.H:8mm | 21 | 4PB IP | M4 | 7.83x12.16x110 | As-cut | 50 | N/A |
| arr-M4.H:8mm | 23 | 4PB IP | M4 | 7.83x12.16x110 | Arrised | 50 | N/A |
| arr-M5.H:8mm | 21 | 4PB IP | M5 | 7.86x12.64x110 | Arrised | 50 | 53.8 |
| arr-M5.L:8mm | 22 | 4PB IP | M5 | 7.84x12.64x110 | Arrised | 50 | 2.2 |
| gro-M3.H:8mm | 20 | 4PB IP | M3 | 7.86x12.35x110 | Ground | 50 | N/A |
| gro-M5.H:8mm | 18 | 4PB IP | M5 | 7.81x12.56x110 | Ground | 50 | N/A |
| gro-M6.H:8mm | 23 | 4PB IP | M6 | 7.71x12.32x110 | Ground | 50 | N/A |

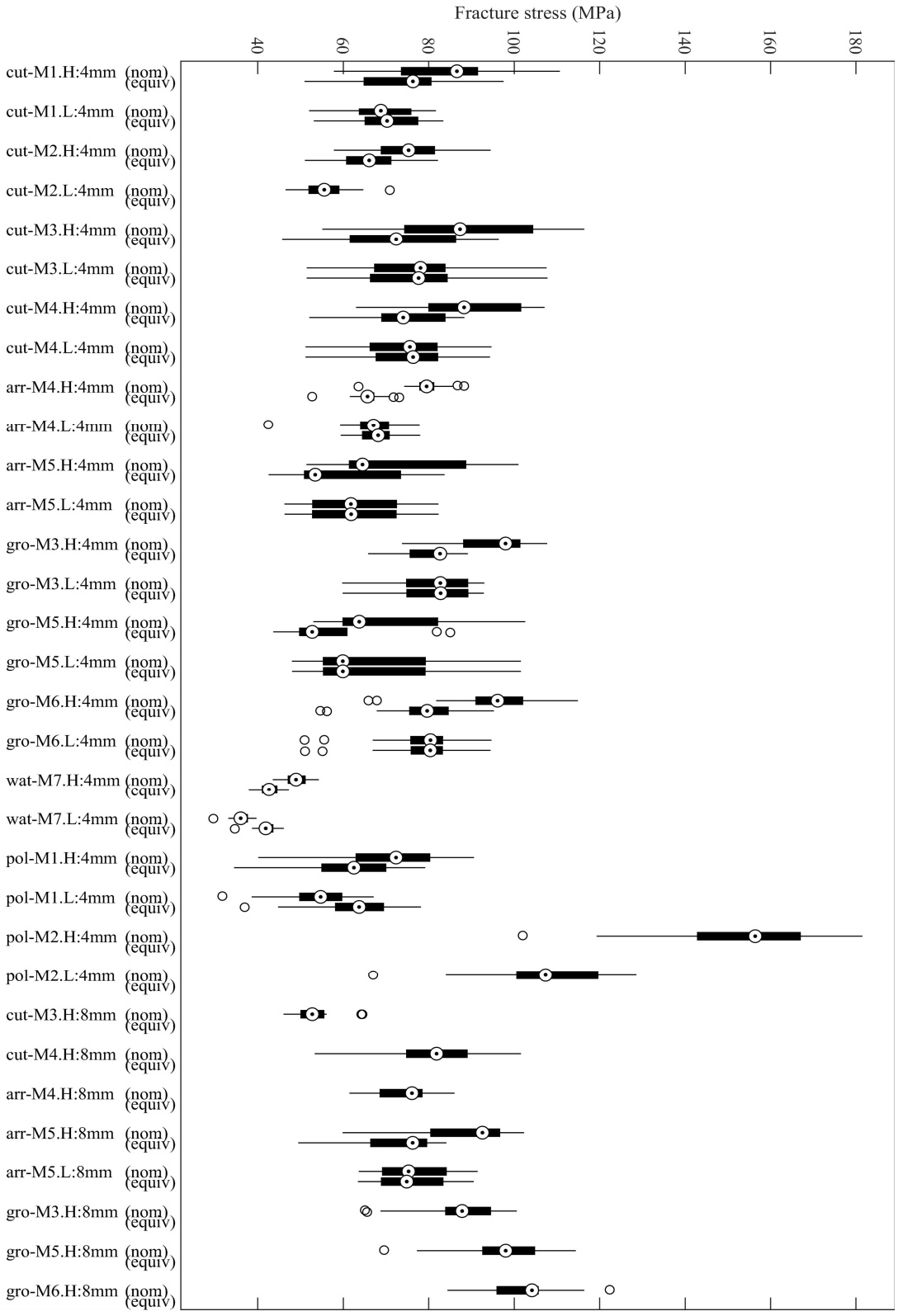


Fig. 43 Boxplots of the nominal and stress rate-equivalent fracture stress values for the data samples in Lindqvist (2013). NB. in some cases the stress rate-equivalent strength was not available in which case only the received (nominal) values are shown.

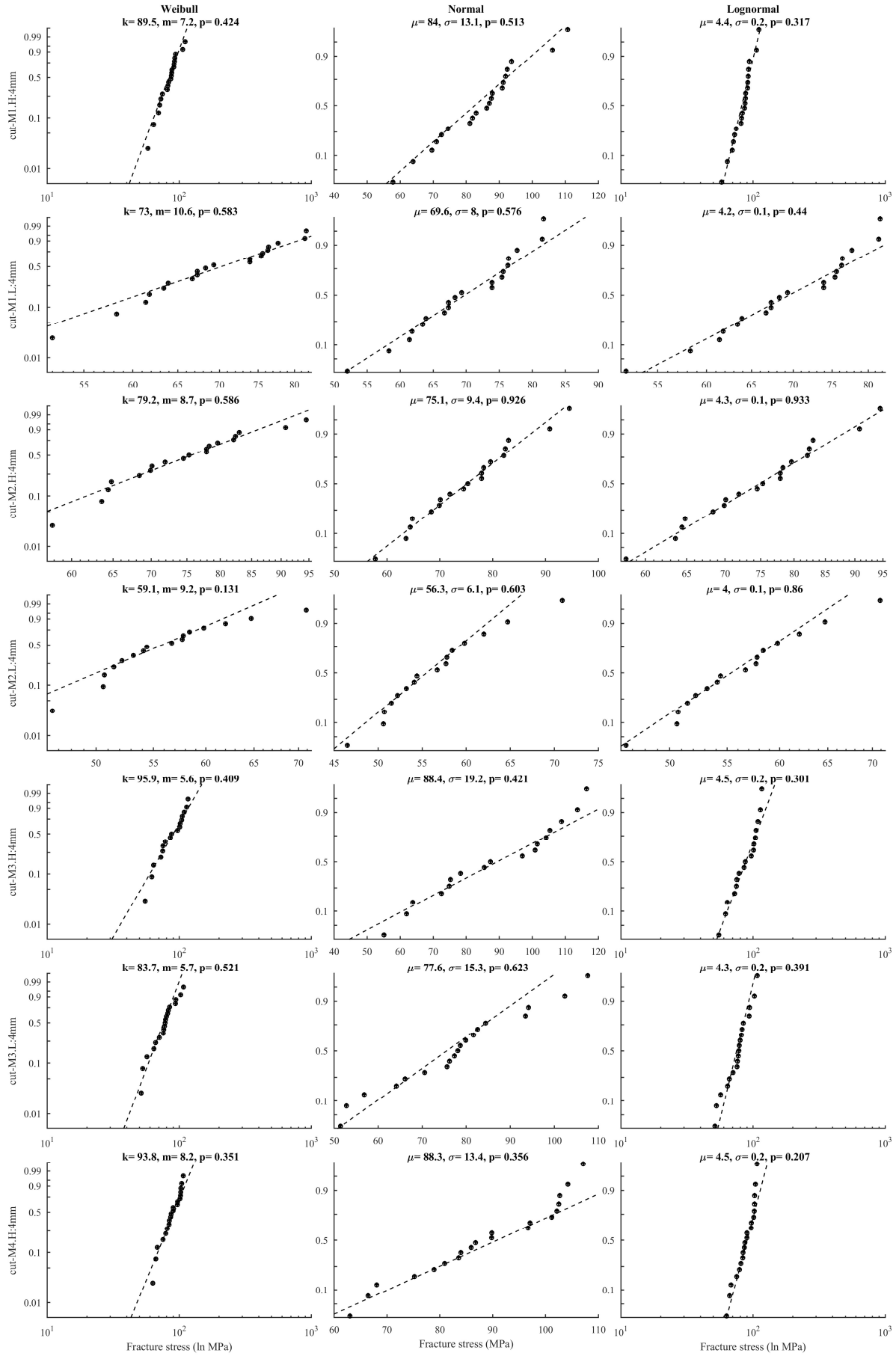


Fig. 44 Probability plots for the data samples in Lindqvist (2013).

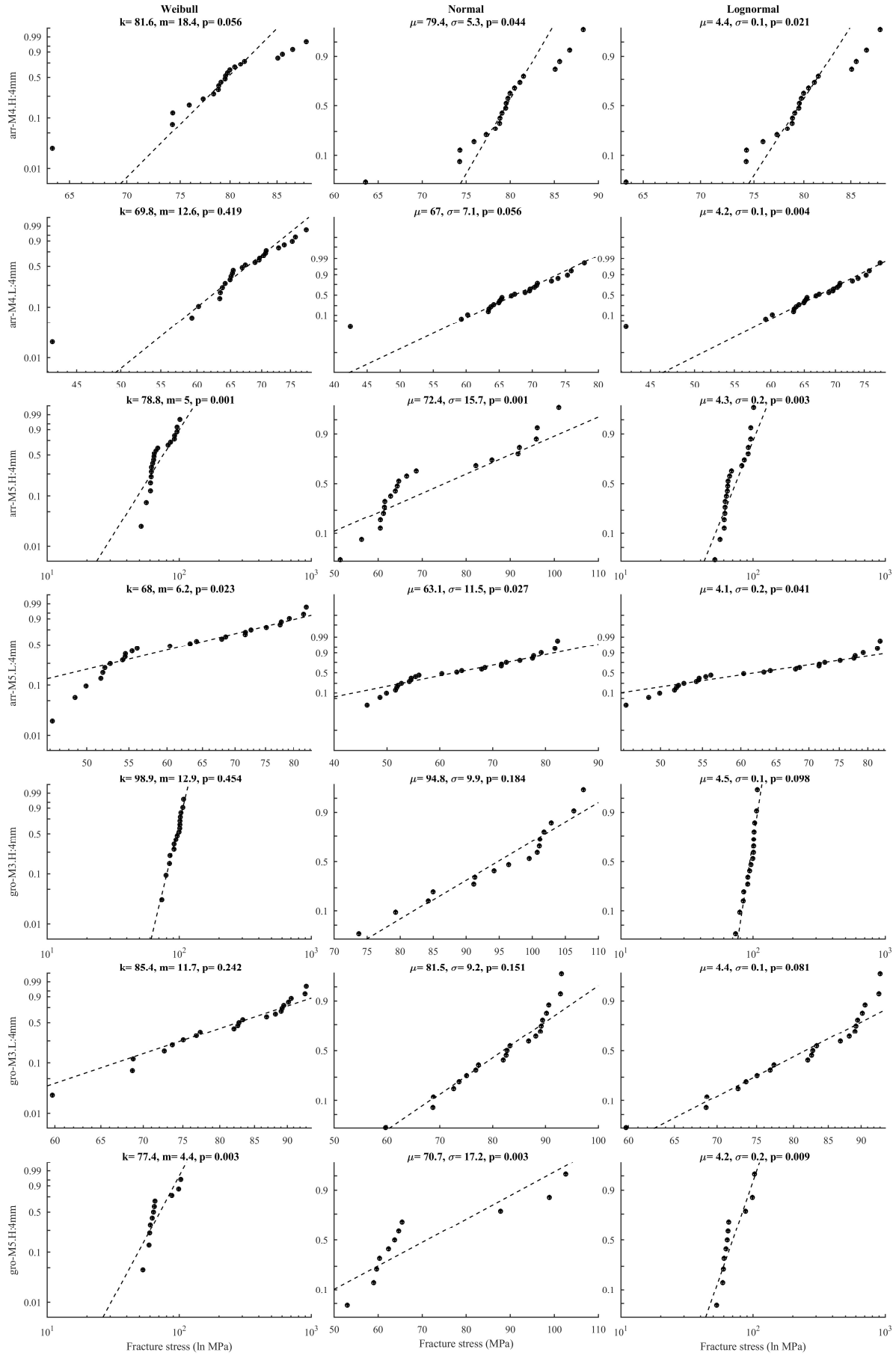


Fig. 45 Probability plots for the data samples in Lindqvist (2013).

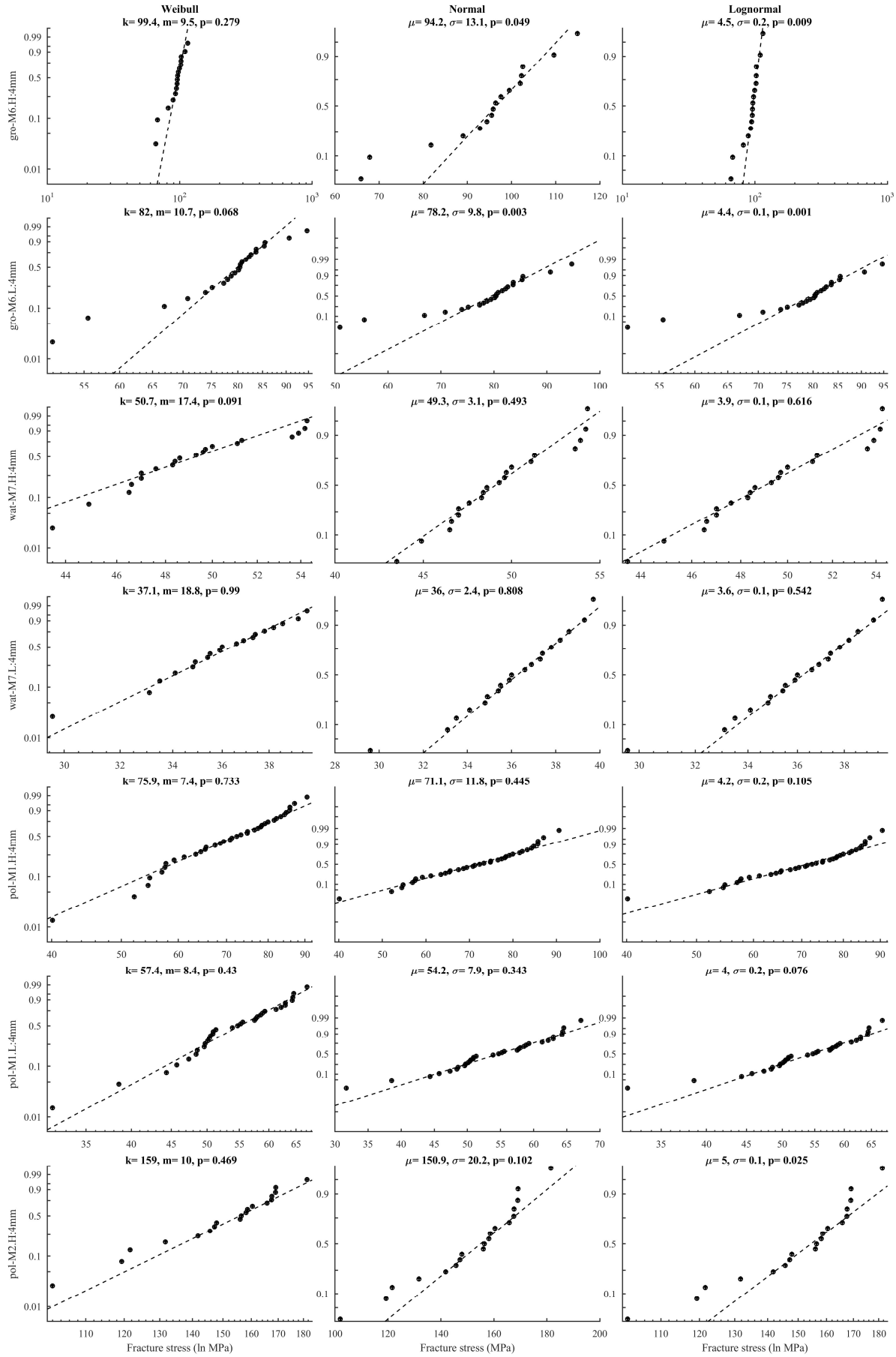


Fig. 46 Probability plots for the data samples in Lindqvist (2013).

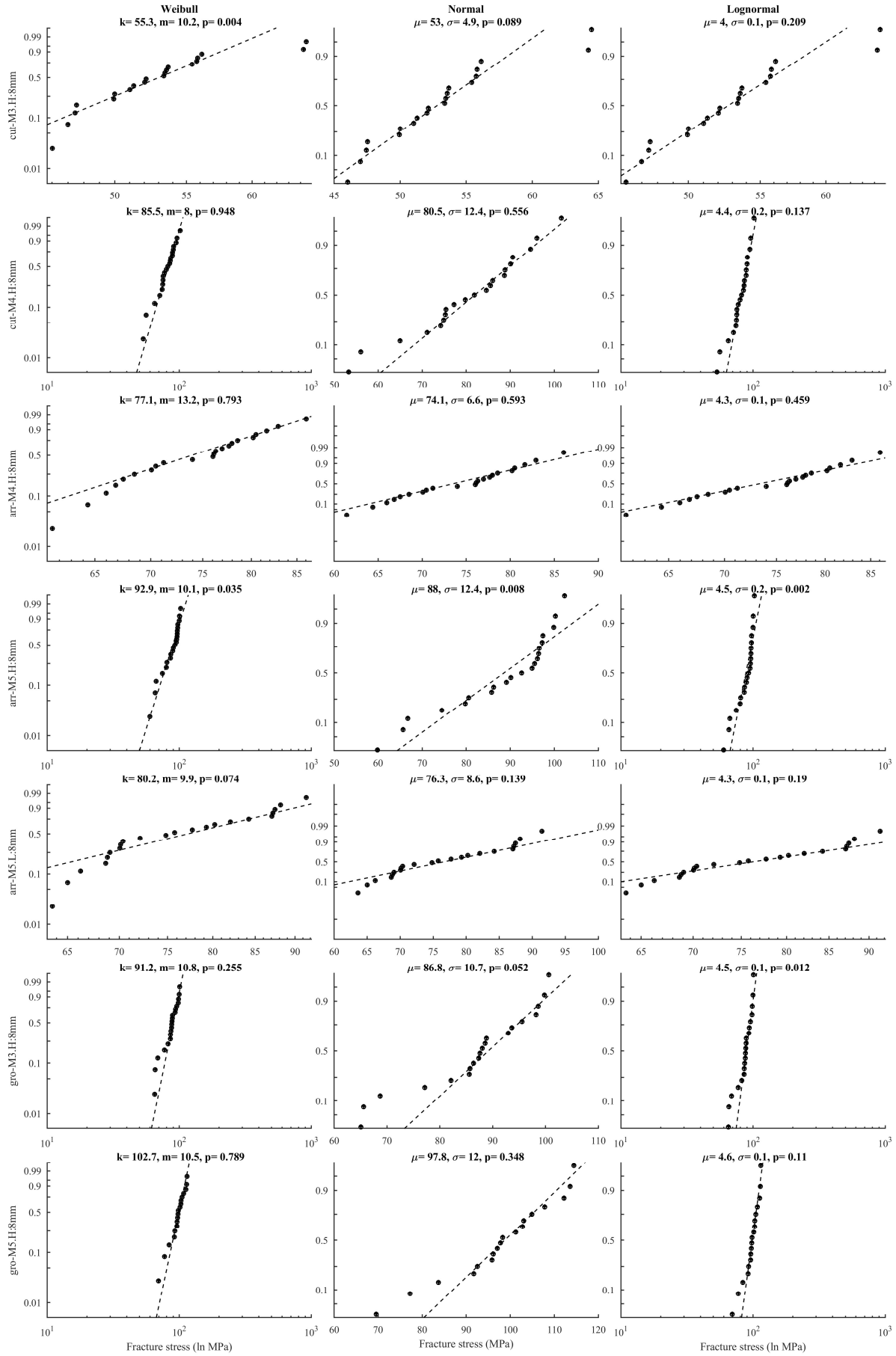


Fig. 47 Probability plots for the data samples in Lindqvist (2013).

*Vandebroek et al. (2014)*

The experiment was conducted with a four-point bending arrangement using an Instron 3369 testing machine. The load and support span were either 250 mm and 500 mm, respectively, or 500 mm and 1000 mm, respectively. The specimens were cut from panes with the thickness 4 mm and 8 mm. The specimen dimensions were 62.5x550 $mm^2$ and 125x1100 $mm^2$. The edge condition was either as-cut or ground. The machine cutting and grinding was carried out by a qualified glass processor. The scoring of the specimens was consistently performed on the air side. The edge processing took place on the same day with the same machine and with the same processing parameters for each set of glass thickness, i.e. 4 mm and 8 mm, and edge type, i.e. as-cut and ground. At least 30 days elapsed from the processing of the edge until the destructive testing. The specimens were subjected to in-plane loading generating an approximate stress rate of 2 MPa $s^{-1}$. The specimens were mounted using rubber intermediates at the load and support contact surfaces. Buckling supports with a Teflon interlayer were employed at mid-span. The temperature and relative humidity during testing was about 25 ºC and 65%, respectively. The specimens that fractured outside the load span were identified and excluded from the analysis. The range of load-duration was approximately 14 sec to 33 sec according to calculations. A summary of details on the experiment is given in Tab. 20. In Fig. 48, a set of boxplots depict the fracture stress characteristics for the nominal strength data. A set of three probability plots for each sample is shown in Fig. 49 including the respective maximum-likelihood parameter estimates and the Anderson-Darling goodness-of-fit statistic. In the probability plots, all points have been marked as edge failures. However, according to the reference, 13% of the ground and 20% of the cut specimen failures on average were identified as originating with either of the surface sides of the glass. These specimens were not identified in the reference.

Table 20: Details on the experiment as reported by Vandebroek et al. (2014). Legend: 4PB=Four-point bending, OP=Out-of-plane.

| Sample ID | No. of spec's | Bending mode | Dimensions ($mm^3$) | Edge condition | Load. span (mm) | Stress rate (MPa $s^{-1}$) |
|---|---|---|---|---|---|---|
| gro-short:4mm | 29 | 4PB IP | 4x62.5x550 | Ground | 250 | 2 |
| gro-long:4mm | 26 | 4PB IP | 4x125x1100 | Ground | 500 | 2 |
| gro-short:8mm | 27 | 4PB IP | 8x62.5x550 | Ground | 250 | 2 |
| gro-long:8mm | 28 | 4PB IP | 8x125x1100 | Ground | 500 | 2 |
| cut-short:4mm | 24 | 4PB IP | 4x62.5x550 | As-cut | 250 | 2 |
| cut-long:4mm | 20 | 4PB IP | 4x125x1100 | As-cut | 500 | 2 |
| cut-short:8mm | 27 | 4PB IP | 8x62.5x550 | As-cut | 250 | 2 |
| cut-long:8mm | 21 | 4PB IP | 8x125x1100 | As-cut | 500 | 2 |

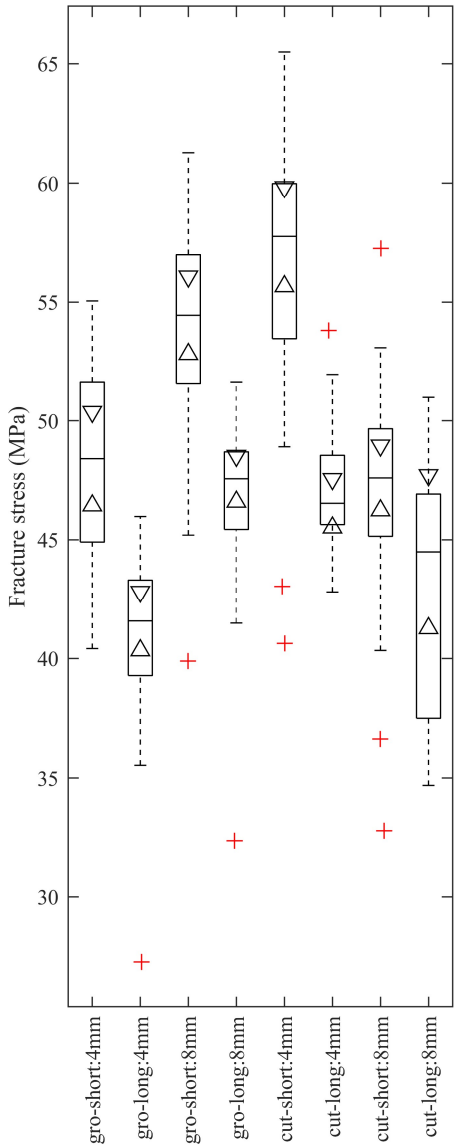


Fig. 48 Boxplots of the fracture stress values for each data sample in Vandebroek et al. (2014).

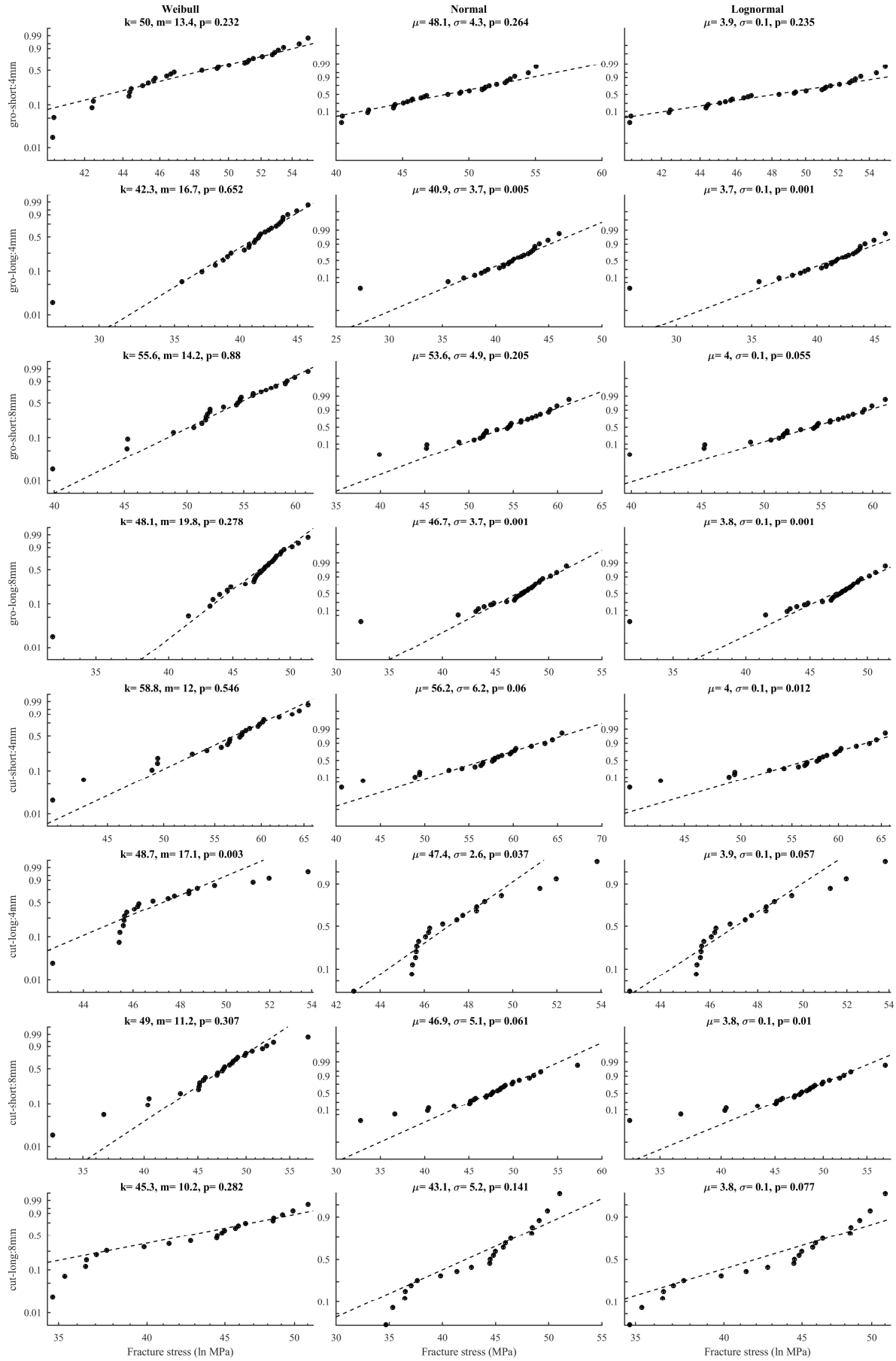


Fig. 49 Probability plots for the data samples in Vandebroek et al. (2014).

*Kozlowski (2014)*

The experiment was conducted with a four-point bending arrangement under displacement control. The load and support span were 500 mm and 1500 mm, respectively. The specimens were cut from panes with the thickness 8 mm. The specimen dimensions were 200x1800 $mm^2$. The edge was machine ground and polished. The specimens were subjected to in-plane loading generating an approximate stress rate of 0.3 MPa $s^{-1}$. The specimens were mounted into the test rig using rubber pads applied at the steel roll contact surfaces at the supports and load introduction points. Two lateral supports were employed at a distance of about 100 mm from the load introduction points. The temperature and relative humidity during testing was not specified but it can be assumed that an indoor environment represents the climatic conditions. The range of load-duration was approximately 2 min and 6 sec to 3 min and 37 sec according to calculations. A summary of details on the experiment is given in Tab. 21. In Fig. 50, a set of boxplots depict the fracture stress characteristics for the nominal strength data as well as the stress rate-equivalent data.

Table 21: Details on the experiment as reported by Kozlowski (2014). Legend: 4PB=Four-point bending, IP=In-plane.

| Sample ID | No. of spec's | Bending mode | Dimensions ($mm^3$) | Edge condition | Load. span (mm) | Stress rate (MPa $s^{-1}$) |
|---|---|---|---|---|---|---|
| pol:8mm | 6 | 4PB IP | 8x200x1800 | Polished | 500 | 0.3 |

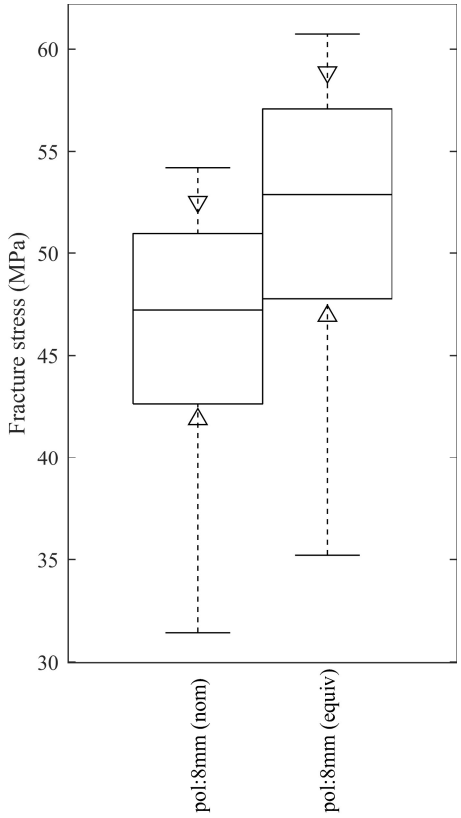


Fig. 50 Boxplots of the fracture stress values in Kozlowski (2014).

*Kleuderlein et al. (2014)*

The experiment was conducted with a four-point bending arrangement. The load and support span were 200 mm and 1090 mm, respectively. The specimens were cut from panes with the thickness 4 mm, 6 mm, and 8 mm. The glass was obtained from six different suppliers in total. The specimen dimensions were 125x1100 $mm^2$. The edge condition was either as-cut, arrised, or ground. The glass manufacturers processed the edges with their usual settings of production parameters. All arrising, grinding, and polishing operations were done by machine. However, the production methods differed between the suppliers. For instance, edging machines with cup wheels were used by half of the manufacturers to arrise the edges while belt edging machines with manual feed were used by the others. Nevertheless, a cup wheel edging machine was used by all manufacturers for the grinding operation. The specimens were subjected to in-plane loading generating an approximate stress rate of 2 MPa $s^{-1}$. The specimens were mounted with four synthetic-coated lateral supports to prevent from tilting. The temperature and relative humidity during testing was not specified but it can be assumed that an indoor environment represents the climatic conditions. Only the specimens that fractured within the load span were considered. The range of load-duration was approximately 17 sec to 45 sec according to calculations. A summary of details on the experiment is given in Tab. 22. In Fig. 51, a set of boxplots depict the fracture stress characteristics for the nominal strength data. A set of three probability plots for each sample is shown in Figs. 52 to 55 including the respective maximum-likelihood parameter estimates and the Anderson-Darling goodness-of-fit statistic. The data results were extracted from the digitized graphs by this author.

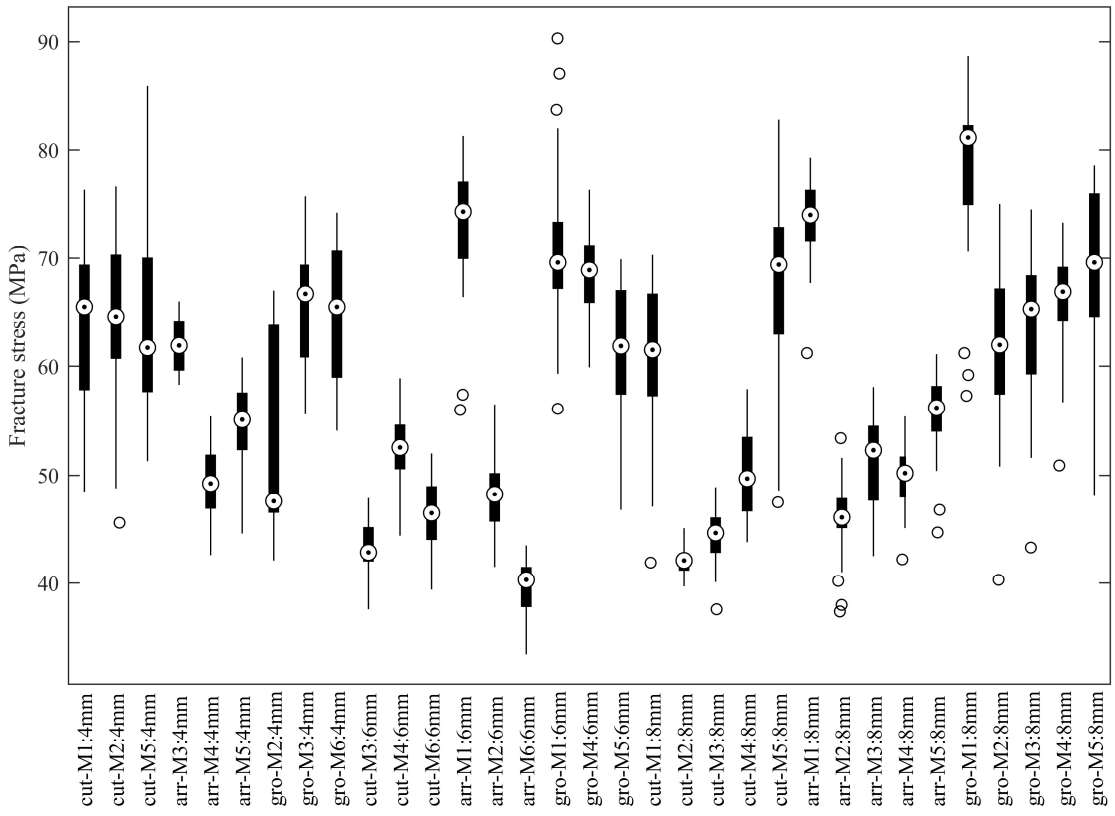


Fig. 51 Boxplots of the nominal fracture stress values for each data sample in Kleuderlein et al. (2014).

Table 22: Details on the experiment as reported by Kleuderlein et al. (2014). Legend: 4PB=Four-point bending, IP=In-plane.

| Sample ID | No. of spec's | Bending mode | Supplier ID | Dimensions ($mm^3$) | Edge condition | Load. span (mm) | Stress rate ($MPa\ s^{-1}$) |
|---|---|---|---|---|---|---|---|
| cut-M1:4mm | 18 | 4PB IP | M1 | 4x125x1100 | Cut | 200 | 2 |
| cut-M2:4mm | 19 | 4PB IP | M2 | 4x125x1100 | Cut | 200 | 2 |
| cut-M5:4mm | 17 | 4PB IP | M5 | 4x125x1100 | Cut | 200 | 2 |
| arr-M3:4mm | 22 | 4PB IP | M3 | 4x125x1100 | Arrised | 200 | 2 |
| arr-M4:4mm | 22 | 4PB IP | M4 | 4x125x1100 | Arrised | 200 | 2 |
| arr-M5:4mm | 23 | 4PB IP | M5 | 4x125x1100 | Arrised | 200 | 2 |
| gro-M2:4mm | 23 | 4PB IP | M2 | 4x125x1100 | Ground | 200 | 2 |
| gro-M3:4mm | 26 | 4PB IP | M3 | 4x125x1100 | Ground | 200 | 2 |
| gro-M6:4mm | 24 | 4PB IP | M6 | 4x125x1100 | Ground | 200 | 2 |
| cut-M3:6mm | 28 | 4PB IP | M3 | 6x125x1100 | Cut | 200 | 2 |
| cut-M4:6mm | 20 | 4PB IP | M4 | 6x125x1100 | Cut | 200 | 2 |
| cut-M6:6mm | 22 | 4PB IP | M6 | 6x125x1100 | Cut | 200 | 2 |
| arr-M1:6mm | 19 | 4PB IP | M1 | 6x125x1100 | Arrised | 200 | 2 |
| arr-M2:6mm | 20 | 4PB IP | M2 | 6x125x1100 | Arrised | 200 | 2 |
| arr-M6:6mm | 26 | 4PB IP | M6 | 6x125x1100 | Arrised | 200 | 2 |
| gro-M1:6mm | 27 | 4PB IP | M1 | 6x125x1100 | Ground | 200 | 2 |
| gro-M4:6mm | 24 | 4PB IP | M4 | 6x125x1100 | Ground | 200 | 2 |
| gro-M5:6mm | 24 | 4PB IP | M5 | 6x125x1100 | Ground | 200 | 2 |
| cut-M1:8mm | 19 | 4PB IP | M1 | 8x125x1100 | Cut | 200 | 2 |
| cut-M2:8mm | 27 | 4PB IP | M2 | 8x125x1100 | Cut | 200 | 2 |
| cut-M3:8mm | 20 | 4PB IP | M3 | 8x125x1100 | Cut | 200 | 2 |
| cut-M4:8mm | 21 | 4PB IP | M4 | 8x125x1100 | Cut | 200 | 2 |
| cut-M5:8mm | 46 | 4PB IP | M5 | 8x125x1100 | Cut | 200 | 2 |
| arr-M1:8mm | 26 | 4PB IP | M1 | 8x125x1100 | Arrised | 200 | 2 |
| arr-M2:8mm | 48 | 4PB IP | M2 | 8x125x1100 | Arrised | 200 | 2 |
| arr-M3:8mm | 20 | 4PB IP | M3 | 8x125x1100 | Arrised | 200 | 2 |
| arr-M4:8mm | 23 | 4PB IP | M4 | 8x125x1100 | Arrised | 200 | 2 |
| arr-M5:8mm | 26 | 4PB IP | M5 | 8x125x1100 | Arrised | 200 | 2 |
| gro-M1:8mm | 22 | 4PB IP | M1 | 8x125x1100 | Ground | 200 | 2 |
| gro-M2:8mm | 26 | 4PB IP | M2 | 8x125x1100 | Ground | 200 | 2 |
| gro-M3:8mm | 53 | 4PB IP | M3 | 8x125x1100 | Ground | 200 | 2 |
| gro-M4:8mm | 28 | 4PB IP | M4 | 8x125x1100 | Ground | 200 | 2 |
| gro-M5:8mm | 21 | 4PB IP | M5 | 8x125x1100 | Ground | 200 | 2 |

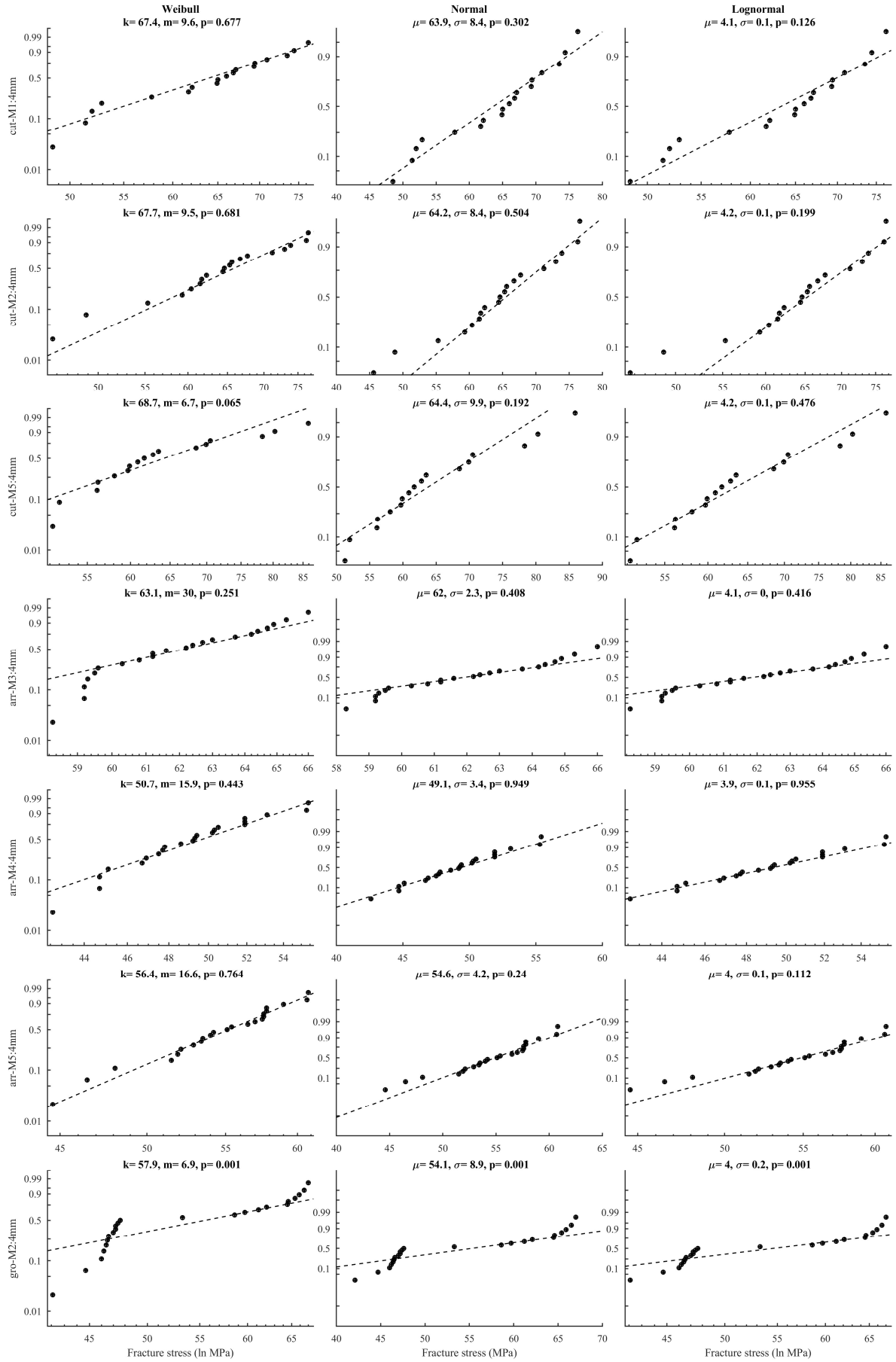


Fig. 52 Probability plots for the data samples in Kleuderlein et al. (2014).

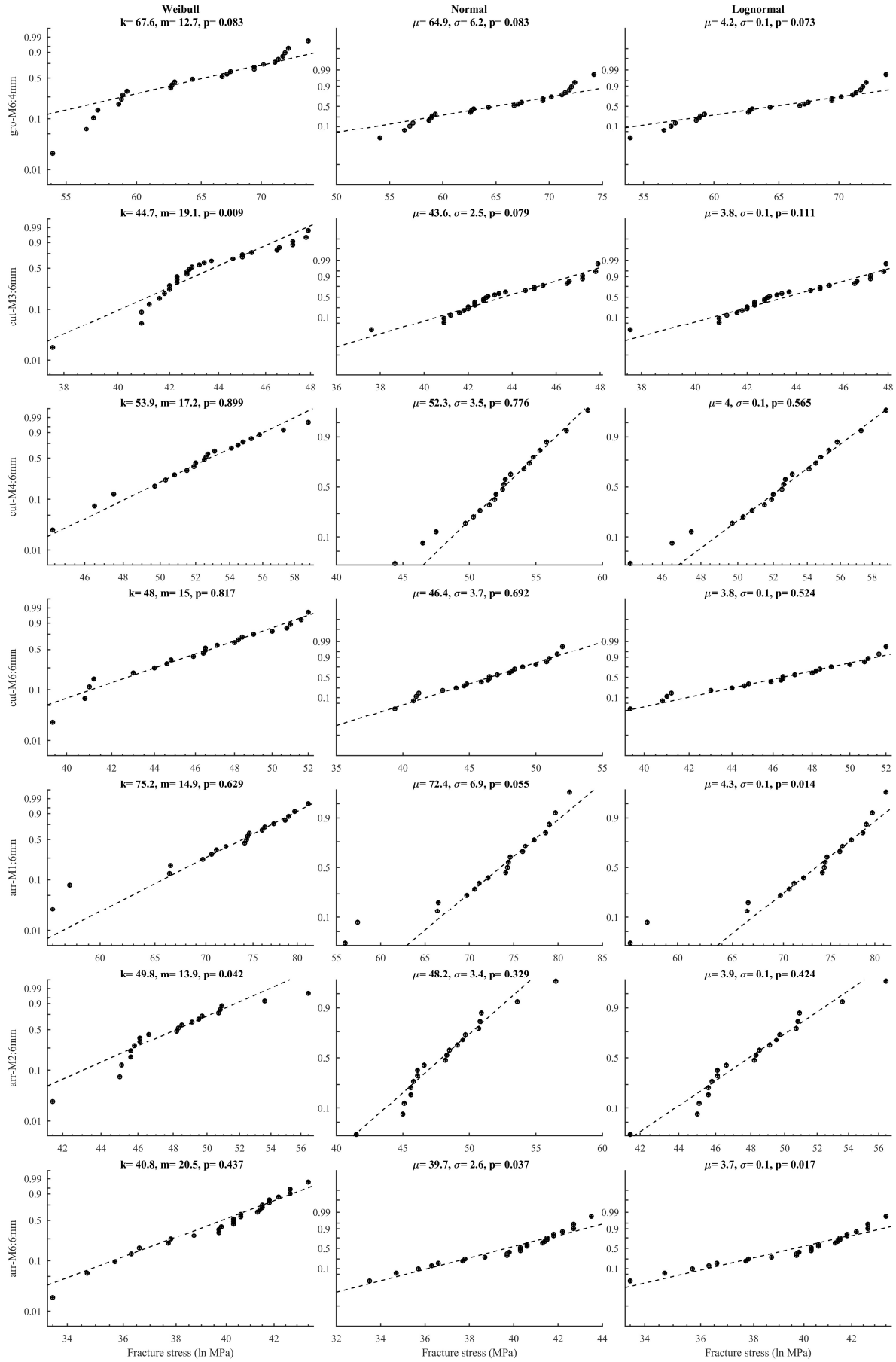


Fig. 53 Probability plots for the data samples in Kleuderlein et al. (2014).

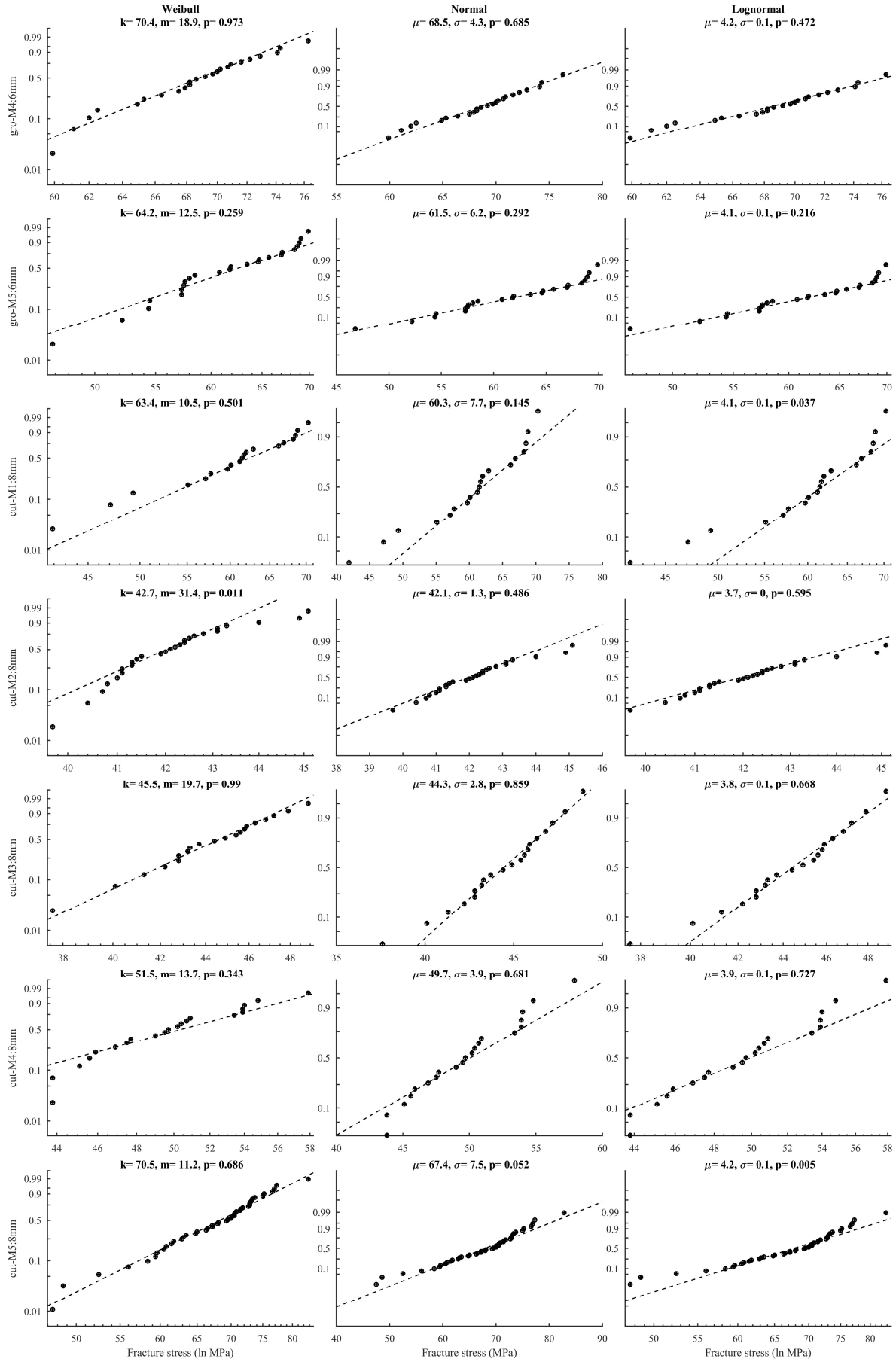


Fig. 54 Probability plots for the data samples in Kleuderlein et al. (2014).

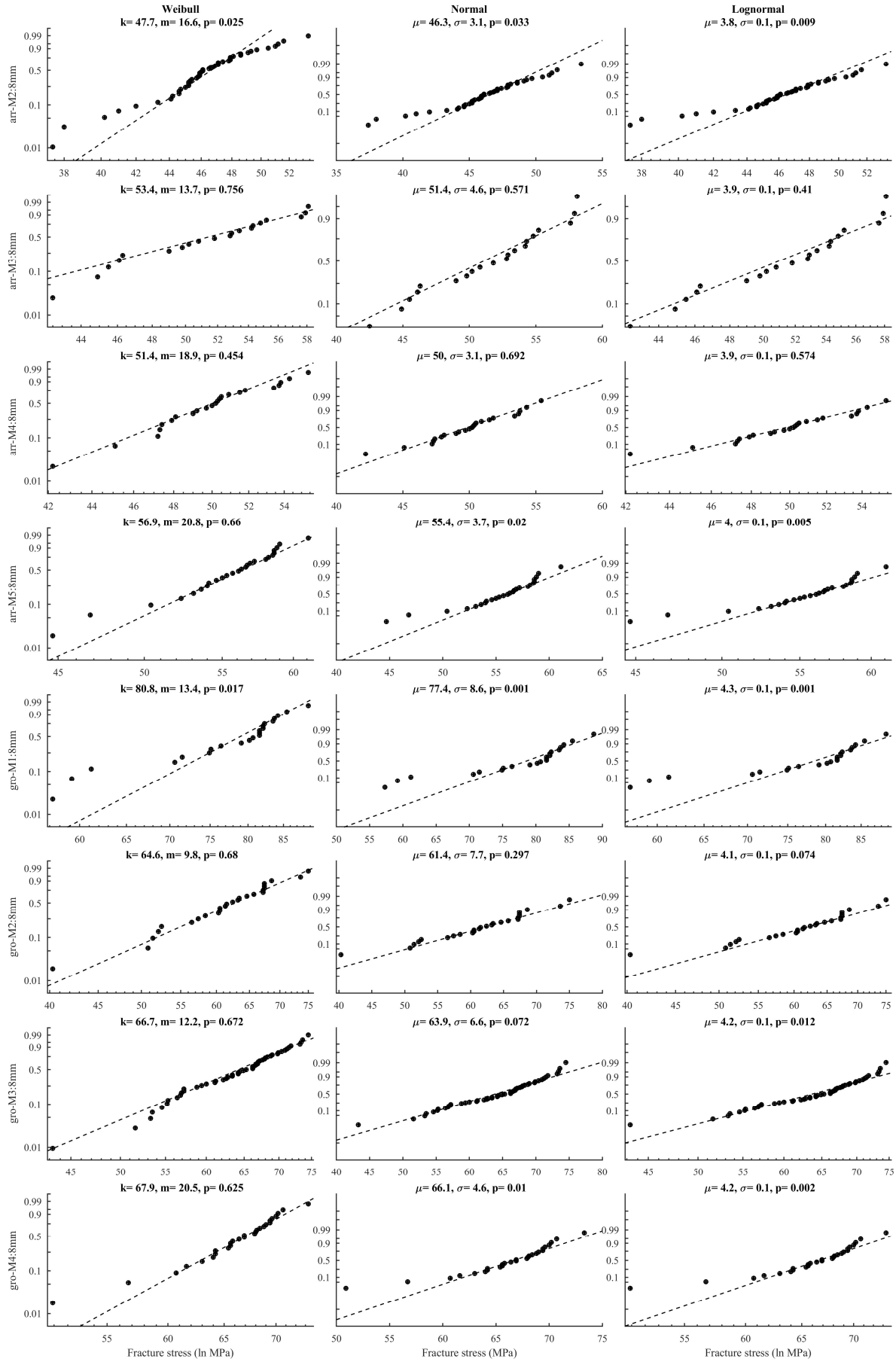


Fig. 55 Probability plots for the data samples in Kleuderlein et al. (2014).

*Schula (2015)*

The experiment was conducted with a coaxial double ring bending setup using a Zwick Z050 THW Allround-Line testing machine. The loading ring diameter was 80 mm and the support ring diameter was 160 mm. The specimens were cut out from panes with a thickness of 6 mm. The specimen dimensions were 250x250 $mm^2$. The specimens were subjected to out-of-plane loading generating a stress rate within the loading ring area of approximately 2 MPa $s^{-1}$. The tin side of the glass was positioned in the tension zone. The specimens were covered in self-adhesive foil on the compression side. The temperature during testing was 27 ºC while the relative humidity was 50%. The time-duration until failure ranged from approximately 25 sec to 51 sec. A summary of details on the experiment is given in Tab. 23. In Fig. 56, a set of boxplots depict the fracture stress characteristics for the nominal strength data. A set of three probability plots for each sample is shown in Fig. 57 including the respective maximum-likelihood parameter estimates and the Anderson-Darling goodness-of-fit statistic.

Table 23: Details from the experiment of Schula (2015). CDR=Coaxial double ring bending.

| Sample ID | No. of spec's | Bending mode | Dimensions ($mm^3$) | Load. ring diameter (mm) | Stress rate (MPa $s^{-1}$) |
|---|---|---|---|---|---|
| 1 | 15 | CDR | 6x250x250 | 80 | 2.0 |

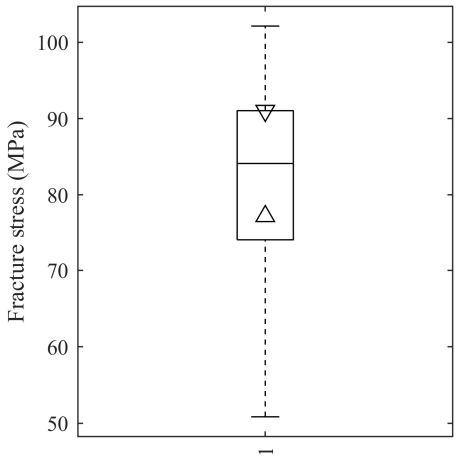


Fig. 56 Boxplots of the nominal fracture stress according to the experimental data in Schula (2015).

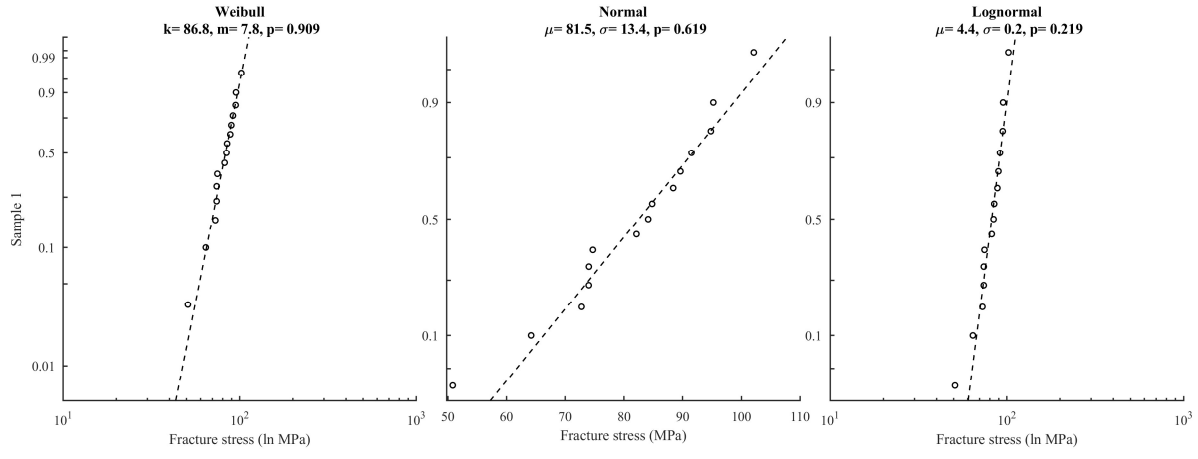


Fig. 57 Probability plots of the data sample in Schula (2015).

*Muniz-Calvente et al. (2016)*

The experiment was conducted with a coaxial double ring bending device and a four-point bending setup using an MTS Bionix uniaxial 100 kN testing machine. The loading and support ring diameters in the double ring bending test were 60 mm and 160 mm, respectively, whereas the load and support span dimensions in the four-point bending test were 200 mm and 1000 mm, respectively. All specimens in the double ring bending test were cut from the same glass pane with a thickness of 5 mm and all specimens in the four-point bending test were cut from the same pane with the thickness 5 mm. The plates in the double ring bending test measured 250x250 $mm^2$ in surface area while the specimens in the four-point bending test measured 360x1100 $mm^2$. The type of edge processing was polished according to personal correspondence with one of the authors. All specimens were subjected to out-of-plane loading generating an approximate stress rate of 2 MPa $s^{-1}$. The type of fracture origin, i.e. edge fracture or surface fracture, in the case of four-point bending was recorded but not detailed in the journal article. The time-duration of loading ranged from approximately 23 secs to 67 secs. A summary of details on the experiment is given in Tab. 24. In Fig. 58, a set of boxplots depict the fracture stress characteristics for the nominal strength data. A set of three probability plots for each sample is shown in Fig. 59 including the respective maximum-likelihood parameter estimates and the Anderson-Darling goodness-of-fit statistic.

Table 24: Details on the experiment as reported by Muniz-Calvente et al. (2016). 4PB=Four-point bending, OP=Out-of-plane, CDR=Coaxial double ring.

| Sample ID | No. of spec's | Bending mode | Dimensions ($mm^3$) | Edge proc. | Load. span/Load. ring diam. (mm) | Stress rate (MPa $s^{-1}$) |
|---|---|---|---|---|---|---|
| CDR | 28 | CDR | 5x250x250 | Polished | 60 | 2 |
| 4PB | 30 | 4PB OP | 5x360x1100 | Polished | 200 | 2 |

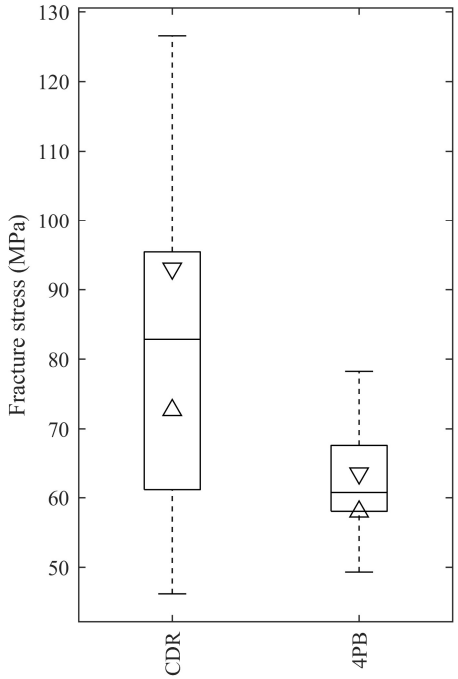


Fig. 58 Boxplots of the nominal fracture stress values in Muniz-Calvente et al. (2016).

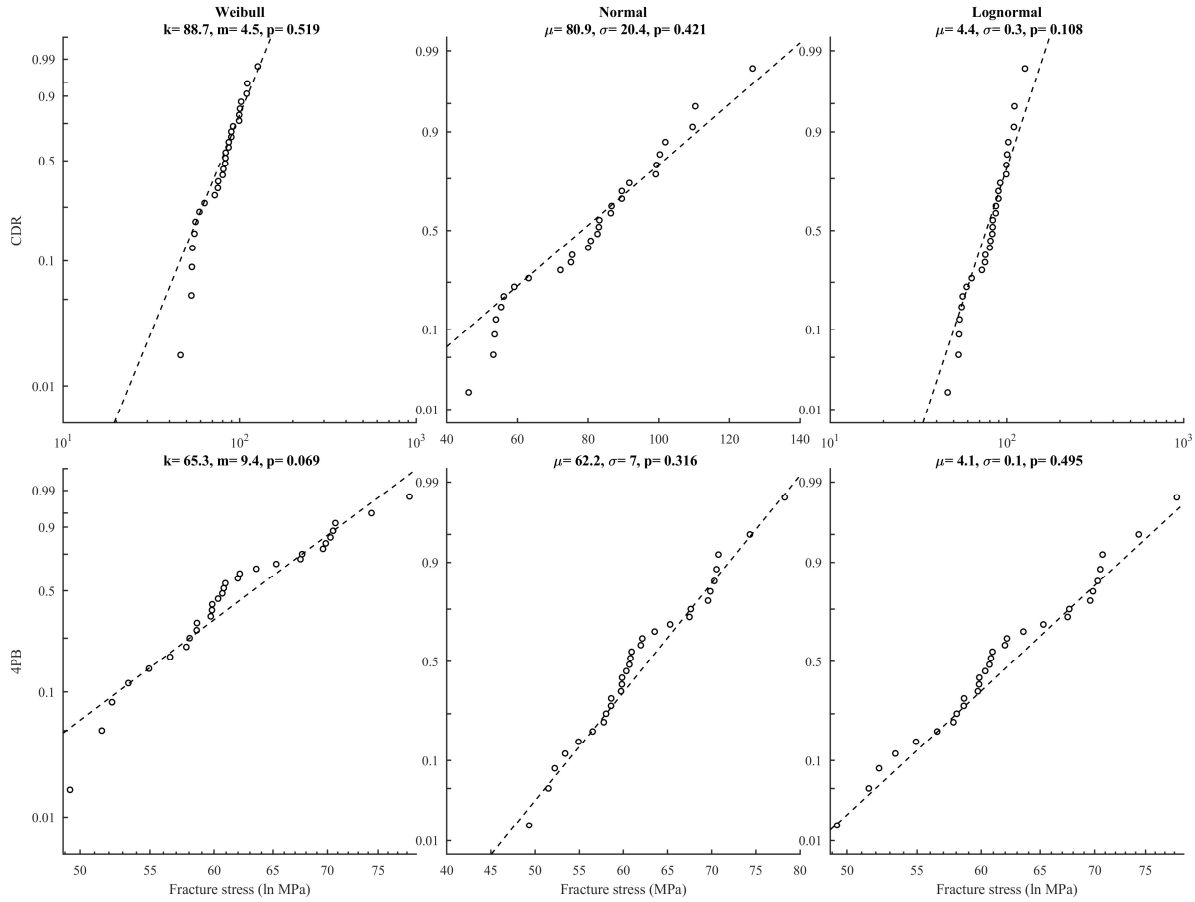


Fig. 59 Probability plots for the data samples in Muniz-Calvente et al. (2016).

*SURVEY OF EXPERIMENTAL DATA ON THE STRENGTH OF ANNEALED FLOAT GLASS*

*Kinsella and Persson (2016)*

The experiment was conducted with the four-point bending setup using an MTS 810 universal testing machine under displacement control. Two different load spans were employed, viz. 300 mm and 450 mm. The support span was 900 mm. All specimens were cut out from the same glass pane with the thickness 8 mm. The specimen dimensions were 100x1000 $mm^2$. The edges were machine ground and polished. The specimens were subjected to out-of-plane loading generating an approximate stress rate of 0.31 MPa $s^{-1}$. All specimens were wrapped in self-adhesive plastic foil in order to control the post-fracture behavior. The fracture origin type, i.e. edge or surface, was not recorded. The load-duration ranged from about 1 min and 24 sec to 4 min and 30 sec. The temperature and relative humidity during testing were not recorded but it can be assumed that an indoor environment represents the climatic conditions. A summary of details on the experiment is given in Tab. 25. In Fig. 60, a set of boxplots depict the fracture stress characteristics for the nominal and stress rate-equivalent strength data. A set of three probability plots for each sample is shown in Fig. 61 including the respective maximum-likelihood parameter estimates and the Anderson-Darling goodness-of-fit statistic.

Table 25: Details on the experiments as reported by Kinsella and Persson (2016). 4PB=Four-point bending, OP=Out-of-plane.

| Sample ID | No. of spec's | Bending mode | Dimensions ($mm^3$) | Edge condition | Load. span (mm) | Stress rate (MPa $s^{-1}$) |
|---|---|---|---|---|---|---|
| pol-short | 44 | 4PB OP | 8x100x1000 | Polished | 300 | 0.32 |
| pol-long | 29 | 4PB OP | 8x100x1000 | Polished | 450 | 0.36 |

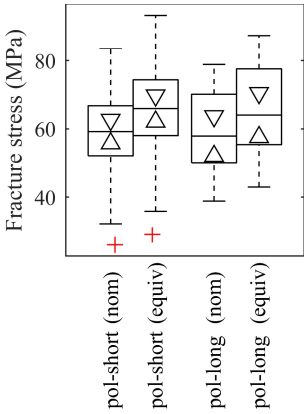


Fig. 60 Boxplots of the (left) nominal and (right) stress rate-equivalent fracture stress values for the data samples in Kinsella and Persson (2016).

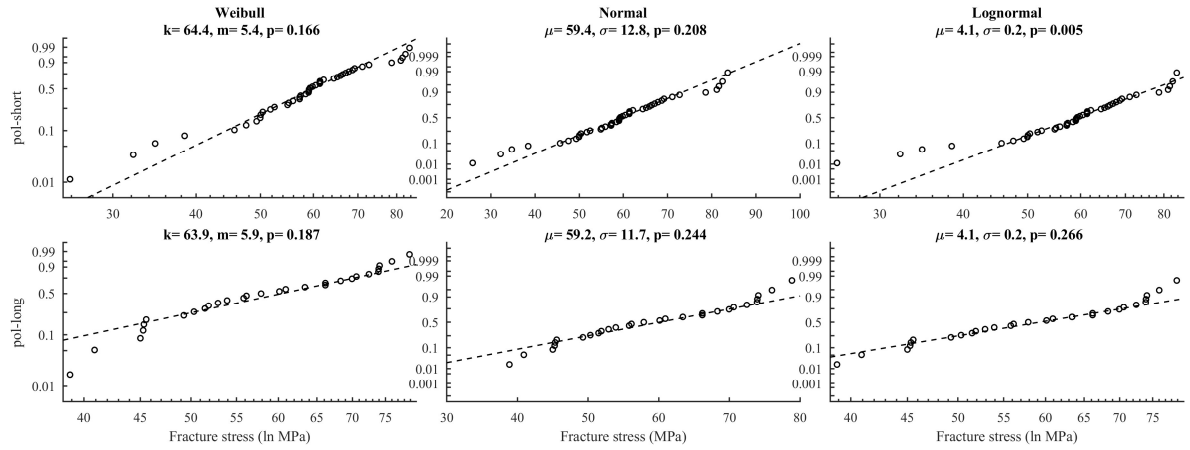


Fig. 61 Probability plots for the data samples in Kinsella and Persson (2016).

*Navarrete et al. (2016)*

The experiment was conducted with the double ring bending setup using an Instron 5500R universal testing machine with a constant load rate of 79 kN $min^{-1}$. The load and support ring diameters were 51 mm and 127 mm, respectively. All specimens were cut out from glass panes using industrial automated cutting. The pane thicknesses were 3, 4, 5, 6, 8, 10, 12, and 19 mm, respectively. The specimen dimensions were 200x200 $mm^2$. The specimens were subjected to out-of-plane loading generating an approximate stress rate according to Tab. 26. All specimens were wrapped in PET foil to control the post-fracture behavior. The load-duration ranged from about 1 sec to 55 sec according to calculations. The average temperature during testing was 20 ºC. The relative humidity during testing was not recorded but it can be assumed that an indoor environment represents the climatic conditions. The specimens were tested with the tin side downwards, i.e. in the tension zone. A total number of 8 specimens were excluded from the record for reasons including the following: the fracture origin could not be determined, the fracture origin was found to lie outside the load ring, the rings were non-coaxial after the test. A summary of details on the experiment is given in Tab. 26. In Fig. 62, a set of boxplots depict the fracture stress characteristics for the nominal and stress rate-equivalent strength data. The failure stress was calculated according to ASTM C 1499-05. A set of three probability plots for each sample is shown in Fig. 63 including the respective maximum-likelihood parameter estimates and the Anderson-Darling goodness-of-fit statistic.

Table 26: Details on the experiments as reported by Navarrete et al. (2016). CDR=Co-axial double ring.

| Sample ID | No. of spec's | Bending mode | Dimensions ($mm^3$) | Edge condition | Load. span/Load. ring diam. (mm) | Stress rate (MPa $s^{-1}$) |
|---|---|---|---|---|---|---|
| 3mm | 8 | CDR | 3x200x200 | As-cut | 51 | 86.0 |
| 4mm | 8 | CDR | 4x200x200 | As-cut | 51 | 48.4 |
| 5mm | 8 | CDR | 5x200x200 | As-cut | 51 | 31.0 |
| 6mm | 9 | CDR | 6x200x200 | As-cut | 51 | 21.5 |
| 8mm | 9 | CDR | 8x200x200 | As-cut | 51 | 12.1 |
| 10mm | 8 | CDR | 10x200x200 | As-cut | 51 | 7.74 |
| 12mm | 9 | CDR | 12x200x200 | As-cut | 51 | 5.37 |
| 19mm | 10 | CDR | 19x200x200 | As-cut | 51 | 2.14 |

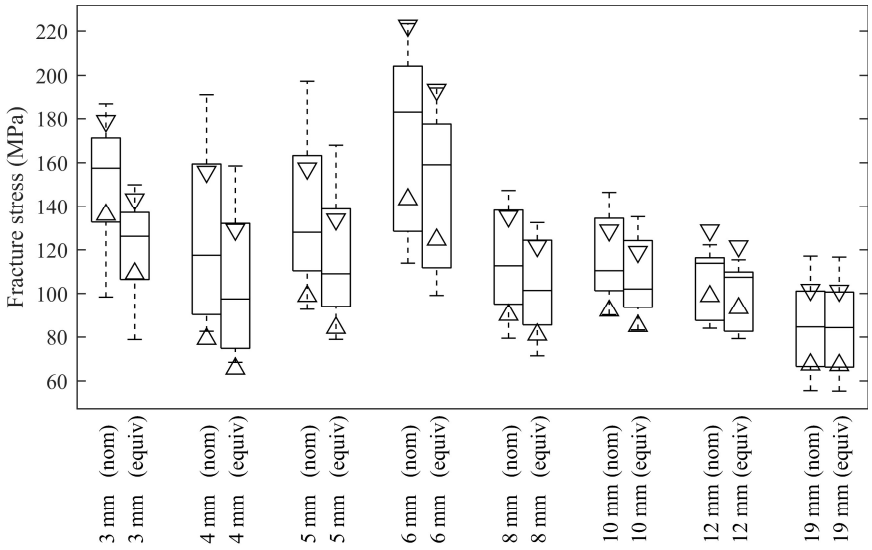


Fig. 62 Boxplots of the (left) nominal and (right) stress rate-equivalent fracture stress values for the data samples in Navarrete et al. (2016).

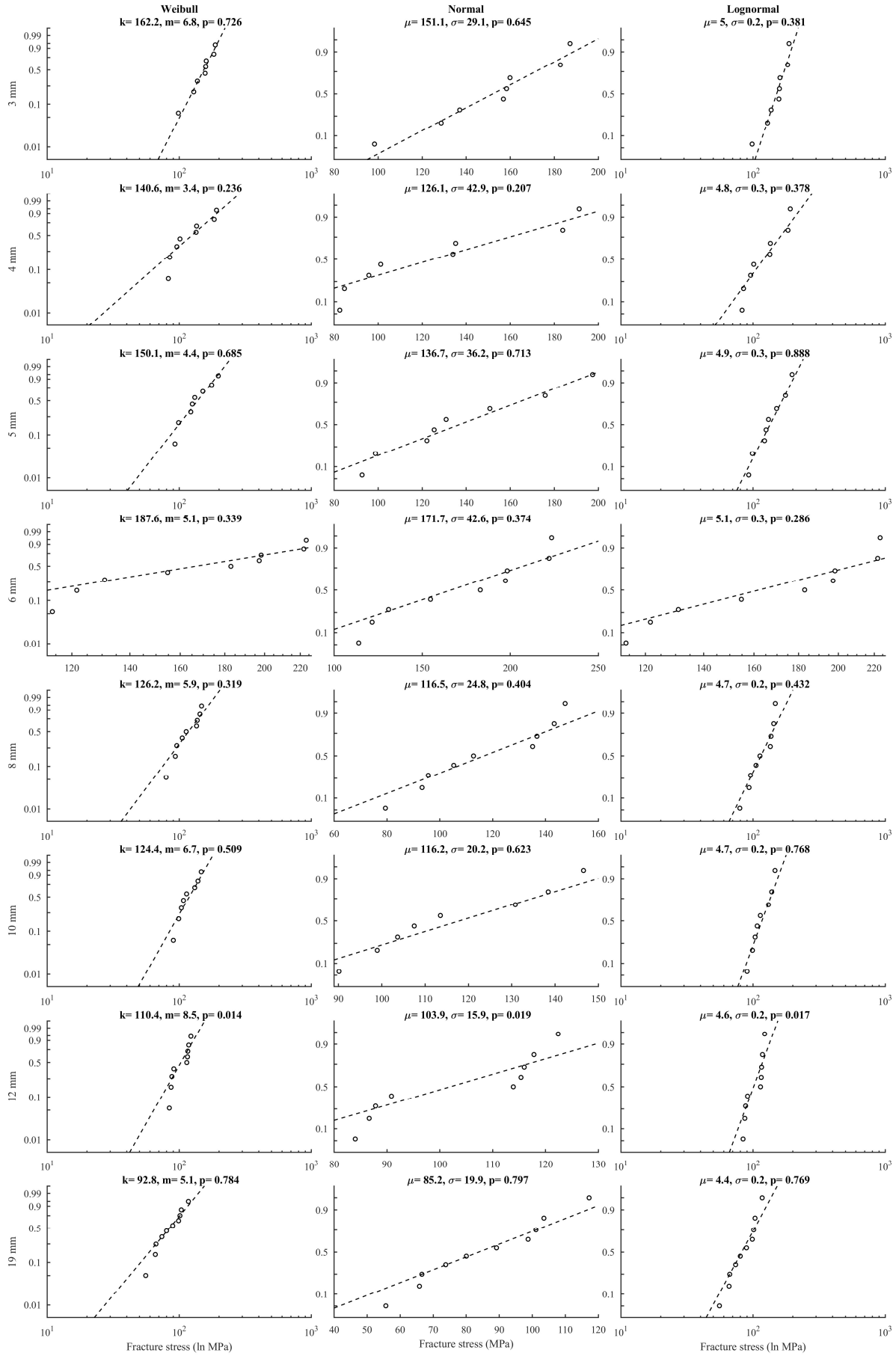


Fig. 63 Probability plots for the data samples in Navarrete et al. (2016).

*Yankelevesky et al. (2017)*

The experiment was conducted with the four-point bending setup under displacement control at about 0.012 mm $s^{-1}$. The load and support span were 100 mm and 200 mm, respectively. All specimens were cut out from glass with a thickness of about 12 mm. The specimen dimensions were 38x250 $mm^2$. The specimens were subjected to out-of-plane loading generating an approximate stress rate of 1.1 MPa $s^{-1}$. The scored edge was placed upwards, i.e. in the compression zone. The origin of failure was identified for each specimen. The load-duration ranged from about 48 sec to 1 min and 58 sec according to calculations. The temperature and relative humidity during testing were 24 ºC and 32%, respectively. A summary of details on the experiment is given in Tab. 27. In Fig. 64, a set of boxplots depict the fracture stress characteristics for the nominal and stress rate-equivalent strength data. A set of three probability plots for the sample is shown in Fig. 65 including the respective maximum-likelihood parameter estimates and the Anderson-Darling goodness-of-fit statistic.

Table 27: Details on the experiment as reported by Yankelevsky et al. (2017). 4PB=Four-point bending, OP=Out-of-plane.

| Sample ID | No. of spec's | Bending mode | Dimensions ($mm^3$) | Edge condition | Load. span (mm) | Stress rate (MPa $s^{-1}$) |
|---|---|---|---|---|---|---|
| 4PB | 56 | 4PB OP | 12x38x250 | As-cut | 100 | 1.1 |

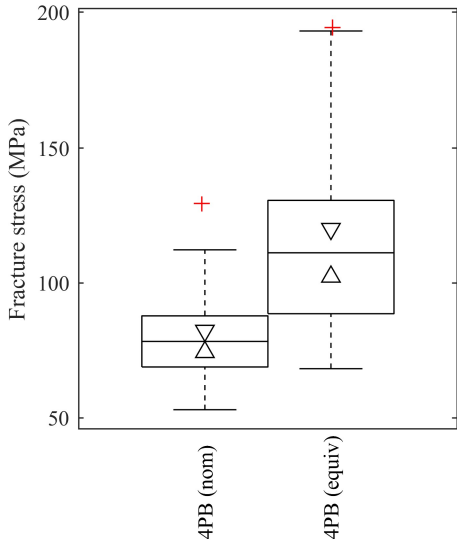


Fig. 64 Boxplots of the (left) nominal and (right) stress rate-equivalent fracture stress values for the data sample in Yankelevsky (2017).

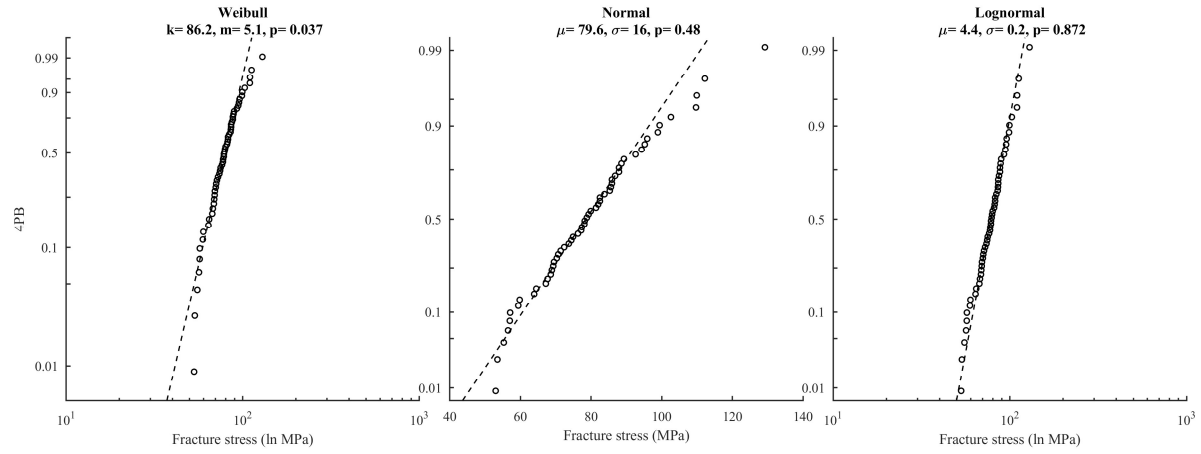


Fig. 65 Probability plots for the data sample in Yankelevsky (2017).

*Osnes et al. (2018)*

The experiment was conducted with a four-point bending device. The loading span varied between 40 mm, 90 mm, and 140 mm, corresponding to three different samples of specimen dimensions. The support span dimensions were 80 mm, 180 mm, and 280 mm, respectively. All specimens were cut out of panes with the nominal thickness 4 mm. The edge condition was as-cut. The specimen dimensions were 20x100 $mm^2$, 40x200 $mm^2$, and 60x300 $mm^2$. The mechanically scribed edge was always placed on the compression side. The specimens were subjected to out-of-plane loading and the loading was applied using displacement control generating an average strain rate of $10 \cdot 10^{-5}$ $s^{-1}$. With the estimation of Young's modulus at $E = 70$ GPa, it follows that the stress rate was approximately 7 MPa $s^{-1}$. The fracture origin type, i.e. edge or surface, was recorded. It was not recorded which of the tin versus air side that was placed in the tension zone. The length of load-duration ranged from approximately 5 sec to 30 sec according to calculations. A summary of details on the experiment is given in Tab. 28. In Fig. 66, a set of boxplots is given for the nominal fracture stress values as well as the stress rate-equivalent values.

Table 28: Details on the experiments as reported by Osnes et al. (2018). Legend: 4PB=Four-point bending, OP=Out-of-plane.

| Sample ID | No. of spec's | Bending mode | Dimensions ($mm^3$) | Edge proc. type | Load. span (mm) | Approx. stress rate (MPa $s^{-1}$) |
|---|---|---|---|---|---|---|
| cut-short | 31 | 4PB OP | 4x20x100 | As-cut | 40 | 7 |
| cut-medium | 31 | 4PB OP | 4x40x200 | As-cut | 90 | 7 |
| cut-long | 31 | 4PB OP | 4x60x300 | As-cut | 140 | 7 |

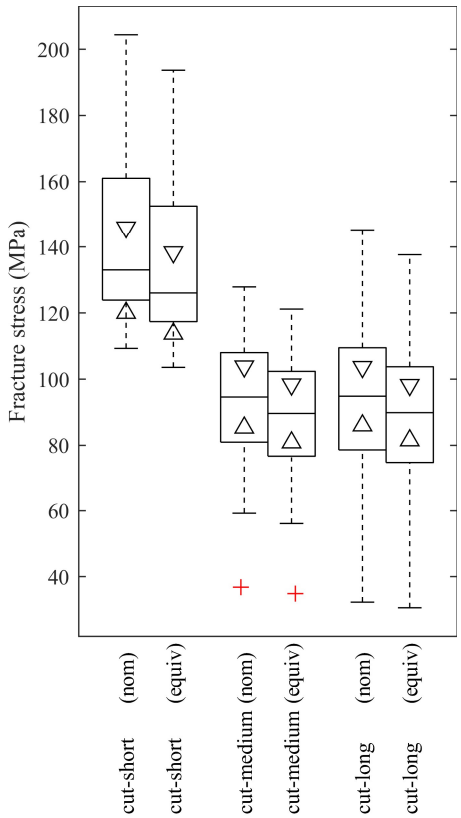


Fig. 66 Boxplots of the nominal and stress rate-equivalent fracture stress values for each data sample in Osnes et al. (2018). Surface failures only.

## 11. References

Anderson, T. W. and Darling, D. A. (1952) 'Asymptotic Theory of Certain "Goodness of Fit" Criteria Based on Stochastic Processes', *Ann. Math. Statist.* The Institute of Mathematical Statistics, (2), pp. 193–212. doi: 10.1214/aoms/1177729437.

Brown, W. G. (1974) *A practicable Formulation for the Strength of Glass and its Special Application to Large Plates*.

Calderone, I. J. (1999) *The equivalent wind loading for window glass design*. Monash University.

Carre, H. (1996) *Etude du comportement à la rupture d'un matériau fragile précontraint : le verre trempé*. Ecole Nationale des Ponts et Chaussées.

Charles, R. J. (1958a) 'Static Fatigue of Glass I', *J Appl Phys*, 29, pp. 1549–1553.

Charles, R. J. (1958b) 'Static Fatigue of Glass II', *J Appl Phys*, 29, pp. 1554–1560.

D'Agostino, R. B. and Stephens, M. A. (eds) (1986) *Goodness-of-fit Techniques*. New York, NY, USA: Marcel Dekker, Inc.

Dalgliesh, W. A. and Taylor, D. A. (1990) 'The strength and testing of window glass', *Can J Civ Eng*, 17, pp. 752–762.

DIN 18008-1 (2010) 'Glas im Bauwesen - Bemessungs- und Konstruktionsregeln - Teil 1: Begriffe und allgemeine Grundlagen.'

Fink, A. (2000) *Ein Beitrag zum Einsatz von Floatglas als dauerhaft tragender Konstruktionswerkstoff im Bauwesen*.

Forbes, C. *et al.* (2011) *Statistical distributions*. 4th edn. John Wiley and sons, Inc.

Garcia-Prieto, M.-A. (2001) *Dimensionamiento probabilistico y analisis experimental de vidrio en rotura*. Universidad de Oviedo.

Haldimann, M. (2006) *Fracture strength of structural glass elements -- analytical and numerical modelling, testing and design*. Ecole Polytechnique Fédérale de Lausanne EPFL.

Hess, R. (2000) *Glasträger*. Zürich, Switzerland.

Huerta, M. C. *et al.* (2011) 'Influence of experimental test type on the determination of probabilistic stress distribution', in *Glass Performance Days 2011*.

Johar, S. (1981) *Dynamic fatigue of flat glass - Phase II*.

Johar, S. (1982) *Dynamic fatigue of flat glass - Phase III*.

Kanabolo, D. C. and Norville, H. S. (1985) *The strength of new window glass using surface characteristics*. Texas Tech University.

Kinsella, D. T. and Persson, K. (2016) 'On the applicability of the Weibull distribution to model annealed glass strength and future research needs', in *Challenging Glass Conference 5*. Ghent, Belgium.

Kirstein, A. F. and Woolley, R. . (1967) 'Symmetrical bending of thin circular elastic plates of equally spaced point supports', *J Res Natl Bur Stds*, 71C, pp. 1–10.

Kleuderlein, J., Ensslen, F. and Schneider, J. (2014) 'Investigation of edge strength dependent on different types of edge processing', in *Engineered Transparency. International Conference at Glasstec*. Düsseldorf, Germany.

Kozlowski, M. (2014) *Experimental and numerical analysis of hybrid timber-glass beams*. Silesian University of Technology.

Lawless, J. F. (2003) *Statistical models and methods for lifetime data*. 2nd edn. John Wiley and Sons, Inc.

Lindqvist, M. (2013) *Structural Glass Strength Prediction Based on Edge Flaw Characterization*. Ecole Polytechnique Fédérale de Lausanne EPFL.

MathWorks Inc. (2018) 'www.mathworks.com'.

McGill, R., Tukey, J. W. and Larsen, W. A. (1978) 'Variations of Box Plots', *Am Stat*. American Statistical Association, Taylor & Francis, Ltd., 32(1), pp. 12–16.

Mencik, J. (1992) *Strength and Fracture of Glass and Ceramics*. Elsevier (Glass Science and Technology).

Muniz-Calvente, M. *et al.* (2016) 'Statistical joint evaluation of fracture results from distinct experimental programs: An application to annealed glass', *Theor Appl Fract Mec*, 85(Part A), pp. 149–157.

Natividad, K. (2014) 'Locations of Fracture Origins and Magnitudes of Maximum Principal Stresses in Rectangular Glass Lites'. Texas Tech University.

Navarrete, B. *et al.* (2016) 'Failure behavior of annealed glass for building windows', *Eng Struct*, 141, pp. 417–426.

Nilsson, A. (1993) *Stochastic characterization of glass strength properties*.

Osnes, K., Børvik, T. and Hopperstad, O. S. (2018) 'Testing and modelling of annealed float glass under quasi-static and dynamic loading', *Eng Fract Mech*. doi: https://doi.org/10.1016/j .engfracmech.2018.05.031.

Overend, M. (2002) *The appraisal of structural glass assemblies*. University of Surrey.

Postigo, S. (2010) *Estudio teorico experimental de impactos humanos contra vidrios de acristalamientos de edificacion*. Universidad de Politecnica de Madrid.

prEN 16612 (2017) 'Glass in building - Determination of the lateral load resistance of glass panes by calculation'.

Schula, S. (2015) *Charakterisierung der Kratzanfälligkeit von Gläsern im Bauwesen*. Springer.

Sglavo, V. M., Muller, C. and Righetti, F. (2007) 'Influence of edge finishing on the resistance to thermal stresses of float glass', in *Glass Performance Days 2007*.

Sheshkin, D. (2004) *Handbook of parametric and nonparametric statistical procedures*. 3rd edn. Chapman Hall/CRC.

Simiu, E. *et al.* (1984) *Ring-on-ring tests and load capacity of cladding glass*.

Vandebroek, M. *et al.* (2012) 'Experimental validation of edge strength model for glass with polished and cut edge finishing', *Eng Fract Mech*, 96, pp. 480–489.

Vandebroek, M. *et al.* (2014) 'Size effect model for the edge strength of glass with cut and ground edge finishing', *Eng Struct*, 79, pp. 96–105.

Veer, F. A., Louter, C. and Bos, F. P. (2009) 'The strength of annealed, heat-strengthened and fully tempered float glass', *Fatigue Fract Eng M*, 32, pp. 18–25.

Veer, F. A., Louter, P. C. and Romein, T. (2006) 'Quality control and the strength of glass', in *ECF 16 conference*.

Veer, F. A. and Rodichev, Y. M. (2011) 'The structural strength of glass: Hidden damage', *Strength Mater+*, 43, pp. 302–315.

Veer, F. A. and Rodichev, Y. M. (2012) 'The strength of water jet cut glass', in *Glass Performance Days 2011*, pp. 434–438.

Wasserman, L. (2006) *All of nonparametric statistics*. Springer.

Weibull, W. (1939) 'A Statistical Theory of the Strength of Materials', *Ingenjörsvetenskapsakademiens handlingar*, 151.

Yankelevsky, D. *et al.* (2017) 'Fracture characteristics of laboratory-tested soda lime glass specimens', *Can J Civ Eng*, 44, pp. 151–160.